



National Library
of Canada

Bibliothèque nationale
du Canada

Acquisitions and
Bibliographic Services Branch

Direction des acquisitions et
des services bibliographiques

395 Wellington Street
Ottawa, Ontario
K1A 0N4

395, rue Wellington
Ottawa (Ontario)
K1A 0N4

Your file *Votre référence*

Our file *Notre référence*

NOTICE

AVIS

The quality of this microform is heavily dependent upon the quality of the original thesis submitted for microfilming. Every effort has been made to ensure the highest quality of reproduction possible.

La qualité de cette microforme dépend grandement de la qualité de la thèse soumise au microfilmage. Nous avons tout fait pour assurer une qualité supérieure de reproduction.

If pages are missing, contact the university which granted the degree.

S'il manque des pages, veuillez communiquer avec l'université qui a conféré le grade.

Some pages may have indistinct print especially if the original pages were typed with a poor typewriter ribbon or if the university sent us an inferior photocopy.

La qualité d'impression de certaines pages peut laisser à désirer, surtout si les pages originales ont été dactylographiées à l'aide d'un ruban usé ou si l'université nous a fait parvenir une photocopie de qualité inférieure.

Reproduction in full or in part of this microform is governed by the Canadian Copyright Act, R.S.C. 1970, c. C-30, and subsequent amendments.

La reproduction, même partielle, de cette microforme est soumise à la Loi canadienne sur le droit d'auteur, SRC 1970, c. C-30, et ses amendements subséquents.

Canada

Lanthanide Ions in the Development of Artificial Nucleases

by Bryan K. Takasaki

*A thesis submitted to the Faculty of Graduate Studies and Research of
McGill University in partial fulfillment of the requirements for the degree of
Doctor of Philosophy*

July, 1994
Department of Chemistry
McGill University
Montreal, Quebec, Canada

© Bryan Takasaki, 1994



National Library
of Canada

Bibliothèque nationale
du Canada

Acquisitions and
Bibliographic Services Branch

Direction des acquisitions et
des services bibliographiques

395 Wellington Street
Ottawa, Ontario
K1A 0N4

395, rue Wellington
Ottawa (Ontario)
K1A 0N4

Your file *Votre référence*

Our file *Notre référence*

THE AUTHOR HAS GRANTED AN
IRREVOCABLE NON-EXCLUSIVE
LICENCE ALLOWING THE NATIONAL
LIBRARY OF CANADA TO
REPRODUCE, LOAN, DISTRIBUTE OR
SELL COPIES OF HIS/HER THESIS BY
ANY MEANS AND IN ANY FORM OR
FORMAT, MAKING THIS THESIS
AVAILABLE TO INTERESTED
PERSONS.

L'AUTEUR A ACCORDE UNE LICENCE
IRREVOCABLE ET NON EXCLUSIVE
PERMETTANT A LA BIBLIOTHEQUE
NATIONALE DU CANADA DE
REPRODUIRE, PRETER, DISTRIBUER
OU VENDRE DES COPIES DE SA
THESE DE QUELQUE MANIERE ET
SOUS QUELQUE FORME QUE CE SOIT
POUR METTRE DES EXEMPLAIRES DE
CETTE THESE A LA DISPOSITION DES
PERSONNE INTERESSEES.

THE AUTHOR RETAINS OWNERSHIP
OF THE COPYRIGHT IN HIS/HER
THESIS. NEITHER THE THESIS NOR
SUBSTANTIAL EXTRACTS FROM IT
MAY BE PRINTED OR OTHERWISE
REPRODUCED WITHOUT HIS/HER
PERMISSION.

L'AUTEUR CONSERVE LA PROPRIETE
DU DROIT D'AUTEUR QUI PROTEGE
SA THESE. NI LA THESE NI DES
EXTRAITS SUBSTANTIELS DE CELLE-
CI NE DOIVENT ETRE IMPRIMES OU
AUTREMENT REPRODUITS SANS SON
AUTORISATION.

ISBN 0-612-00137-7

Canada

To my parents,

Frank and Chiyeko

Abstract

The kinetics and mechanism of hydrolysis of both activated and unactivated phosphate diesters in the presence of aqueous solutions of Ce(III) salts are studied in detail. In the presence of 20 mM Ce(ClO₄)₃ (pH 8, 37° C) a DNA dinucleotide (dApdA) is converted to the nucleoside (dA) and inorganic phosphate with a half-life of approximately 100 minutes. This reaction is oxygen dependent and a mechanism involving the activation of oxygen by Ce(III) to give a Ce(IV) coordinated peroxide dianion as the active species is proposed.

The addition of 20 mM hydrogen peroxide to 2mM La(III) (pH 7.0, 25° C) results in a 34,000 fold increase in the rate of BNPP hydrolysis over that observed in the presence of 2mM La(III) alone and an overall 5×10^8 fold rate increase over the uncatalyzed rate. Incorporation of ¹⁸O from hydrogen peroxide into the inorganic phosphate product and evidence from the reaction kinetics and potentiometric titrations indicate that the mechanism involves nucleophilic attack of a La(III) coordinated peroxide dianion upon the substrate.

La(III) hydroxide clusters formed from the combination of La(III) (20 mM) and NaOH (40 mM) rapidly converts an RNA dinucleotide (ApA) to the monophosphates (2'-AMP and 3'-AMP) ($t_{1/2}$ =8 sec at pH 8.7, 20 °C). The presence of molecular oxygen does not improve the efficiency of Ce(III) in cleaving ApA; however, it does assist in the cleavage of the monophosphates which are not cleaved by Ce(III) in the absence of O₂ or La(III).

Résumé

Les analyses cinétiques et mécanistiques détaillées de l'hydrolyse des esters de phosphate activés et non activés sont rapportées. En présence de 20 mM $\text{Ce}(\text{ClO}_4)_3$ (pH 8, 37 °C), un dinucléotide de l'ADN (dApdA) est converti en nucléoside (dA) et en phosphate inorganique avec une demie-vie approximative de 100 minutes. La réaction nécessite la présence d'oxygène et on propose un mécanisme où l'activation de l'oxygène par le Ce(III) donne un dianion de peroxyde coordonné au Ce(IV) comme agent actif.

L'addition de 20 mM de peroxyde d'hydrogène à une solution de 2 mM de La(III) (pH 7.0, 25 °C) augmente le taux d'hydrolyse de BNPP 34 000 fois par rapport à la même réaction en absence de peroxyde d'hydrogène. Ceci représente une augmentation du taux de 5×10^8 fois par rapport à la réaction non catalysée. L'incorporation de ^{18}O de peroxyde d'hydrogène dans le produit (phosphate inorganique), les analyses cinétiques et les titrages potentiométrique indiquent que le mécanisme implique l'attaque nucléophile du dianion peroxyde (coordonné au La(III)) sur le substrat.

Les complexes formés par la combinaison du La(III) et de NaOH convertissent rapidement un dinucléotide d'ARN (ApA) en mono-phosphates correspondants (2'-AMP et 3'-AMP) ($t_{1/2}=8$ sec, pH 8.7, 20 °C). La présence d'oxygène moléculaire n'améliore pas l'efficacité du Ce(III) dans l'hydrolyse de l'ApA, mais il assiste le cleavage des monophosphates qui sont coupés par le Ce(III) en absence d'oxygène ou par le La(III).

Acknowledgements

I wish to gratefully acknowledge

my research supervisor, Prof. Jik Chin, for his advice, guidance and encouragement throughout my post-graduate studies at McGill.

I would like to thank the dedicated undergraduate students:

Erik Rubin, Wai-Lam Chan, Curtis Keith and Christophe Farès who were of invaluable assistance in performing experiments.

I would like to thank all of my colleagues in Room 230

Daphne Wahnou, Barry Linkletter, James Connolly, Dr. Jung Hee Kim, Dr. Vrej Jubian, Dr. Stephen Kawai, Mary Jane Young, Mark Wall, Jin Seog Seo, Philip Hurst, William Cheung and Dr. Nick Williams for their friendship, and for making it a joy to come into the lab.

I would like to thank:

Dr. Nick Williams for proofreading the manuscript and for his helpful comments and criticism,
Dr. Rosemary Hynes for the X-ray structural determinations,
Kosta Yannopoulos and Eric Marsault for translating the abstract,
Dr. Françoise Sauriol for her assistance in NMR experiments.

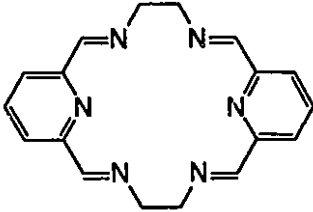
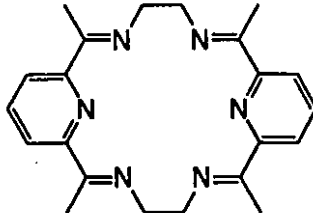
I would like to thank:

Jen and my friends at 4606 Hutchison and in the McGill Christian Fellowship for their love and support.

I would like to thank the Natural Sciences and Engineering Research Council of Canada (NSERC) for their financial support.

Glossary of symbols and abbreviations

A	adenosine
Å	angstrom
°C	degrees celsius
2',3'-cAMP	2',3'-cyclic adenosine monophosphate
2'-AMP	adenosine 2'-monophosphate
3',5'-cAMP	3',5'-cyclic adenosinemonophosphate
3'-AMP	adenosine 3'-monophosphate
3'-dAMP	2'-deoxyadenosine-3'-monophosphate
5'-dAMP	2'-deoxyadenosine-5'-monophosphate
Abs	absorbance
ApA	adenyl(3'-5')adenosine
BNPP	bis-(p-nitrophenyl)phosphate
cyclen	1,4,7,10-tetraazacyclododecane
dA	2'-deoxyadenosine
dApdA	2'-deoxyadenyl(3'-5')-2'-deoxyadenosine
δ	chemical shift (nmr)
D	density
DMP	dimethylphosphate
DNA	deoxyribonucleic acid
DPP	diphenylphosphate
EDTA	ethylenediaminetetraacetic acid
eq.	equation

equiv.	equivalent(s)
<i>et al.</i>	and others
HEPES	[4-(2-hydroxyethyl)-1-piperazine ethanesulfonic acid]
HP	Hewlett Packard
HPLC	high pressure liquid chromatography
HPNPP	2-hydroxypropyl-p-nitrophenylphosphate
hr	hours(s)
k	rate constant
k_{obs}	observed pseudo first-order rate constant
K	equilibrium constant
L	liter
L_1	
L_2	
λ	wavelength
Ln	lanthanide
M	molar (moles/L)
MeOH	methanol
min	minute(s)
μL	microliter
mL	milliliter

mM	millimolar
MW	molecular weight
nmr	nuclear magnetic resonance
NPP	p-nitrophenylphosphate
PhOH	phenol
P _i	inorganic phosphate
PP	phenylphosphate
ppm	parts per million
prod.	product
r	correlation coefficient
RNA	ribonucleic acid
sec	second(s)
TMS	tetramethylsilane
TpT	thimidyl(3'-5')thymine
trpn	tris(3-aminopropyl)amine
UpU	uridyl(3'-5')uridine
UV-vis	ultraviolet-visible
V	volume
Z	charge

Table of Contents

Abstract	i
Résumé.....	ii
Acknowledgements	iii
Glossary of symbols and abbreviations	iv
1. Introduction	
1.1. Nucleic Acids	1
1.2. Artificial Restriction enzymes	2
1.3. Oxidative Cleavage and its Application	5
1.3.1. Phenanthroline•Copper	5
1.3.2. Fe•EDTA	6
1.3.3. Footprinting	7
1.3.4. Affinity Cleavage	7
1.3.4.1. Peptide Binding to the Minor Groove	8
1.3.4.2. Triple Helix Formation	9
1.4. Hydrolytic Cleavage of Phosphate Esters	10
1.4.1. Mechanism of Uncatalyzed Hydrolysis	10
1.4.2. Enzyme Catalyzed Hydrolytic Cleavage.....	12
1.4.2.1. RNase A	12
1.4.2.2. Ribozymes	14
1.4.3. Metal Ion Promoted Hydrolysis	16
1.5. Plan of Study	19
2. Lanthanide ions in the Cleavage of RNA and RNA Analogs	
2.1. Introduction and literature review	20
2.2. Results and Discussion	23
2.2.1. X-Ray crystallography	23
2.2.2. Lanthanide ion Concentration Dependence of the LnL1 and Ln(III) mediated cleavage of HPNPP	27
2.3. Conclusion.....	34
2.4. Experimental	36
2.4.1. Chemicals	36
2.4.2. Synthesis	36

2.4.2.1. complexes	36
2.4.2.2. HPNPP	37
2.4.3. X-ray crystallography	37
2.4.4. UV-vis kinetics.....	38
Appendix 2.1 Pseudo First-Order Rate Constants	39
Appendix 2.2 Derivation of Rate Equations	41
Appendix 2.3 X-Ray Crystal Data	43
Structure A - CeC ₂₀ H ₂₈ N ₈ O ₁₂ P	43
Structure B CeC ₂₀ H ₂₄ N ₈ O ₁₈ P . 1.5H ₂ O	48
3. Unusual Behavior in the Ce(III) mediated cleavage of BNPP	
3.1. Introduction	53
3.2. The effect of lanthanide ions on the hydrolysis of BNPP	54
3.3. The unusual case of Ce(III)	55
3.4. Hydroxide consumption in the formation of the active species.	59
3.5. Oxygen Dependence	61
3.6. Effect of pH and [Ce(III)] on the duration of the lag time.....	62
3.7. UV-vis observation of the active species.	64
3.8. Theoretical explanation of the induction period.	66
3.9. Conclusions	69
3.10. Experimental	77
3.10.1. Chemicals	77
3.10.2. UV-vis spectroscopy	77
3.10.3. pH-stat	77
3.10.4. Titrations	78
3.10.5. UV-vis observation of the active species.	78
Appendix 3.1 Derivation of (3.2)	79
4. Ce(III) + DNA analogs	
4.1. Introduction	81
4.2. Results and discussion	82
4.2.1. Dimethyl Phosphate (DMP)	82
4.2.2. Diphenyl Phosphate	84
4.2.3. dApdA cleavage by Ce(III)•O ₂	85
4.2.4. Linear Free Energy Relationship.....	86
4.2.5. Product analysis of dApdA cleavage	89
4.3. Conclusion.....	92
4.4. Experimental	93
4.4.1. Chemicals	93
4.4.2. DMP cleavage	93
4.4.3. Diphenyl phosphate cleavage	93
4.4.4. dApdA cleavage	94
5. Cooperativity between La(III) and Hydrogen Peroxide in Phosphate Diester Cleavage	

5.1. Introduction	95
5.2. Results and Discussion	98
5.2.1. Lanthanide Ions and Hydrogen Peroxide Cooperativity	98
5.2.2. Other Phosphate Diesters	99
5.2.3. pH Dependence	101
5.2.4. Concentration Dependence	104
5.2.5. Proposed Mechanism	105
5.2.6. Substrate Binding	108
5.3. Proposed Mechanism	112
5.4. Conclusion.....	116
5.5. Experimental	118
5.5.1. Chemicals	118
5.5.2. UV-vis kinetics.....	118
5.5.3. Cleavage of 2',3'-cAMP	118
5.5.4. ³¹ P nmr	119
5.5.5. Potentiometric Titrations	119
Appendix 5.1 Pseudo First-Order Rate Constants	120
6. The Effect of Lanthanide Ions on the Cleavage of RNA	
6.1. Introduction	122
6.2. Results and Discussion	124
6.2.1. Ce(III) promoted cleavage of ApA	124
6.2.2. La(III) promoted hydrolysis of ApA	128
6.2.2.1. pH dependence.....	130
6.2.2.2. La(III) Concentration Dependence	132
6.3. Conclusion.....	134
6.4. Experimental	135
6.4.1. ApA cleavage.....	135
6.4.2. pH rate profile	135
6.4.3. La(III) Concentration Dependence	136
6.4.4. Oxygen dependence of the Ce(III) reaction.....	136
6.4.5. Potentiometric Titration of La(III)/OH ⁻	136
Appendix 6.1 Derivations of Rate Expressions.....	137
Appendix 6.2 Pseudo First-Order Rate Constants	139
7. Recent Developments in the use of Lanthanide Ions in the Development of Artificial Nucleases	140
Contribution to Knowledge.....	147
References	149

1. Chapter 1. Introduction

1.1. Nucleic Acids

The nucleic acids, ribonucleic acid (RNA) and deoxyribonucleic acid (DNA), represent one of the most important classes of molecules found in all living organisms. The structure of these biopolymers seems to be perfectly designed for the fulfillment of their roles as the preservers and messengers of genetic information in the cell.

Both classes of nucleic acids are polymers of nucleoside units linked by a phosphate diester backbone. The nucleosides are composed of a purine or pyrimidine base attached to either a ribose (RNA) or a deoxyribose (DNA) sugar which is in turn linked to the phosphate ester backbone. The highly specific hydrogen bonding interactions between specific base pairs allows for the replication and transmission of the information stored in the sequence of bases of DNA needed for the synthesis of proteins.

The aspect of the structure of nucleic acids which is of particular interest in this study is the phosphate diester backbone which links the important sequence of nucleosides. In keeping with the role of DNA as the storehouse of the genetic code, the phosphate diester linkage of DNA is extremely stable. Its half-life at neutral pH and 25° C is estimated to be two hundred million years (Chin *et al.*, 1989). This enormous stability preserves the valuable information

from degradation but it also requires the development of enzymes capable of effecting a 10^{12} fold increase in the rate of cleavage.

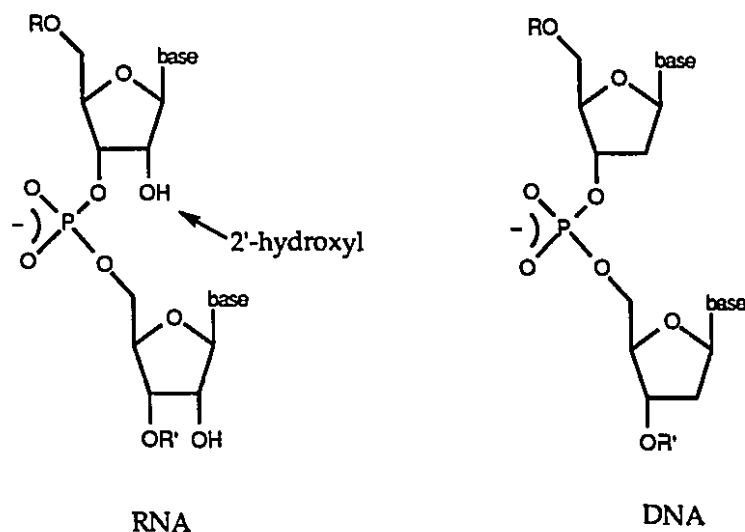


Figure 1.1 Basic structures of RNA and DNA illustrating the fundamental structural differences which account for their difference in reactivity.

The more disposable and ubiquitous RNA which plays several roles in the transmission of information from DNA to the synthesis of polypeptides differs from DNA primarily in the presence of the 2'-OH group on the ribose sugar. This hydroxyl group is well placed to act as an intramolecular nucleophile thus facilitating the hydrolysis of the phosphate diester which renders RNA inherently much less stable than DNA. Enzymes therefore only need to bring about a 10^9 fold increase in the rate of cleavage of RNA.

1.2. Artificial Restriction enzymes

Recent advances in genetic technology have created a strong demand for reagents capable of DNA recognition and site specific cleavage. The success of sequencing and gene location programmes such as the Human Genome Project

has resulted in a great deal of interest in gene manipulation techniques. These techniques may make it possible to treat diseases caused by genetic anomalies by replacing defective genes with the normal gene. This may lead to cure of diseases such as cystic fibrosis.

Furthermore, researchers are currently blocking the expression of certain genes by selectively binding the messenger RNA (mRNA) of the gene using anti-sense oligonucleotides. These anti-sense strands represent the complementary sequence of the sense mRNA and therefore bind to the target mRNA by duplex formation. This strategy has already been used to prevent the expression of certain genes in many different organisms and could be used to prevent the replication of viruses by arresting the vital process of gene transcription and expression (Weintraub, 1990). This technique is being improved upon by designing alternative linkages to replace the phosphate backbone which are resistant to degradation by cellular nucleases and which are more effective at penetrating the cell membrane (Uhlmann & Peyman, 1990). Its effectiveness could also be markedly improved if the target RNA could be destroyed by an appropriate cleaving group attached to the anti-sense strand.

Restriction enzymes play a key role in the enormous and growing field of gene manipulation. They are used to cut large sections of the genome into manageable sized pieces which can be analyzed. They are used extensively in research devoted to locating certain genes on the chromosome. Restriction enzymes are also indispensable in various gene manipulation technologies which involve splicing certain sections of DNA into chromosomes or plasmids. These and many other uses of restriction enzymes currently employed by researchers could be expanded and refined with the development of artificial restriction enzymes.

Artificial restriction enzymes offer the possibility of being custom designed for particular applications. There are only a limited number of sequences which can be recognized by the natural enzymes. The custom designed reagent could be tailor-made to recognize any sequence whether it be only a few base pairs in length or a very specific target sequence of 10-12 base pairs. The synthetic reagents could also conceivably be much cheaper to manufacture and use than the natural enzymes which need to be isolated and purified. These and many other advantages of artificial restriction enzymes make their development a very exciting and tantalizing goal for researchers in a variety of fields. Although many of the exciting possibilities mentioned above have not yet been realized, there have been many significant advances made in both the development of sequence recognition technology and cleavage groups. The research described in this thesis is devoted primarily to the design and development of cleavage groups.

A number of different reagents have been developed in order to cleave DNA. They can be divided into two general classes of reagents; oxidative and hydrolytic. The vast majority of synthetic DNA cleavage reagents developed to date rely on an oxidative pathway while enzymes cleave DNA by a hydrolytic mechanism. The oxidative cleavage of DNA is facile and rapid; however, it destroys the sugar moiety of the nucleotide producing fragments which cannot be easily religated. Despite this drawback, oxidative cleavage groups have been used to great advantage in many innovative studies. Efforts to mimic the enzymatic hydrolytic cleavage of DNA with simple systems has proven to be very difficult. Although a great deal of progress has been made in this endeavor there are still no synthetic reagents capable of effecting rapid hydrolytic cleavage of DNA under physiological conditions.

1.3. Oxidative Cleavage and its Application

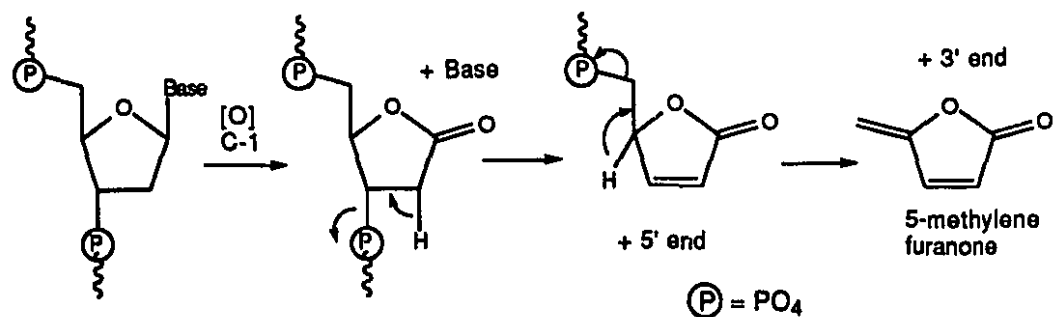
Many efficient systems which can cleave DNA oxidatively have been developed and exploited (for a recent review see Sigman *et al.*, 1993). Most of these systems involve the hydroxyl radical or some other free radical oxygen species. For the sake of brevity only two such systems will be examined here. The first is the 2:1 1,10 phenanthroline-cuprous complex $[(OP)_2Cu^+]$ and the other is based on Fenton chemistry using the $Fe^{\bullet}EDTA$ complex.

1.3.1. Phenanthroline•Copper

Fourteen years ago David Sigman and co-workers discovered that the 2:1 1,10-phenanthroline-cuprous complex $[(OP)_2Cu^+]$ and hydrogen peroxide could rapidly cleave DNA (Sigman *et al.*, 1979). They have since explored the mechanism of this reaction in some detail and have exploited its nucleolytic properties in a number of interesting studies (Sigman, 1986).

In order to gain insight into the mechanism of cleavage, Sigman and co-workers undertook a careful examination of the scission products and reactive intermediates (Goyne & Sigman, 1987; Kuwabara *et al.*, 1986; Sigman *et al.*, 1979). The formation of 5'- and 3'-phosphomonoester termini, free bases and 5-methylene furanone suggest that the cleavage results from the abstraction of the C-1 hydrogen. (see scheme 1.1)

Scheme 1.1 Proposed mechanism for the scission of DNA by $(OP)_2Cu^+$



Further studies indicate that the active species generated from the combination of hydrogen peroxide and $(OP)_2Cu^+$ remains bound to the copper. They postulate that the active species is either a copper oxene or a copper coordinated hydroxyl radical. The reaction therefore requires that the copper be held in close proximity to the C-1 hydrogen of the deoxyribose. Modifications to the 1,10-phenanthroline ligand result in loss of reactivity and suggest that it is the interaction of the phenanthroline ligand with the minor groove of DNA which positions the active copper-hydroxyl species for attack on the sugar.

Sigman and his co-workers have used the Cu^+ complex with a single phenanthroline ($OP\bullet Cu^+$) in the development of artificial chemical nucleases capable of site specific cleavage of a target oligonucleotide. In order to do this, Chen & Sigman have attached the $OP\bullet Cu^+$ cleaving group to various ligands capable of binding to specific oligonucleotide sequences. They have attached 1,10-phenanthroline to a 21-nucleotide-long deoxyoligonucleotide and demonstrated cleavage of both complementary DNA (Chen & Sigman, 1986) and RNA (Chen & Sigman, 1988) strands. They have also attached the $OP\bullet Cu^+$ unit to DNA binding proteins thus transforming the protein into a site specific nuclease (Chen & Sigman, 1987; Sigman *et al.*, 1993).

1.3.2. $Fe\bullet EDTA$

Redox active metals such as Fe and Cu can catalyze the reduction of hydrogen peroxide generating hydroxide ion and the hydroxyl radical. For the reaction to cycle, the metal must be reduced via a one-electron reduction. This can be accomplished using superoxide, ascorbic acid or other similar reducing agents. The overall reaction is known as Fenton Chemistry and has been used extensively to cleave DNA. The mechanism of cleavage is still not well

understood but it is widely believed that the diffusible and highly reactive hydroxyl radical is responsible for the cleavage (Sigman *et al.*, 1993). The reaction is likely to proceed via C-1 or 4-H hydrogen abstraction from the deoxyribose. (For a different proposed mechanism see Sawyer *et al.*, 1993)

Cleaving groups such as Fe•EDTA which cleave DNA through Fenton Chemistry can be used to explore the interactions between DNA-binding reagents and the target DNA in a number of ways, the two most general techniques are footprinting and affinity cleavage.

1.3.3. Footprinting

In footprinting experiments, the binding reagent is allowed to bind to the DNA which is then attacked by an indiscriminate cleaving group which cleaves the exposed parts of the DNA. This leaves a "footprint" of intact DNA where the binding interaction shielded the target DNA from attack by the cleaving group. This technique has been used by Tullius & Dombroski (1986) to explore the interaction of Cro proteins with DNA. Cech's group has used a similar technique to distinguish between the protected "inside" sections and the exposed "outside" portions of a ribozyme (Latham & Cech, 1989) as well as to help visualize the higher order folding of a ribozyme (Celander & Cech, 1991).

1.3.4. Affinity Cleavage

In affinity cleavage studies, the DNA cleaving element is covalently linked to the binding group. The interaction of the binding group with the target DNA brings the cleaving group into close proximity to a particular portion of the DNA. Analysis of the scission products reveal valuable information concerning the mode of binding and the affinity of the binding group for the target.

Peter Dervan and his co-workers have used the Fe•EDTA group in a series of elegant affinity cleavage studies to explore the interaction of two classes

of DNA binding reagents: peptides which bind to the minor groove (Dervan, 1986) and oligonucleotides which bind to the major groove.

1.3.4.1. Peptide Binding to the Minor Groove

The natural products netropsin and distamycin A are di- and tripeptides respectively (Figure 1.2) which bind to the minor groove of DNA at sites of 4 or 5 successive A,T base pairs. Dervan *et al.* have covalently linked the Fe•EDTA cleavage group to these peptides and have used affinity cleavage to explore the interaction of these peptides with DNA (Dervan, 1986; Mrksich & Dervan, 1993a; 1993b). They have also used this technique to evaluate modifications made to the peptides in order to recognize different sequences and to improve the affinity of the peptides for DNA (Wade *et al.*, 1992).

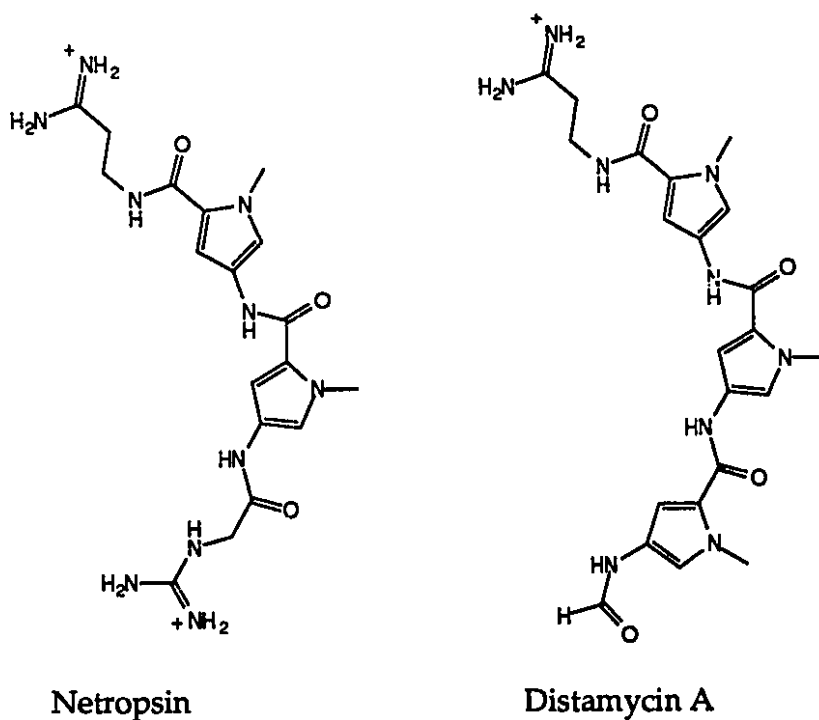


Figure 1.2 Structures of peptides which bind to the minor groove of DNA.

1.3.4.2. Triple Helix Formation

One of the most versatile ways of recognizing specific sequences of double stranded helical DNA is through the binding of an oligonucleotide in the major groove to form a triple helix. Pyrimidine oligonucleotides form Hoogsteen-type hydrogen bonds to the purine bases of the Watson-Crick duplex. Thymine binds specifically to the adenine-thymine (AT) base pair to form a T•AT triple while protonated cytosine (C⁺) binds specifically to guanine-cytosine (GC) base pairs to form a C⁺GC triplet. (Figure 1.3)

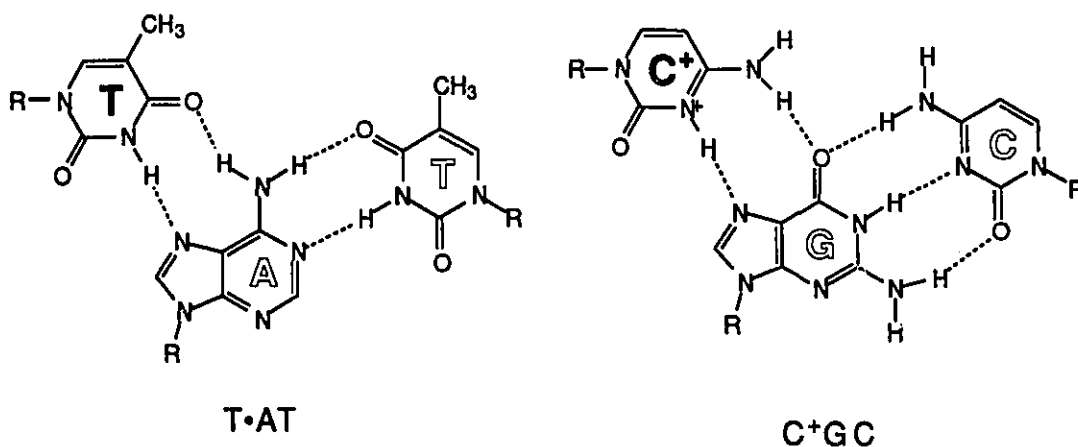


Figure 1.3 Structure of T•AT and C⁺GC base triplets illustrating both Watson-Crick and Hoogsteen type hydrogen bonding. The Watson-Crick base pairs are shown with outline type and the third strand is shown in shaded type.

Other natural base triplets have been identified (Griffin & Dervan, 1989) and non-natural bases are being designed in order to make possible the recognition of all four base pairs (Griffin *et al.*, 1992; Koh & Dervan, 1992). These advances promise to make triple helix formation a very versatile and powerful tool for chemists seeking to recognize specific sequences of DNA. This technique has already been combined with the Fe•EDTA cleaving group to form a reagent

capable of site specific cleavage of human chromosomal DNA (Strobel & Dervan, 1991).

1.4. Hydrolytic Cleavage of Phosphate Esters

1.4.1. Mechanism of Uncatalyzed Hydrolysis

The mechanism of hydrolysis of phosphate esters has been extensively studied (Cox & Ramsay, 1964; Thatcher & Kluger, 1989). Hydrolysis of phosphate esters has normally been viewed as occurring through one of two major mechanistic pathways: associative and dissociative. In the associative mechanism, the nucleophile attacks the phosphorus center to give a pentacoordinate intermediate which breaks down with loss of the leaving group to give the products. In the dissociative mechanism, unimolecular cleavage of the P-O bond leads to a metaphosphate intermediate to which the nucleophile is added to give products. A concerted mechanism constitutes the third possible pathway where attack of the nucleophile and loss of the leaving group occur without the formation of an intermediate.

A helpful way of viewing the possible mechanisms is shown in Figure 1.4. The reaction pathway begins in the bottom left corner and ends at the top right corner. The horizontal edges of the box represent the attack of the nucleophile and the vertical edges represent the loss of the leaving group (breaking of the P-Y bond). The stepwise mechanisms proceed along the edges and involve the intermediates drawn in the corners while the concerted pathways bypass the corners and the transition state may resemble either of the intermediates drawn in the corners.

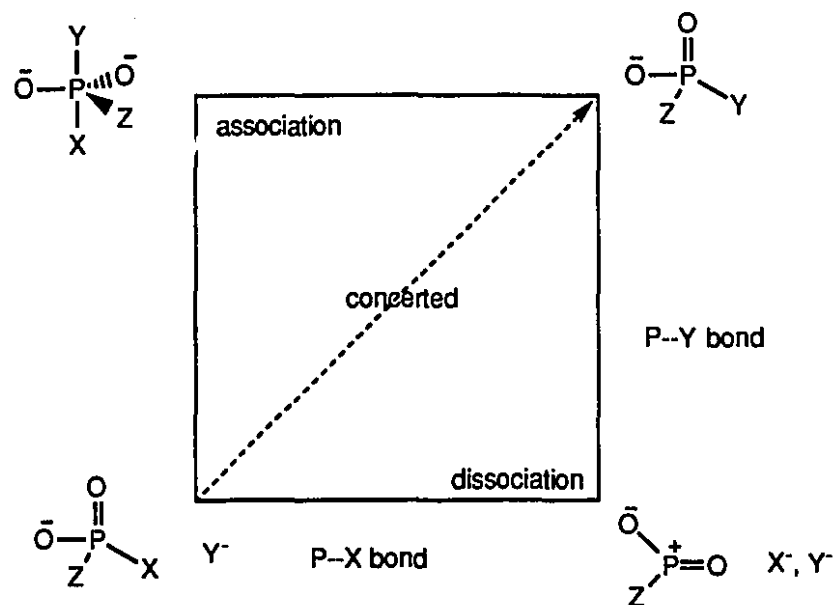


Figure 1.4 Three dimensional energy plot for nucleophilic substitution at phosphorus. The horizontal axis represents departure of the leaving group and the vertical axis represents attack of the nucleophile. (The free energy would normally be represented as coming out of the plane of the paper.)

The mechanism most commonly observed in the hydrolysis of phosphate diesters is the associative mechanism ($S_N2(P)$) while the dissociative mechanism is more commonly observed in the hydrolysis of phosphate monoesters. Since the primary focus of this thesis involves the hydrolysis of nucleic acids which are diesters this discussion will focus on the associative mechanism.

Attack of a nucleophile on the tetrahedral phosphorus center of phosphate esters leads to trigonalbipyramidal phosphorus (TBP) which may have a sufficient lifetime to be considered an intermediate. A number of rules concerning the positions of substituents on the TBP have been developed (Westheimer, 1968). Most significantly, it has been observed that the nucleophile always attacks from the apical position and by the principle of microscopic reversibility, the leaving group must also leave from the apical position.

Substituents on the TBP can rearrange through pseudorotation where two equatorial ligands are exchanged with the two apical ligands. In this way any TBP structure can rotate to three different possible isomers. If there is no pseudo-rotation of the TBP, then the attack of the nucleophile from one apical position and departure of the leaving group from the other leads to inversion of configuration at the phosphorus and is called an "in-line nucleophilic attack" ($S_N2(P)$).

1.4.2. Enzyme Catalyzed Hydrolytic Cleavage

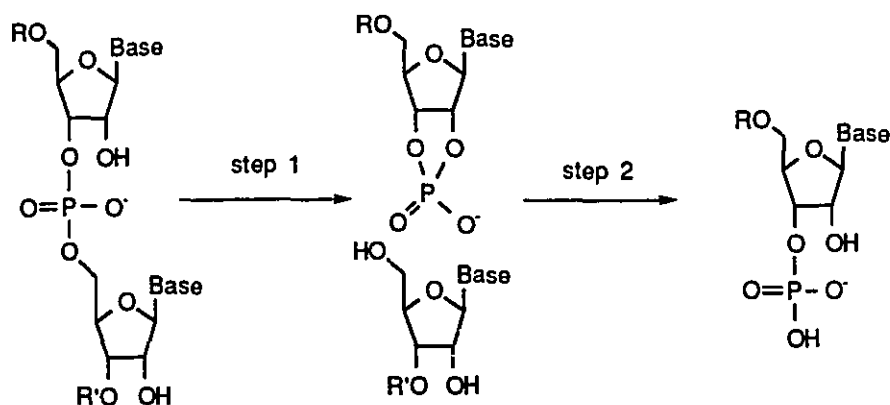
There are a wide variety of enzymes (nucleases) which catalyze the hydrolysis of nucleic acids. These enzymes employ a number of different strategies in enhancing the reactivity of the otherwise very stable phosphate diester linkage. In this section we will consider two very different types of nucleases as examples of the different strategies employed by nature in order to effect the rapid cleavage of nucleic acids.

1.4.2.1. RNase A

One of the most carefully and extensively studied nucleases is Bovine Pancreatic Ribonuclease A (RNase A). This enzyme which consists of a single polypeptide chain (124 amino acid residues) is easily purified and has therefore been extensively studied (Blackburn & Moore, 1982; Richards & Wyckoff, 1961). The mechanism is known to proceed through an isolable cyclic phosphate intermediate and therefore involves the two steps shown in Scheme 1.2.

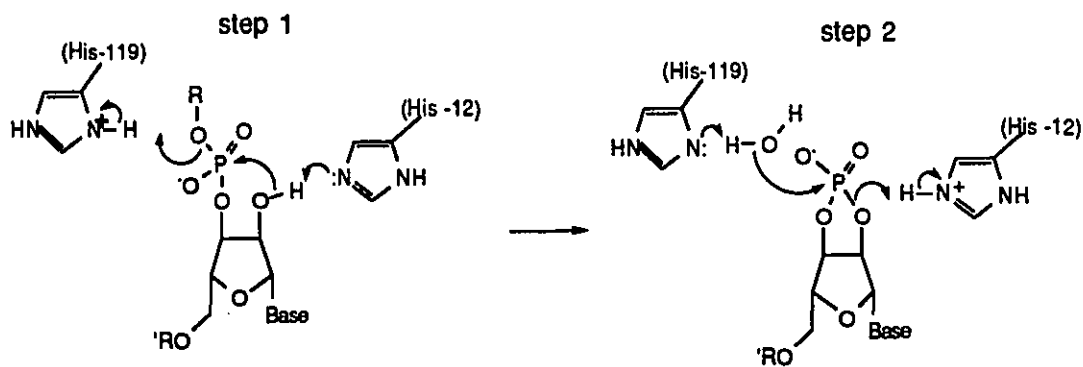
Chemical modification studies have implicated His-119 and His-12 as residues found in the active site which are necessary for catalytic activity (Weil & Seibles, 1967). The bell-shaped pH activity curve of the enzyme with a maximum near neutrality led to the proposal that the two essential histidine residues of RNase A acted as general acid and general base catalysts (Findlay *et al.*, 1961).

Scheme 1.2



According to the proposed mechanism (Findlay *et al.*, 1961) shown in Scheme 1.3 the unprotonated histidine acts as a general base in assisting the internal attack of the 2'-OH of the ribose on the phosphate while the protonated histidine acts as a general acid protonating the leaving group. Their roles are then reversed in the second step involving the breakdown of the cyclic intermediate.

Scheme 1.3



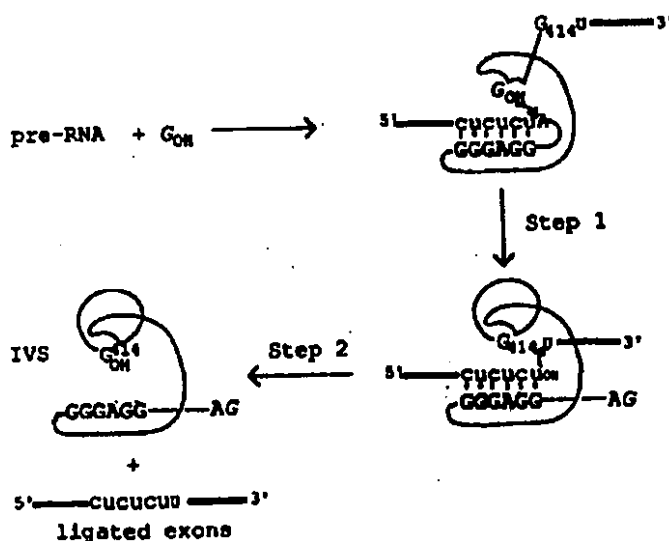
More recent crystallographic data have further supported the now generally accepted general acid/general base catalysis by His-119 and His-12 (Fersht, 1985). Ronald Breslow and his group have done a series of studies on the effects of imidazole buffers on the hydrolysis of RNA in attempt to better understand the fine details of the role of the histidine residues in RNase A

(Anslyn & Breslow, 1989; Breslow & Huang, 1990; Breslow *et al.*, 1989; Breslow & Labelle, 1986). Although some sloppiness in the presentation and analysis of this work has received sharp criticism (Haim, 1992; Menger, 1991; Menger & Haim, 1992), Breslow's work has still made a significant contribution to the understanding of the role of imidazole buffers in the catalysis of RNA hydrolysis (Breslow, 1993).

1.4.2.2. Ribozymes

The discovery that RNA could act as an enzyme revolutionized the understanding of chemistry in biological systems and revealed a whole new class of enzymes capable of cleaving and ligating RNA. The first catalytically active RNA molecule (ribozyme) discovered was the self-splicing intron of the large subunit ribosomal RNA of the *Tetrahymena thermophila*. (Cech *et al.*, 1981) This ribozyme catalyzes its own excision from the larger section of RNA according to Scheme 1.4

Scheme 1.4



Reproduced from *J. Bio. Chem.* © 1992 by The American Society for Biochemistry and Molecular Biology Inc..

In the first step a guanosine binds to the ribozyme and the 3'-hydroxyl group of the bound guanosine attacks the phosphate diester linkage at the 5' splice site. This transesterification results in the cleavage of the RNA and attachment of the guanosine to the 5'-end of the intron by a normal 3'-5'-phosphodiester linkage. In the second step the 3'-hydroxyl group of the 5'-exon attacks the phosphorus at the 3'-splice site. This transesterification results in the ligation of the two exons and excision of the intron (Cech, 1990; Cech *et al.*, 1992).

Shortened forms of this ribozyme have been used to catalyze the cleavage or ligation of external RNA (Zaug *et al.*, 1986; Zaug & Cech, 1986) and even DNA (Herschlag & Cech, 1990). Furthermore, because the sequence specificity of the cleavage and ligation reactions is based on base-pairing of the substrate to the internal guide sequence (IGS) of the ribozyme, variation of the IGS allows for control of the sequence specificity of the ribozyme (Zaug *et al.*, 1986).

The mechanism of the ribozyme catalyzed reaction has been studied in detail and has been reviewed (Cech *et al.*, 1992). One aspect of the mechanism which is of particular relevance to this work is the role of metal ions in the functioning of the ribozyme. All of the ribozymes discovered and studied to date are metalloenzymes (Pyle, 1993). Divalent cations are essential for the function of ribozymes for both structural and chemical reasons.

Using Fe•EDTA free radical chemistry (cf. sec. 1.3.2.2) Celander and Cech (1991) probed the effect of divalent metal ions on the tertiary structure of the *Tetrahymena* ribozyme. They found that the formation of the active tertiary structure required three Mg(II) ions. Replacement of Mg(II) with Ca(II) or Sr(II) produced the same folding structure as the active form of the ribozyme but showed no catalytic activity, thus indicating a special role for Mg(II).

The chemical role of the Mg(II) ion was established by an elegant study (Piccirilli *et al.*, 1993) where the 3' oxygen atom at the cleavage site of an RNA substrate was replaced by sulphur. This substitution resulted in a 1,000 fold decrease in the rate of cleavage by the ribozyme when only Mg(II) was present. Addition of Mn(II) or Zn(II) to the reaction restored the former reactivity of the ribozyme. This change in reactivity can be explained by the observation that Mg(II) does not coordinate well to sulphur while Mn(II) and Zn(II) do. These results indicate that the Mg(II) contributes to the ribozyme activity by coordinating to the 3' oxygen of the substrate thus stabilizing the developing negative charge on the leaving group (Figure. 1.5).

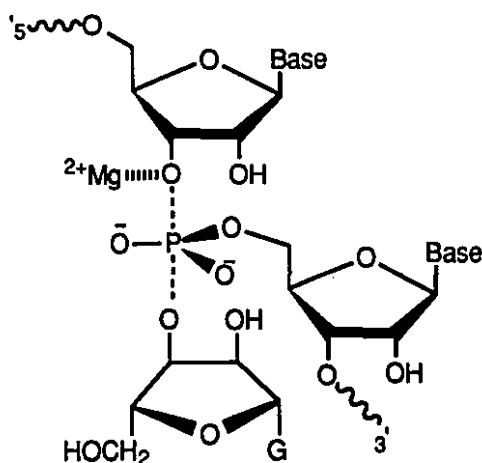


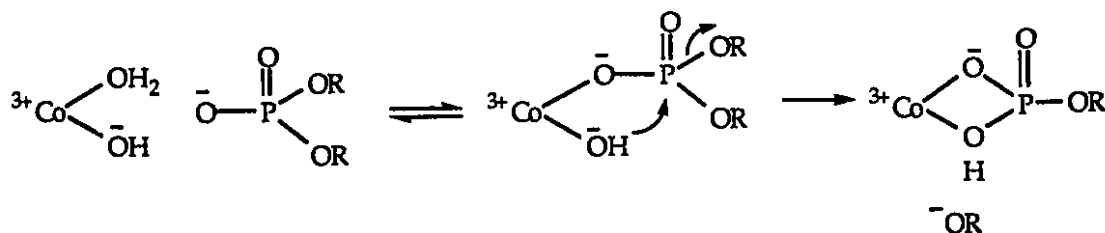
Figure 1.5 Postulated transition state for *Tetrahymena* ribozyme mediated cleavage of RNA substrate. The 3'-hydroxyl of the guanosine is shown attacking the phosphorous centre at the cleavage site of the substrate RNA in an in-line $S_N2(P)$ reaction. The Mg(II) ion is shown coordinated to the 3'-hydroxyl of the leaving group. The overall reaction results in scission of the substrate RNA strand and addition of guanosine to the 5' end of the 3' fragment.

1.4.3. Metal Ion Promoted Hydrolysis

The enormous stability of the phosphate diester backbone of DNA ($t_{1/2}$ =200 million years) (Chin *et al.*, 1989) makes it an unsuitable substrate for

catalysts which provide less than 10 orders of magnitude rate enhancement. For this reason, most metal ion catalysts have been tested on more reactive DNA analogs such as bis-(*p*-nitrophenyl)phosphate (BNPP) (cf. Scheme 3.1) Thus far, the most successful reagents developed for the hydrolytic cleavage of DNA analogs are *cis*-diaqua cobalt(III) complexes (Chin, 1991a,b). Upon binding to the [(trpn)Co(OH₂)(OH)]²⁺ complex, the phosphate diester BNPP is hydrolyzed 10⁸ times faster than when free in solution (Chin *et al.*, 1989). Similar rate enhancement is also observed with another *cis*-diaqua complex in the hydrolysis of the much less reactive phosphate diester, dimethyl phosphate (Kim & Chin, 1992).

Scheme 1.6



The *cis*-diaqua Co(III) complex brings about the impressive rate enhancement by combining Lewis Acid activation of the bound substrate with intramolecular nucleophilic attack by the adjacent metal bound hydroxide (scheme 1.6). This mechanism is supported by the pH dependence of the reaction which is consistent with aqua-hydroxy form of the Co(III) complex being the active form (Chin *et al.*, 1989) as well as the strong correlation between reactivity and the ability of the Co(III) complex to form four membered rings such as proposed in Scheme 1.6 (Chin *et al.*, 1988; 1989).

Another group of metal ions which has been used to cleave phosphate ester bonds is the lanthanide ions. Butcher and Westheimer (1955) showed that lanthanum hydroxide gels give modest rate enhancement in the hydrolysis of

phosphate monoesters. Lanthanide ions have also been shown to cleave tRNA (Eichhorn & Butzow, 1965) and lanthanide ion complexes have been used to cleave phosphate triesters (Hay & Govan, 1990). Even though the early work using lanthanide ions to hydrolyze phosphate esters was done in the fifties and sixties it is only in the past few years that the mechanism of their action has been studied in greater detail (see section 2.1). This renewed interest in the use of lanthanide ions in the design of reagents capable of phosphate ester cleavage may lead to the design of new catalysts capable of rapid hydrolytic cleavage of RNA and DNA.

1.5. Plan of Study

The principle goal of this research is to design a simple metal ion catalyst capable of effecting the rapid hydrolysis of the phosphate diester backbone of DNA. This represents a significant challenge since DNA is an extremely stable polymer. The half-life of the phosphate diester backbone of DNA at neutral pH and 25° C is estimated to be two hundred million years.(Chin *et al.*, 1989) Therefore in order to hydrolyze DNA under these conditions with a half-life of hours, a catalyst would need to increase the rate of hydrolysis by at least 10^{12} fold.

Cis-diaqua cobalt (III) complexes have been shown to give 10^{10} fold increase in the rate of hydrolysis of phosphate diesters through the combination of Lewis Acid and metal hydroxide activation (Chin, 1991b). In order to obtain the additional two orders of magnitude of rate enhancement required to hydrolyze DNA rapidly I chose to turn from transition metals to lanthanide ions. It has long been known that lanthanide ions catalyze the hydrolysis of phosphate monoesters (Butcher & Westheimer, 1955) and RNA (Eichhorn & Butzow, 1965). In order to better understand the role of lanthanide ions in the hydrolysis of RNA I investigated the mechanism of lanthanide ion promoted hydrolysis of RNA and RNA analogs through kinetic and crystallographic studies. I also explored ways of extending the range of substrates cleaved by lanthanide ions to include DNA analogs and DNA itself.

Chapter 2.

Lanthanide ions in the Cleavage of RNA and RNA Analogs

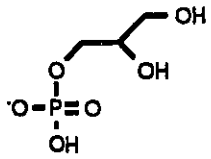
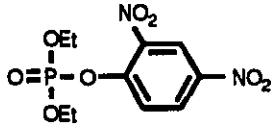
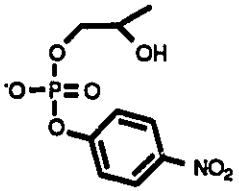
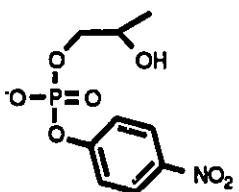
2.1. Introduction and literature review

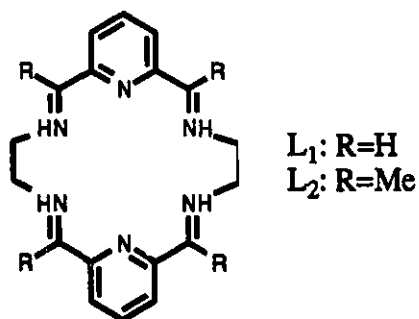
At the time of the initiation of this research on the effect of lanthanide(III) (Ln(III)) ions on the hydrolysis of phosphate diesters very little work on the topic had been reported in the literature. Lanthanide ions and lanthanide ion complexes had been shown to give modest rate enhancements in the hydrolysis of phosphate monoesters (Butcher & Westheimer, 1955) and triesters (Hay & Govan, 1990). Ln(III) salts had also been shown to cleave tRNA (Eichhorn & Butzow, 1965); however, little was known about the mechanism of this reaction. After beginning this research in 1990, three research groups (those of: R. Breslow at Columbia University, J. Morrow at SUNY at Buffalo and M. Komiyama at the University of Tokyo) published papers describing the effect of lanthanide ions and lanthanide ion complexes on the hydrolysis of RNA and RNA analogs (Table 2.1).

Four papers, which were all published within a year of each other, report similar findings. The lanthanide ions and their complexes yield considerable rate enhancements in the transesterification of phosphate diesters which incorporate a hydroxyl group well positioned for nucleophilic attack upon the phosphorous center of the phosphate. The most interesting results were those which

demonstrated the rapid cleavage of the phosphate diester linkage of actual RNA dinucleotides using lanthanide ions.

Table 2.1 Literature Review of Ln(III) ions in the Cleavage of Phosphate Esters

substrate	catalyst	rate enhancement	reference
	La(OH) ₃	> 10 ³	(Butcher & Westheimer, 1955)
	Ln(III)L ₁	10 ³	(Hay & Govan, 1990)
	Eu(III), Tb(III), Yb(III)	10 ³ - 10 ⁴	(Breslow & Huang, 1991)
	La(III), Nd(III), Eu(III), Gd(III), Tb(III), Lu(III)	10 ⁴	(Morrow <i>et al.</i> , 1992a)
ApUp	La(III)L ₂ , Eu(III)L ₂ , Gd(III)L ₂ , Tb(III)L ₂ , Lu(III)L ₂		(Morrow <i>et al.</i> , 1992b)
ApA	Tm(III)		(Komiyama <i>et al.</i> , 1992)



Morrow *et al.* (1992b) showed that 0.49 mM Ln(III)L₂ complex hydrolyzes the dinucleotide ApUp at 37° C, pH 7.15 with a half-life of approximately 4-5 hrs. Komiyama *et al.* (1992) showed that 10 mM of Tm(III) at 30° C, pH 8 hydrolyzes ApA with a half life of 10 minutes. They suggest that the rate acceleration is due to a metal hydroxide species which acts as a general base catalyst activating the 2'-hydroxyl group of the ribose group which then attacks the phosphate (Figure 2.1) (Komiyama *et al.*, 1992). However, they offer little evidence for this mechanism.

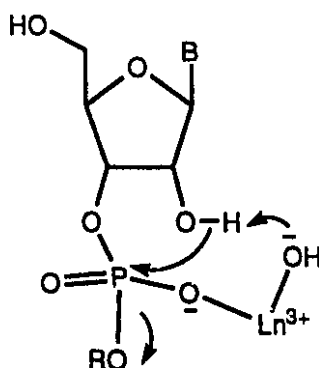


Figure 2.1 Structure of coordinated RNA showing Ln(III) bound hydroxide ion acting as a general base catalyst in the nucleophilic attack of the 2'-hydroxyl group upon the phosphorus center as proposed by Komiyama *et al.* (1992).

Despite the number of papers by different research groups presenting the same results very little was revealed about the mechanism of the impressive rate enhancements achieved using the lanthanide ions. What is clear from the published results is that the cleavage of ApA involves nucleophilic attack of the 2'-hydroxyl upon the phosphorous center of the phosphate (Komiyama *et al.*, 1992) and that the Ln(III) ion without a ligand is more effective than the Ln(III)L₂ complex (Komiyama *et al.*, 1992; Morrow *et al.*, 1992b). In order to better understand the mechanism of this reaction, the mode of binding of phosphate

esters to the lanthanide ion was studied through X-ray crystallography and by determining the lanthanide ion concentration dependence of the reaction.

2.2. Results and Discussion

2.2.1. X-Ray crystallography

In all of the reports of lanthanide ion complexes catalyzing the cleavage of phosphate esters it is suggested that the substrate is coordinated to the metal ion during the cleavage reaction; however, there have been no reports of spectroscopic or structural evidence of a phosphate ester coordinated to a lanthanide Schiff base complex. Several crystal structures have been reported for different lanthanide ions schiff base complexes with different counterions (Abid *et al.*, 1984; Arif *et al.*, 1987; Benetollo *et al.*, 1989; 1990; Bombieri *et al.*, 1986; 1991; Smith *et al.*, 1989); however, no structures have been reported showing binding of phosphate esters. I was able to grow two different X-ray quality crystals with dimethyl phosphate coordinated to the Ce(III)L₁ complex. The structures were solved by Dr. Rosemary C. Hynes. The crystallographic data for both crystals are given in Table 2.2. Tables of atomic parameters, bond lengths and angles are given in Appendix 2.3.

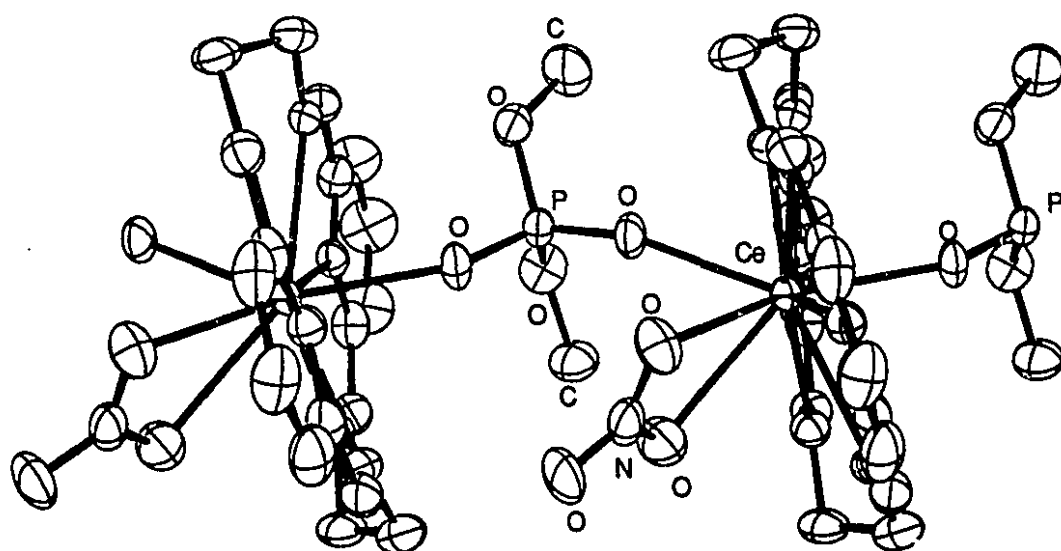


Figure 2.2 ORTEP diagram of crystal structure A ($\text{CeC}_{20}\text{H}_{28}\text{N}_8\text{O}_{12}\text{P}$) Ellipses are drawn at 50% probability.

Structure A - $\text{CeC}_{20}\text{H}_{28}\text{N}_8\text{O}_{12}\text{P}$

The crystal structure is composed of chains of CeL_1 units linked by bridging dimethyl phosphate ligands. Each unit also incorporates one chelated NO_3^- and one NO_3^- acting as a counter ion. Each dimethyl phosphate is coordinated to two Ce(III) ions through the phosphoryl oxygens. There are also two water molecules in the lattice hydrogen bonded to each other (Figure 2.2)

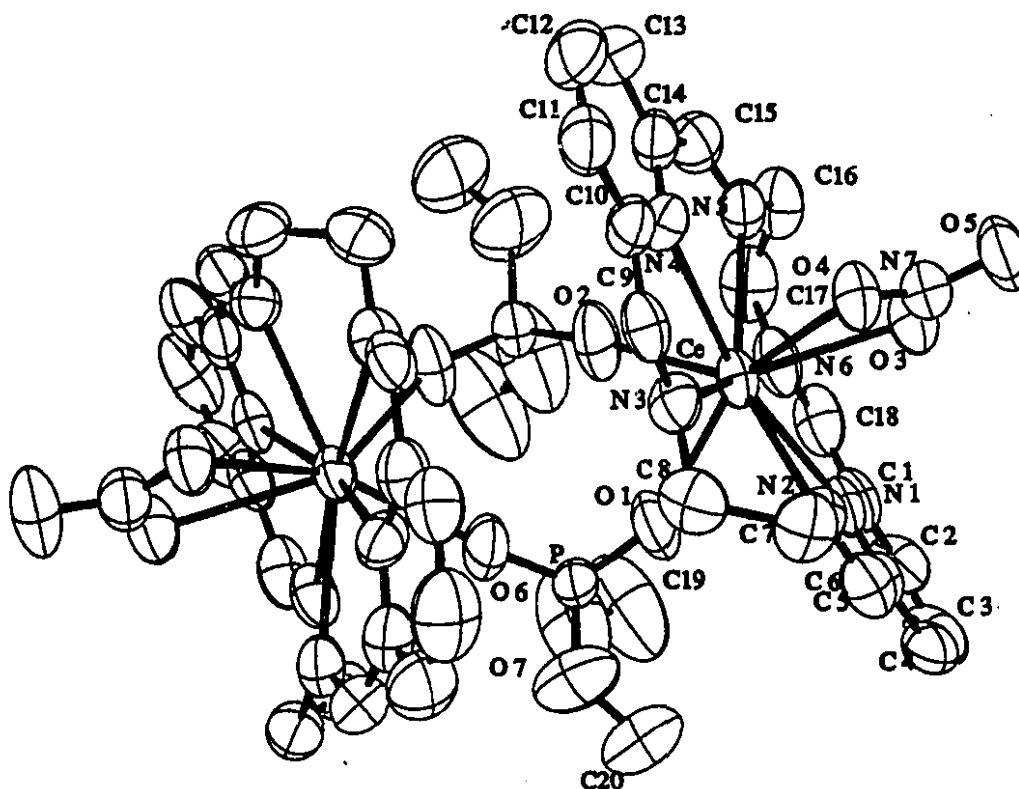


Figure 2.3 ORTEP diagram of crystal structure B ($\text{CeC}_{20}\text{H}_{24}\text{N}_8\text{O}_{10}\text{P} \cdot 1.5\text{H}_2\text{O}$). Ellipsoids are drawn at 50% probability.

Structure B - $\text{CeC}_{20}\text{H}_{24}\text{N}_8\text{O}_{10}\text{P} \cdot 1.5\text{H}_2\text{O}$

The structure consists of doubly bridged dimeric units of CeL_1 and dimethyl phosphate arranged about a 2-fold symmetry axis. The CeL_1 moieties are tilted towards each other opposite the methyl groups of the dimethyl phosphate bridges. Each CeL_1 moiety is coordinated to a chelated NO_3^- and is linked to another CeL_1 moiety through two bridging dimethyl phosphate groups. The lattice also incorporates two NO_3^- counter ions and three solvent water molecules per dimeric unit (Figure 2.3).

Table 2.2 Crystallographic data

Structure	A	B
Formula	CeC ₂₀ H ₂₈ N ₈ O ₁₂ P	CeC ₂₀ H ₂₄ N ₈ O ₁₀ P.1.5H ₂ O
MW (g/mole)	743.57	731.54
Crystal system	Monoclinic	Monoclinic
Space group	P 2 ₁ /c	C 2/c
a (Å)	19.061 (5)	13.531 (4)
b (Å)	7.1386 (16)	25.307 (5)
c (Å)	22.087 (5)	17.761 (4)
β (°)	111.858 (19)	93.988 (22)
V (Å ³)	2789.3 (12)	6067 (3)
Z	4	8
D _{calc} (g/cm ³)	1.771	1.602
Transmission coefficient	0.48-0.65	0.64-0.78
Crystal dimensions (mm)	0.45 x 0.33 x 0.25	0.20 x 0.20 x 0.20
Scan mode	θ/2θ	ω
Reflections measured	3617	4151
Unique reflections	3489	3955
Reflections with I>2.5σ(I)	3243	2546
No. of parameters	380	373
R _F ^a	0.028	0.050
R _w ^b	0.036	0.057
GOF ^c	2.33	1.90

$${}^a R_F = \sum (|F_0| - |F_C|) / \sum |F_0|;$$

$${}^b R_w = [\sum w(|F_0| - |F_C|)^2 / \sum w|F_0|^2]^{1/2};$$

$${}^c \text{GOF} = [\sum w(|F_0| - |F_C|)^2 / (\text{NO} - \text{NV})]^{1/2}$$

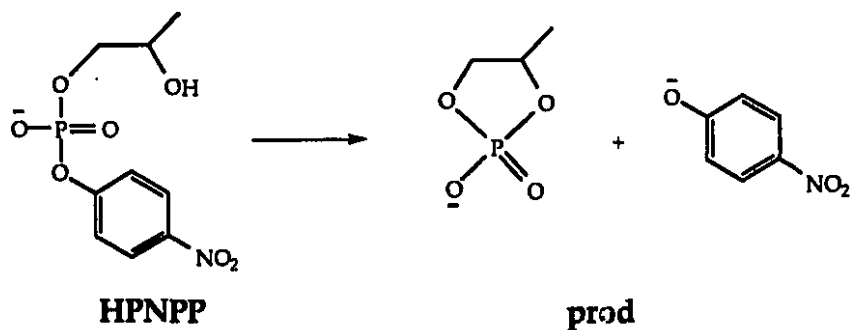
Two different crystal structures have been determined which incorporate a phosphate diester coordinated to a Ce(III) ion bound to a macrocyclic hexamine schiff base ligand (L₁). In both cases the phosphate diester was found to coordinate to two Ce(III) ions thus acting as a bridging ligand.

It is difficult to judge how much the crystal structure reveals about the solution behavior of the CeL_1 complex and its interaction with phosphate diesters. It is clear that the phosphate diester is capable of coordinating to the $Ce(III)$ center through a phosphoryl oxygen. The bridging structures obtained suggest that the CeL_1 complex might be providing double Lewis Acid activation of the bound substrate by forming a 2:1 metal to substrate complex. However, this is not supported by the concentration dependence of the reaction which is described in the next section.

2.2.2. Lanthanide ion Concentration Dependence of the LnL_1 and $Ln(III)$ mediated cleavage of HPNPP

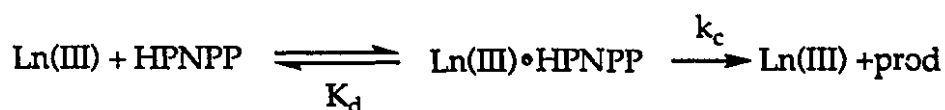
In order to gain a clearer understanding of the role of the lanthanide ion and the effect of the ligand on the metal ion reactivity, the pseudo first-order rate constant for the cleavage of the RNA analog, 2-hydroxypropyl-*p*-nitrophenyl phosphate (HPNPP) was determined as a function of lanthanide ion concentration. The structure of HPNPP combines the *p*-nitrophenoxide leaving group with a well positioned hydroxyl group which can imitate the role of the ribose 2'-hydroxyl group in the cleavage of RNA (Scheme 2.1).

Scheme 2.1

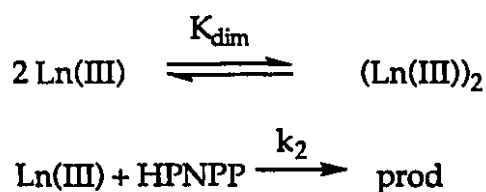


At low Ln(III) and Ln(III)L₁ concentrations the pseudo first-order rate constant increases linearly with increasing metal ion concentration and in all cases except those of LaL₁ and CeL₁ the kinetics begin to saturate at higher metal ion concentrations. Two possible mechanisms which are consistent with this type of behaviour are shown in Schemes 2.2 and 2.3.

Scheme 2.2



Scheme 2.3



In Scheme 2.2, pre-equilibrium binding of the substrate to the metal ion is followed by transesterification of the bound substrate. This is consistent with the observed saturation behavior because at high concentrations of lanthanide ion all of the substrate is bound and increasing the metal concentration cannot further increase the concentration of the coordinated substrate. In Scheme 2.3, the saturation behaviour is caused by the formation of an inactive dimeric lanthanide species ((Ln(III))₂) at high concentrations of lanthanide ion.

The lanthanide ion concentration dependence predicted by Scheme 2.2 can be expressed by (2.1) where k_{obs} is the observed pseudo-first order rate constant, [Ln(III)] is the total Ln(III) or LnL₁ concentration, K_d is the disassociation constant of the metal-bound substrate complex and k_c is the first-order rate constant for the reaction of the bound substrate (derivations in Appendix 2.2)

$$k_{\text{obs}} = k_c[\text{Ln(III)}]/([\text{Ln(III)}]+K_d) \quad (2.1)$$

The lanthanide ion concentration dependence of the observed first-order rate constant predicted by Scheme 2.3 can be expressed by (2.2) where k_2 is the second-order rate constant for reaction of Ln(III) with HPNPP, K_{dim} is the equilibrium constant for the dimerization of Ln(III) and $[\text{Ln(III)}]$ is the total Ln(III) concentration (derivations in Appendix 2.2)

$$k_{\text{obs}} = k_2 \left(\frac{-1 + \sqrt{1 + 8K_{\text{dim}}[\text{Ln(III)}]}}{4K_{\text{dim}}} \right) \quad (2.2)$$

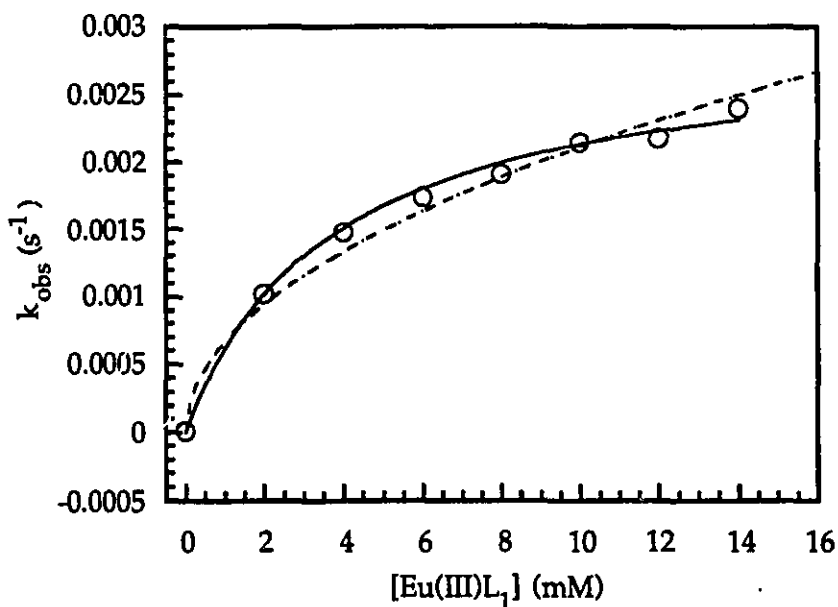


Figure 2.4 $[\text{Eu(III)L}_1]$ dependence of the pseudo first-order rate constant for the Eu(III)L_1 mediated hydrolysis of HPNPP (5×10^{-5} M) at 50 °C, pH 7.0 (0.10 M HEPES). The solid line represents the calculated curve derived from (2.1) where $k_c = 0.0029 \pm 0.0001 \text{ s}^{-1}$ and $K_d = 3.78 \pm 0.2 \text{ mM}$; the dashed line represents the calculated curve derived from (2.2) where $k_2 = 0.086 \pm 5 \text{ s}^{-1}$ and $K_{\text{dim}} = 8.2 \pm 900 \times 10^3 \text{ mM}^{-1}$.

Although both Schemes predict saturation behaviour in the concentration dependence of the observed rate they are kinetically distinguishable. The rate equation (2.1) derived from Scheme 2.2 predicts a zero-order dependence of k_{obs} on $[Ln(III)]$ at high $[Ln(III)]$ while that (2.2) derived from Scheme 2.3 predicts a half-order dependence on $[Ln(III)]$ at high concentrations of $Ln(III)$. When the two Schemes are compared, it is the equation (2.1) derived from Scheme 2.2 which provides the better fit to the data (Figure 2.4). In fact, the non-linear least squares algorithm used to fit the equation to the data yielded values for the parameters k_2 and K_{dim} with errors which far exceed the magnitude of the parameters themselves (see caption to Figure 2.4). Although only one example is shown in Figure 2.4, in all cases, equation (2.1) yielded the fit with the higher correlation coefficient.

The superior fit to the data using (2.1) suggests that the reaction involves pre-equilibrium binding of the substrate to the lanthanide ion as depicted in Scheme 2.1. This observation is consistent with that observed previously by Morrow *et al.* (1992).

Figures 2.5 and 2.6 show the $Ln(III)L_1$ and $Ln(III)$ concentration dependence of the observed first-order rate constant for the transesterification of HPNPP. The calculated curves are all derived from (2.1). The constants calculated from the curve fits are shown in tables 2.3 & 2.4 where k_2 is the apparent second-order rate constant for the reaction of $Ln(III)$ or LnL_1 with HPNPP. For LaL_1 and CeL_1 which do not display saturation behavior under the conditions studied, k_2 is calculated from the slope of the k_{obs} vs $[LnL_1]$ plots. In all other cases $k_2 = k_c / K_d$.

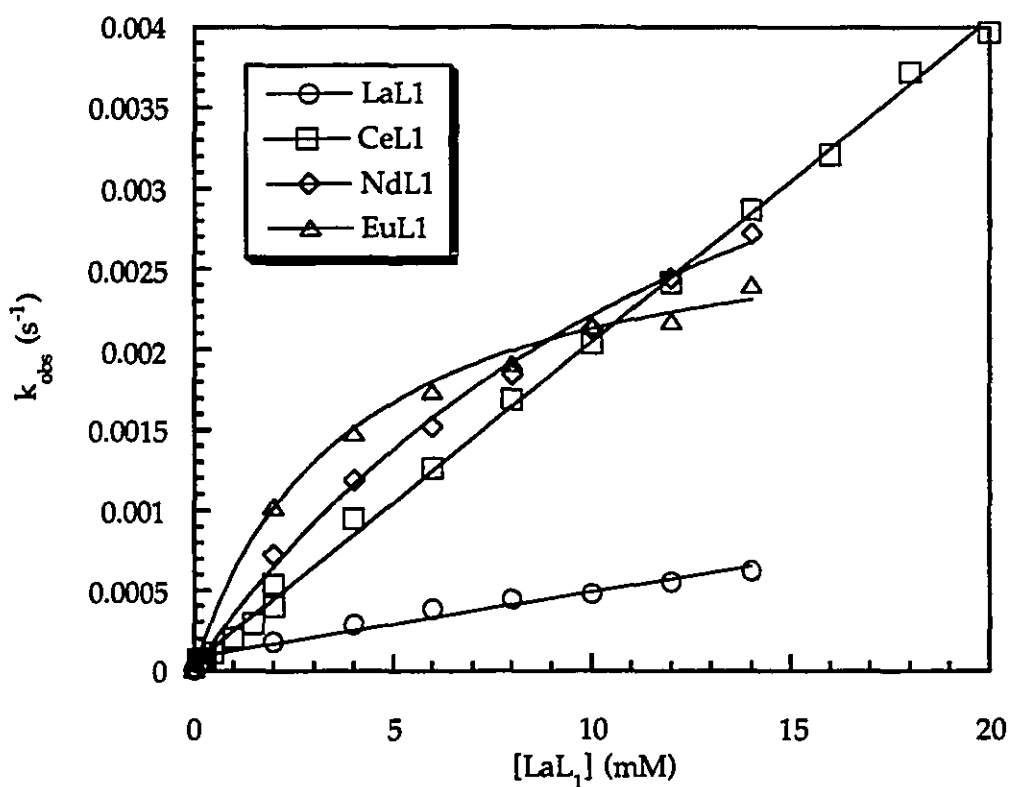


Figure 2.5 $[\text{LnL}_1]$ dependence of the first-order rate constant for the LnL_1 mediated hydrolysis of HPNPP. Reactions performed at 50° C, pH 7.0 in 0.10 M HEPES buffer. The calculated curves for NdL_1 and EuL_1 are derived from the non-linear least squares fit of (2.1) to the data.

Table 2.3 Kinetic constants calculated from the $[\text{LnL}_1]$ dependence of the first-order rate constant for the hydrolysis of HPNPP.

complex	K_d (mM)	k_c (s ⁻¹)	k_2 (M ⁻¹ s ⁻¹)
LaL_1			0.040 ± 0.004
CeL_1			0.20 ± 0.002
NdL_1	15.2 ± 1	$5.60 \pm 0.5 \times 10^{-3}$	0.35 ± 0.7
EuL_1	3.78 ± 0.2	$2.93 \pm 0.1 \times 10^{-3}$	0.72 ± 0.7

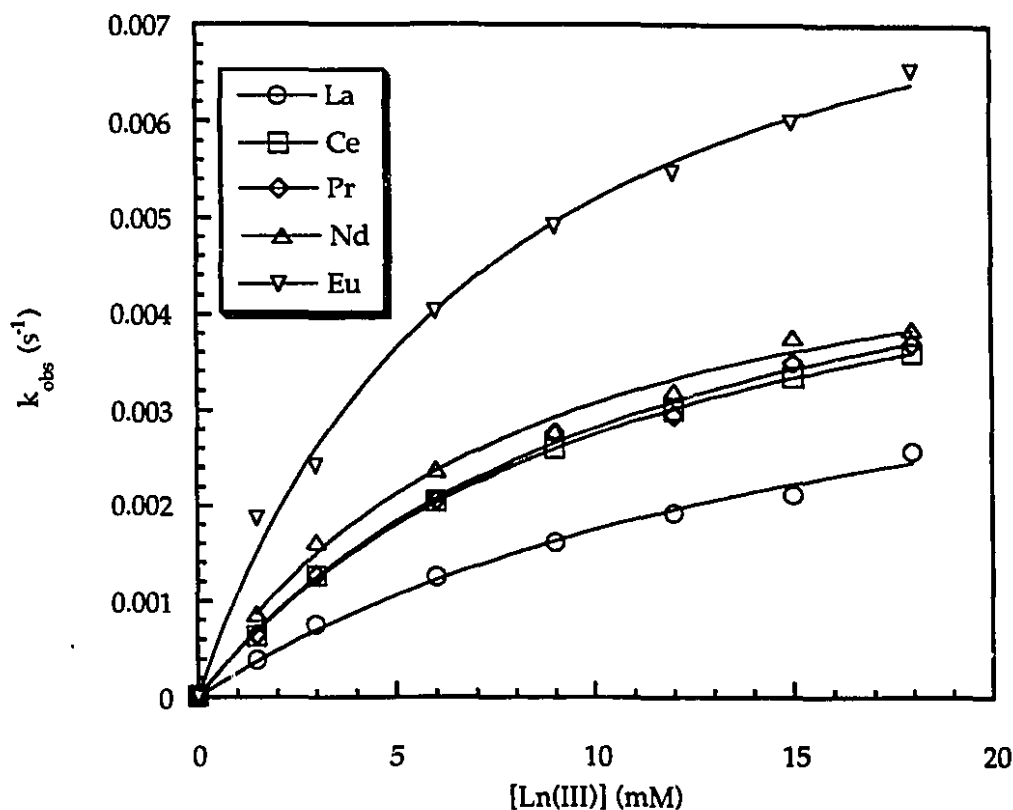


Figure 2.6 [Ln(III)] dependence of the first-order rate constant for the Ln(III) mediated hydrolysis of HPNPP. Reactions were monitored at 50° C at pH 7.0 in 0.10 M HEPES buffer. Curves are based on the non-linear least squares fit of (2.1) to the data.

Table 2.4 Kinetic constants calculated from the [Ln(III)] dependence of the first-order rate constant for the hydrolysis of HPNPP.

lanthanide(III)	K_m (mM)	k_c (s^{-1})	k_2 ($M^{-1} s^{-1}$)
La(III)	18.5 ± 2	$4.98 \pm 0.5 \times 10^{-3}$	0.27 ± 0.05
Ce(III)	11.3 ± 0.2	$5.87 \pm 0.1 \times 10^{-3}$	0.52 ± 0.02
Pr(III)	11.8 ± 0.6	$6.13 \pm 0.3 \times 10^{-3}$	0.52 ± 0.05
Nd(III)	8.21 ± 0.5	$5.59 \pm 0.3 \times 10^{-3}$	0.68 ± 0.07
Eu(III)	7.45 ± 0.4	$9.04 \pm 0.4 \times 10^{-3}$	1.21 ± 0.1

With both, the lanthanide ions salts (Ln(III)) and the schiff base complexes (LnL₁), the apparent second-order rate constant increases through the lanthanide series from La(III) to Eu(III). This is most likely due to the decrease in atomic radius as one moves from left to right across the series of lanthanides. This decrease in atomic radius most likely results in an increase in Lewis Acidity and therefore slightly better rate enhancements. This trend is consistent with that observed previously (Morrow *et al.*, 1992a).

A more careful analysis of the kinetic data reveals that the LnL₁ complexes behave quite differently than the Ln(III) salts. In the case of the uncomplexed lanthanide ions there is only a small variation in the values of K_d and k_c with the different metal ions. However, in the case of the schiff base complexes (LnL₁) there is a considerable variation in the K_d values. The binding of the substrate to the metal ion is so weak in the cases of LaL₁ and CeL₁ that the data shows no sign of saturating even at concentrations of lanthanide ion complex as high as 20 mM. The binding grows stronger with the smaller lanthanide ions but this is accompanied by a drop in the value of k_c.

The more pronounced effects of changing atomic radius on the ability to bind the phosphate ester substrates to the schiff base complexes is most likely due to the pronounced effect of atomic radius on the conformation of the ligand. Crystal structures of the schiff base ligands L₁ and L₂ complexed to various lanthanide ions have been reported in the literature. These structures reveal that small differences in the atomic radius can result in substantial changes in the conformation of the ligand (Bunzli & Wiessner, 1984). The interactions of the sterically bulky ligand most likely inhibits the binding of the substrate to the larger lanthanide ions.

2.3. Conclusion

What is the role of the lanthanide ion in the cleavage of RNA and RNA analogues? It seems clear from the saturation kinetics observed with increasing concentration of lanthanide ion in the cleavage of HPNPP that the substrate is activated through complexation with the metal ion. The X-ray crystal structure suggests that the phosphate diester binds through the phosphoryl oxygen. This all suggests that, like transition metal catalysts, the lanthanide ion accelerates the rate of cleavage of a phosphate diester through Lewis Acid activation of the bound substrate. However, unlike *cis*-diaqua cobalt(III) complexes, it appears that the lanthanide ions do not possess a well positioned metal-hydroxide to act as a nucleophile. This hypothesis is supported by the observation that Ln(III) ions are far more effective than Co(III) at hydrolyzing RNA where the 2'-hydroxyl acts as a nucleophile, while the *cis*-diaqua cobalt(III) complex is far more efficient than the Ln(III) ions at cleaving phosphate diesters which lack the intramolecular hydroxyl nucleophile (Figure 2.6).

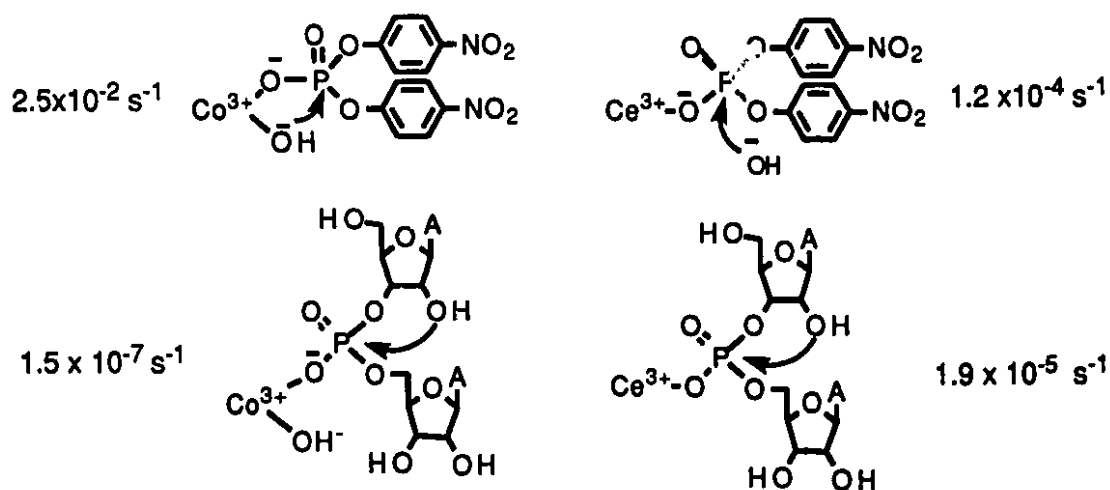


Figure 2.6 Comparison of the observed first-order rate constants for Co(cyclen)³⁺ (10 mM) and CeL₁(III) (10 mM) promoted hydrolysis of BNPP (10⁻⁴ M) and ApA (10⁻³ M) at pH 7.0 and 50 °C.

The lanthanide ions provide strong Lewis Acid activation of phosphate diesters through coordination of one or both of the phosphoryl oxygens. This strong Lewis Acid activation may be due to chelation of the phosphate diester to the lanthanide ions giving double Lewis Acid activation of the chelated substrate. Chelation of the phosphate diester to the metal ion is more likely to take place in the case of the lanthanide ions than with Co(III) complexes because the higher coordination numbers (10-12) possible with the lanthanide ions allows for smaller angles between ligands and favors the formation of the four membered rings formed upon chelation of a phosphate ester. This activation is sufficient to give rapid hydrolysis of RNA; however, it lacks the reactive metal bound hydroxide required to bring about rapid hydrolysis of DNA or DNA analogs. One approach to designing a catalyst capable of rapid cleavage of a DNA analog is to combine the strong Lewis Acidity of Ln(III) with a well positioned intramolecular nucleophile.

2.4. Experimental

2.4.1. Chemicals

All of the lanthanide(III) salts were purchased from Strem Chemicals Company. The HEPES was purchased from Aldrich Chemical Company.

2.4.2. Synthesis

2.4.2.1. complexes

$\text{LaL}_1(\text{NO}_3)_3$, $\text{CeL}_1(\text{NO}_3)_3$, $\text{NdL}_1(\text{NO}_3)_3$ and $\text{EuL}_1(\text{NO}_3)_3$ were synthesized by template synthesis according to the literature procedure (Arif *et al.*, 1987; Abid *et al.* 1984) and characterized by ^1H nmr (Table 2.4).

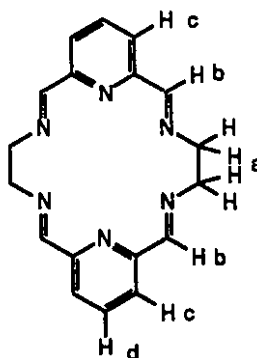


Table 2.4 ^1H nmr Characterization of $\text{LnL}_1(\text{NO}_3)_3$.

complex	a 8H s	b 4H s	c 4H d	d 2H t
$\text{LaL}_1(\text{NO}_3)_3$	4.15 ppm	8.85 ppm	8.09 ppm	8.41 ppm
$\text{CeL}_1(\text{NO}_3)_3$	6.49 ppm	15.17 ppm	10.15 ppm	10.08 ppm
$\text{NdL}_1(\text{NO}_3)_3$	12.03 ppm	27.65 ppm	13.06 ppm	11.73 ppm
$\text{EuL}_1(\text{NO}_3)_3$	-8.10 ppm	-22.59 ppm	1.61 ppm	4.43 ppm

2.4.2.2. HPNPP

HPNPP was synthesized according to the literature procedure (Brown & Usher, 1965).

2.4.3. X-ray crystallography

Slow evaporation of an aqueous solution of a 1:1 mixture of $\text{CeL}_1(\text{NO}_3)_3$ (546 mg, 1.0 mmole) and sodium dimethyl phosphate (148 mg, 1.0 mmole) initially yielded orange crystals ($\text{CeC}_{20}\text{H}_{24}\text{N}_8\text{O}_{10}\text{P} \cdot 1.5\text{H}_2\text{O}$). Upon further evaporation of the water, red crystals formed ($\text{CeC}_{20}\text{H}_{28}\text{N}_8\text{O}_{12}\text{P}$). Crystals suitable for X-ray diffraction study were obtained for both types of crystals. The crystal structure was solved by Dr. Rosemary C. Hynes.

Structure A - $\text{CeC}_{20}\text{H}_{28}\text{N}_8\text{O}_{12}\text{P}$

An orange crystal of dimensions 0.145 mm x 0.33 mm x 0.25 mm was obtained from the slow evaporation of water from an aqueous solution of $\text{CeL}_1(\text{NO}_3)_3$ and dimethyl phosphate. The intensity data were collected on a Rigaku diffractometer controlled by TEXRAY software using the ω scan mode. The space group was found to be monoclinic P 21/c with $a=19.061(5)$, $b=7.1386(16)$, $c=22.087(5)$, $\beta=111.858(19)^\circ$ and $V=2789.3(12) \text{ \AA}^3$. The last least squares cycle was calculated with 70 atoms, 380 parameters and 3242 out of 3489 reflections and was refined to $R_f=0.028$ and $R_w=0.036$. Merging R was 4.8% for 128 pairs of symmetry related reflections. The structure was solved by direct methods. Hydrogens were included in calculated positions. All non-hydrogen atoms were refined anisotropically.

Structure B - $\text{CeC}_{20}\text{H}_{24}\text{N}_8\text{O}_{10}\text{P} \cdot 1.5\text{H}_2\text{O}$

A red crystal of dimensions 0.20 mm x 0.20 mm x 0.20 mm was obtained from further evaporation of water from an aqueous solution of $\text{CeL}_1(\text{NO}_3)_3$ and dimethyl phosphate. The intensity data were collected on a Rigaku diffractometer controlled by TEXRAY software using the $\theta/2\theta$ scan mode. The space group was found to be monoclinic, C 2/c with $a=13.531(4)$, $b=25.307(5)$, $c=17.761(4)$, $\beta=93.988(22)^\circ$ and $V=6067(3) \text{ \AA}^3$. The last least squares cycle was calculated with 67 atoms, 373 parameters and 2546 out of 3955 reflections and was refined to $R_f=0.050$ and $R_w=0.055$. The merging R for 196 pairs of symmetry-related reflections was 2.3%. The structure was solved by direct methods followed by a difference Fourier. Hydrogen atoms were included in calculated positions. The structure was refined to convergence by full-matrix least-squares. All non-hydrogens were refined anisotropically except the solvent water oxygens, which were assigned occupancies of 0.5 and refined isotropically.

2.1.4. UV-vis kinetics

The cleavage of HPNPP was followed by monitoring the increase in absorbance at 400 nm due to the appearance of the *p*-nitrophenoxide ion. All absorbance measurements were made on a Hewlett Packard HP 8452 diode array UV-vis spectrophotometer equipped with a seven cell transport and jacketed cells attached to a circulating water bath for temperature control.

The data were acquired and saved using the Hewlett Packard software. All data analysis was done using software I developed using the Borland C++ programming environment. Rate constants were calculated by a non-linear least-squares fit of the first-order rate equation to the absorbance data. All reported rate constants are based on the analysis of 30-300 points representing at least 90% reaction.

Appendix 2.1 Pseudo First-Order Rate Constants

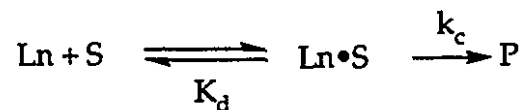
Table 2.1.1 Pseudo First-Order Rate Constants for the Ln(III)L₁ Promoted Cleavage of HPNPP (5 × 10⁻⁵ M) at pH 7.0 (0.1 M HEPES), 50 °C.

[Ln(III)L ₁] (mM)	k _{obs} × 10 ⁵ (s ⁻¹)			
	La(III)L ₁	Ce(III)L ₁	Nd(III)L ₁	Eu(III)L ₁
0	0.886	0.886	0.886	0.886
0.1		7.05		
0.2		6.66		
0.3		7.36		
0.5		10.8		
1.0		19.8		
1.5		28.8		
2.0	17.9	53.5	72.1	102
4.0	28.5	94.7	119	148
6.0	37.8	126	152	174
8.0	44.3	169	184	191
10.0	47.6	204	212	214
12.0	55.1	241	244	218
14.0	61.9	287	272	240
16.0		321		
18.0		372		
20.0		397		

Table 2.1.2 Pseudo First-Order Rate Constants for the Ln(III) Promoted Cleavage of HPNPP (5×10^{-5} M) at pH 7.0 (0.1 M HEPES), 50 °C.

[La(III)] (mM)	$k_{\text{obs}} \times 10^3$ (sec ⁻¹)				
	La(III)	Ce(III)	Pr(III)	Nd(III)	Eu(III)
1.5	0.385	0.635	0.647	0.866	1.86
3.0	0.752	1.26	1.27	1.62	2.42
6.0	1.25	2.04	2.05	2.38	4.03
9.0	1.61	2.60	2.76	2.79	4.91
12.0	1.92	3.00	2.95	3.20	5.47
15.0	2.12	3.35	3.50	3.77	6.00
18.0	2.57	3.60	3.70	3.86	6.54

Appendix 2.2 Derivation of Rate Equations



where Ln=Ln(III); S=HPNPP; Ln•S=Ln(III)•HPNPP; P=prod

$$K_d = \frac{[\text{Ln}][\text{S}]}{[\text{Ln} \cdot \text{S}]} \quad (2.2.1)$$

if $[\text{Ln}] \gg [\text{S}]$ then

$$[\text{S}]_T = [\text{S}] + [\text{Ln} \cdot \text{S}] \quad (2.2.2)$$

substitute (2.2.1) into (2.2.3)

$$K_d = \frac{[\text{Ln}]([\text{S}]_T - [\text{Ln} \cdot \text{S}])}{[\text{Ln} \cdot \text{S}]} \quad (2.2.3)$$

rearrange (2.2.3)

$$[\text{Ln} \cdot \text{S}] = \frac{[\text{Ln}][\text{S}]_T}{K_d + [\text{Ln}]} \quad (2.2.4)$$

rate equation

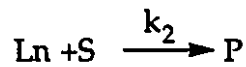
$$d[\text{P}]/dt = k_c[\text{Ln} \cdot \text{S}] \quad (2.2.5)$$

substitute (2.2.4) into (2.2.5)

$$\frac{d[\text{P}]}{dt} = \frac{-d[\text{S}]_T}{dT} = \frac{k_c[\text{Ln}][\text{S}]_T}{K_d + [\text{Ln}]} \quad (2.2.6)$$

integrate (2.2.6)

$$k_{\text{obs}} = \frac{k_c[\text{Ln}]}{K_d + [\text{Ln}]} \quad (2.2.7)$$



$$K_{\text{dim}} = \frac{[\text{Ln}_2]}{[\text{Ln}]^2} \quad (2.2.8)$$

$$[\text{Ln}]_{\text{T}} = [\text{Ln}] + 2[\text{Ln}_2] \quad (2.2.9)$$

substitute (2.2.8) into (2.2.9)

$$[\text{Ln}]_{\text{T}} = [\text{Ln}] + 2[\text{Ln}]^2 \quad (2.2.10)$$

use the quadratic formula to solve for $[\text{Ln}]$

$$[\text{Ln}] = \frac{-1 + \sqrt{1 + 8K_{\text{dim}}[\text{Ln}]_{\text{T}}}}{4K_{\text{dim}}} \quad (2.2.11)$$

the rate equation is

$$d[\text{P}]/dt = k_2[\text{S}][\text{Ln}] \quad (2.2.12)$$

substitute (2.2.11) in (2.2.12)

$$d[\text{P}]/dt = -d[\text{S}]/dt = k_2[\text{S}] \left(\frac{-1 + \sqrt{1 + 8K_{\text{dim}}[\text{Ln}]_{\text{T}}}}{4K_{\text{dim}}} \right) \quad (2.2.13)$$

integrate (2.2.13)

$$k_{\text{obs}} = \frac{k_2 \left(-1 + \sqrt{1 + 8K_{\text{dim}}[\text{Ln}]_{\text{T}}} \right)}{4K_{\text{dim}}} \quad (2.2.14)$$

Appendix 2.3 X-Ray Crystal Data

Crystal Structure A - $\text{CeC}_{20}\text{H}_{28}\text{N}_8\text{O}_{12}\text{P}$

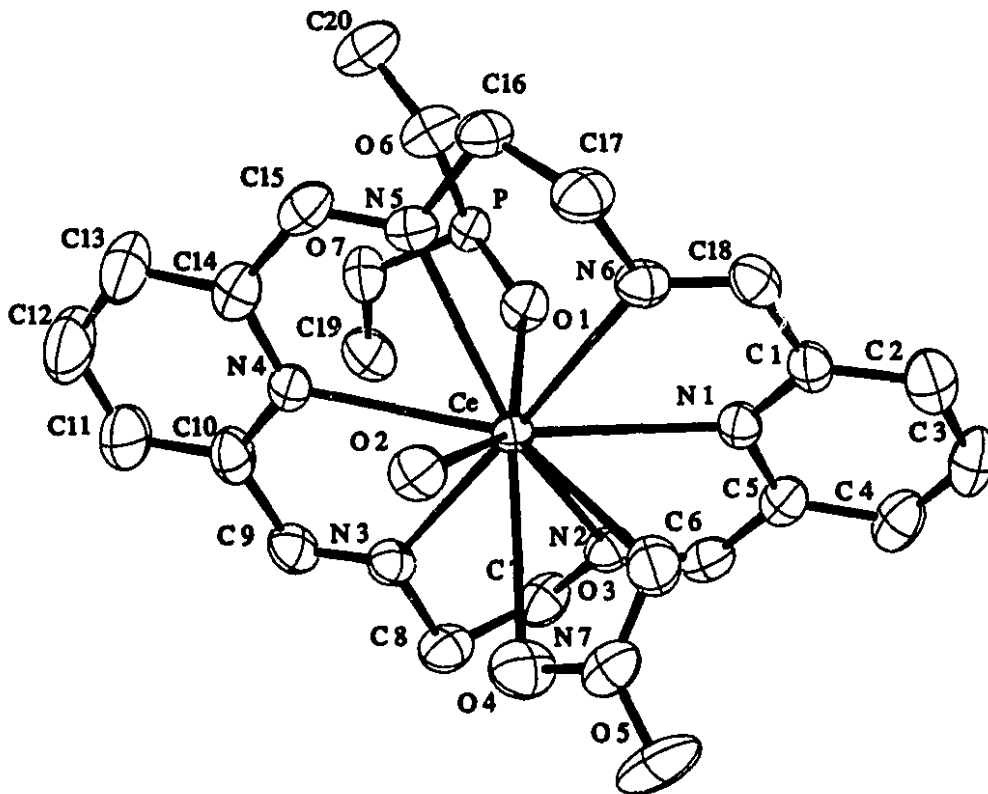


Figure 2.3.1 Labeled ORTEP diagram of structure A

Table 2.3.1 Atomic Parameters x, y, z, and Beq of Structure A (E. S. Ds. refer to the last digit printed).

	x	y	z	Beq
Ce	0.817655 (13)	0.28780 (3)	0.050700 (11)	1.818 (15)
P	0.74192 (7)	-0.20191 (16)	0.00436 (6)	2.17 (6)
O 1	0.79743 (16)	-0.0476 (4)	0.03119 (14)	2.76 (15)
O 2	0.77101 (17)	0.6033 (4)	0.01088 (14)	2.92 (15)
O 3	0.92966 (18)	0.5322 (5)	0.08469 (17)	3.67 (18)
O 4	0.87110 (20)	0.5403 (5)	0.15071 (16)	4.11 (18)
O 5	0.96961 (23)	0.7177 (5)	0.16754 (19)	5.22 (21)
O 6	0.69762 (18)	-0.1497 (5)	-0.06963 (15)	3.49 (17)
O 7	0.67669 (18)	-0.1922 (5)	0.03201 (16)	3.57 (17)
O 8	0.3727 (3)	0.2413 (7)	0.2843 (3)	7.2 (3)
O 9	0.2637 (3)	0.3605 (8)	0.2355 (3)	8.3 (3)
O10	0.2761 (3)	0.0654 (8)	0.24501 (24)	7.9 (3)
N 1	0.96228 (20)	0.1784 (5)	0.06928 (18)	2.34 (18)
N 2	0.90666 (20)	0.1257 (5)	0.16442 (16)	2.63 (18)
N 3	0.76358 (22)	0.2422 (5)	0.14771 (18)	2.59 (18)
N 4	0.66479 (20)	0.2626 (5)	0.02334 (18)	2.26 (19)
N 5	0.71646 (22)	0.2668 (5)	-0.07497 (18)	2.42 (20)
N 6	0.86877 (22)	0.3152 (5)	-0.04655 (17)	2.62 (19)
N 7	0.92412 (22)	0.6008 (6)	0.13498 (19)	3.09 (20)
N 8	0.3031 (3)	0.2240 (8)	0.25381 (23)	4.5 (3)
C 1	0.9914 (3)	0.2186 (6)	0.02405 (24)	2.60 (24)
C 2	1.0683 (3)	0.2080 (7)	0.0370 (3)	3.5 (3)
C 3	1.1169 (3)	0.1604 (7)	0.0987 (3)	3.7 (3)
C 4	1.0886 (3)	0.1269 (7)	0.1452 (3)	3.53 (24)
C 5	1.01046 (25)	0.1349 (7)	0.12936 (22)	2.69 (22)
C 6	0.9764 (3)	0.0983 (7)	0.17787 (21)	2.95 (24)
C 7	0.8749 (3)	0.0727 (8)	0.21298 (21)	3.49 (25)
C 8	0.8178 (3)	0.2186 (7)	0.21410 (22)	3.4 (3)
C 9	0.6945 (3)	0.2370 (7)	0.13835 (23)	3.04 (25)
C10	0.6377 (3)	0.2484 (7)	0.0718 (3)	3.2 (3)
C11	0.5608 (3)	0.2432 (9)	0.0599 (3)	4.7 (3)
C12	0.5104 (3)	0.2474 (10)	-0.0034 (4)	5.6 (4)
C13	0.5369 (3)	0.2574 (9)	-0.0538 (3)	4.7 (3)
C14	0.6144 (3)	0.2632 (7)	-0.03831 (24)	2.98 (24)
C15	0.6458 (3)	0.2654 (7)	-0.08945 (23)	2.92 (24)
C16	0.7446 (3)	0.2612 (7)	-0.12873 (22)	2.97 (23)
C17	0.8157 (3)	0.3778 (8)	-0.10961 (21)	3.38 (25)
C18	0.9369 (3)	0.2802 (6)	-0.03985 (23)	2.72 (23)
C19	0.6936 (3)	-0.2492 (8)	0.0988 (3)	4.2 (3)
C20	0.6339 (3)	-0.2496 (8)	-0.1113 (3)	4.6 (3)
OW1	0.5307 (3)	0.4409 (8)	0.2063 (3)	9.5 (4)
OW2	0.4419 (3)	0.5677 (8)	0.2731 (3)	10.4 (4)

Table 2.3.2 Bond distances in Å of structure A

Ce-O(1)	2.438(3)	N(2)-C(6)	1.265(6)
Ce-O(2)	2.461(3)	N(2)-C(7)	1.464(6)
Ce-O(3)	2.640(3)	N(3)-C(8)	1.455(6)
Ce-O(4)	2.737(3)	N(3)-C(9)	1.256(6)
Ce-N(1)	2.745(4)	N(4)-C(10)	1.354(6)
Ce-N(2)	2.711(4)	N(4)-C(14)	1.343(6)
Ce-N(3)	2.721(4)	N(5)-C(15)	1.263(6)
Ce-N(4)	2.753(4)	N(5)-C(16)	1.474(6)
Ce-N(5)	2.731(4)	N(6)-C(17)	1.454(6)
Ce-N(6)	2.676(4)	N(6)-C(18)	1.276(6)
P-O(1)	1.489(3)	C(1)-C(2)	1.386(7)
P-O(2) a	1.484(3)	C(1)-C(18)	1.474(7)
P-O(6)	1.580(3)	C(2)-C(3)	1.376(8)
P-O(7)	1.578(3)	C(3)-C(4)	1.346(8)
O(2)-Pb	1.484(3)	C(4)-C(5)	1.399(7)
O(3)-N(7)	1.254(6)	C(5)-C(6)	1.468(7)
O(4)-N(7)	1.261(6)	C(7)-C(8)	1.515(8)
O(5)-N(7)	1.225(5)	C(9)-C(10)	1.468(7)
O(6)-C(20)	1.414(6)	C(10)-C(11)	1.390(7)
O(7)-C(19)	1.446(6)	C(11)-C(12)	1.369(9)
O(8)-N(8)	1.249(7)	C(12)-C(13)	1.386(10)
O(9)-N(8)	1.205(7)	C(13)-C(14)	1.387(7)
O(10)-N(8)	1.228(8)	C(14)-C(15)	1.463(7)
N(1)-C(1)	1.342(6)	C(16)-C(17)	1.511(7)
N(1)-C(5)	1.339(6)		

Table 2.3.3 Bond Angles (°) of Structure A.

O(1)-Ce-O(2)	145.43(10)	Ce-O(4)-N(7)	95.7(3)
O(1)-Ce-O(3)	139.21(10)	P-O(6)-C(20)	123.6(3)
O(1)-Ce-O(4)	140.92(10)	P-O(7)-C(19)	118.3(3)
O(1)-Ce-N(1)	80.27(10)	Ce-N(1)-C(1)	119.9(3)
O(1)-Ce-N(2)	75.40(11)	Ce-N(1)-C(5)	119.6(3)
O(1)-Ce-N(3)	86.58(11)	C(1)-N(1)-C(5)	117.8(4)
O(1)-Ce-N(4)	79.18(10)	Ce-N(2)-C(6)	121.6(3)
O(1)-Ce-N(5)	76.17(10)	Ce-N(2)-C(7)	120.2(3)
O(1)-Ce-N(6)	90.61(11)	C(6)-N(2)-C(7)	118.2(4)
O(2)-Ce-O(3)	69.09(10)	Ce-N(3)-C(8)	118.2(3)
O(2)-Ce-O(4)	70.25(10)	Ce-N(3)-C(9)	123.8(3)
O(2)-Ce-N(1)	121.53(11)	C(8)-N(3)-C(9)	118.0(4)
O(2)-Ce-N(2)	137.72(11)	Ce-N(4)-C(10)	121.0(3)
O(2)-Ce-N(3)	101.45(11)	Ce-N(4)-C(14)	121.5(3)
O(2)-Ce-N(4)	76.66(10)	C(10)-N(4)-C(14)	117.5(4)
O(2)-Ce-N(5)	70.28(10)	Ce-N(5)-C(15)	122.7(3)
O(2)-Ce-N(6)	80.64(11)	Ce-N(5)-C(16)	119.3(3)
O(3)-Ce-O(4)	46.91(11)	C(15)-N(5)-C(16)	117.9(4)
O(3)-Ce-N(1)	58.98(11)	Ce-N(6)-C(17)	117.4(3)
O(3)-Ce-N(2)	81.82(11)	Ce-N(6)-C(18)	123.5(3)
O(3)-Ce-N(3)	111.00(11)	C(17)-N(6)-C(18)	119.1(4)
O(3)-Ce-N(4)	141.57(10)	O(3)-N(7)-O(4)	116.8(4)
O(3)-Ce-N(5)	121.03(11)	O(3)-N(7)-O(5)	120.8(4)
O(3)-Ce-N(6)	71.48(11)	O(4)-N(7)-O(5)	122.4(5)
O(4)-Ce-N(1)	90.88(11)	O(8)-N(8)-O(9)	120.3(6)
O(4)-Ce-N(2)	67.47(11)	O(8)-N(8)-O(10)	118.3(5)
O(4)-Ce-N(3)	65.13(11)	O(9)-N(8)-O(10)	121.3(6)
O(4)-Ce-N(4)	105.41(11)	N(1)-C(1)-C(2)	122.2(5)
O(4)-Ce-N(5)	140.01(11)	N(1)-C(1)-C(18)	115.9(4)
O(4)-Ce-N(6)	117.55(11)	C(2)-C(1)-C(18)	121.8(5)
N(1)-Ce-N(2)	59.53(11)	C(1)-C(2)-C(3)	119.2(5)
N(1)-Ce-N(3)	120.13(11)	C(2)-C(3)-C(4)	119.1(5)
N(1)-Ce-N(4)	159.44(10)	C(3)-C(4)-C(5)	119.6(4)
N(1)-Ce-N(5)	115.23(11)	N(1)-C(5)-C(4)	122.0(4)
N(1)-Ce-N(6)	59.68(11)	N(1)-C(5)-C(6)	116.0(4)
N(2)-Ce-N(3)	60.62(11)	C(4)-C(5)-C(6)	122.0(4)
N(2)-Ce-N(4)	114.94(11)	N(2)-C(6)-C(5)	120.8(4)
N(2)-Ce-N(5)	151.58(11)	N(2)-C(7)-C(8)	109.3(4)
N(2)-Ce-N(6)	119.05(11)	N(3)-C(8)-C(7)	108.0(4)
N(3)-Ce-N(4)	58.98(11)	N(3)-C(9)-C(10)	120.0(4)
N(3)-Ce-N(5)	117.54(12)	N(4)-C(10)-C(9)	116.1(4)
N(3)-Ce-N(6)	177.16(11)	N(4)-C(10)-C(11)	122.6(5)
N(4)-Ce-N(5)	58.93(12)	C(9)-C(10)-C(11)	121.3(5)
N(4)-Ce-N(6)	120.04(11)	C(10)-C(11)-C(12)	118.8(5)
N(5)-Ce-N(6)	61.23(12)	C(11)-C(12)-C(13)	119.6(5)
O(1)-P-O(2)a	118.04(18)	C(12)-C(13)-C(14)	118.4(5)
O(1)-P-O(6)	105.30(18)	N(4)-C(14)-C(13)	123.0(5)
O(1)-P-O(7)	111.04(19)	N(4)-C(14)-C(15)	116.0(4)
O(2)a-P-O(6)	110.99(18)	C(13)-C(14)-C(15)	121.0(5)
O(2)a-P-O(7)	108.87(19)	N(5)-C(15)-C(14)	120.6(4)
O(6)-P-O(7)	101.26(19)	N(5)-C(16)-C(17)	108.5(4)
Ce-O(1)-P	147.05(18)	N(6)-C(17)-C(16)	109.3(4)
Ce-O(2)-Pb	164.71(19)	N(6)-C(18)-C(1)	119.6(4)
Ce-O(3)-N(7)	100.6(3)		

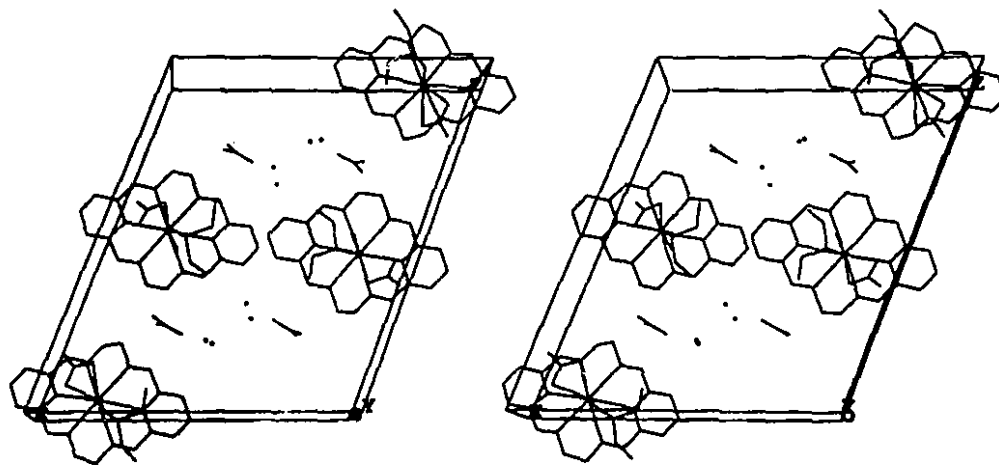


Figure 2.3.2 Packing diagram of structure A.

Structure B $\text{CeC}_{20}\text{H}_{24}\text{N}_8\text{O}_{18}\text{P} \cdot 1.5\text{H}_2\text{O}$

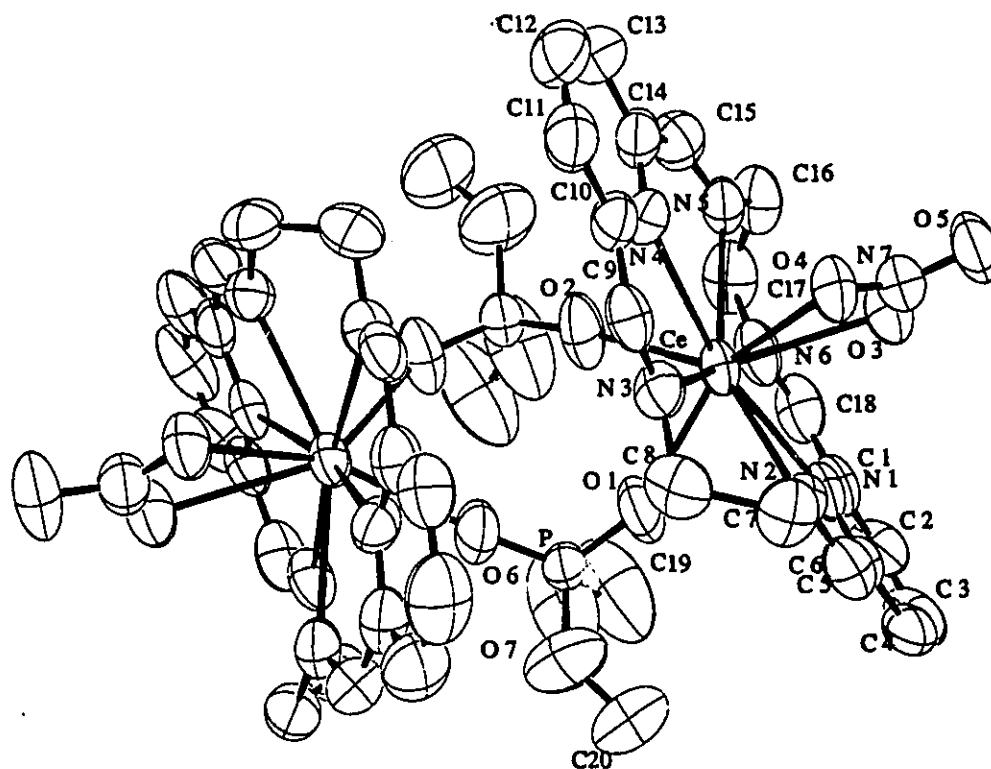


Figure 2.3.3 Labeled Ortep diagram of structure B.

Table 2.3.4 Atomic Parameters x, y, z and Beq of Structure B (E. S. Ds. refer to the last digit printed)

	x	y	z	Beq
Ce	0.21655 (5)	0.36858 (3)	0.78850 (4)	4.09 (3)
P	0.02642 (23)	0.41933 (13)	0.64003 (18)	4.48 (15)
O 1	0.1169 (6)	0.4021 (4)	0.6809 (5)	7.3 (5)
O 2	0.0663 (6)	0.3995 (4)	0.8378 (5)	7.3 (5)
O 3	0.4091 (6)	0.3645 (3)	0.8345 (4)	6.0 (5)
O 4	0.3405 (5)	0.2893 (3)	0.8129 (5)	5.4 (4)
O 5	0.4957 (6)	0.2940 (4)	0.8505 (5)	7.8 (5)
O 6	0.0155 (9)	0.4800 (4)	0.6319 (8)	13.1 (9)
O 7	0.0225 (10)	0.4028 (6)	0.5548 (6)	13.8 (10)
O 8	0.0639 (10)	0.1038 (4)	0.5577 (6)	11.4 (8)
O 9	0.2019 (10)	0.1356 (6)	0.5773 (7)	14.7 (10)
O10	0.1129 (10)	0.1232 (4)	0.6703 (5)	10.8 (8)
N 1	0.3257 (6)	0.4364 (4)	0.7110 (5)	4.8 (5)
N 2	0.2887 (7)	0.3379 (4)	0.6602 (5)	4.6 (5)
N 3	0.1488 (7)	0.2797 (3)	0.7235 (5)	4.5 (5)
N 4	0.1507 (7)	0.2906 (3)	0.8762 (5)	4.6 (5)
N 5	0.2383 (7)	0.3772 (4)	0.9412 (5)	5.3 (5)
N 6	0.2678 (7)	0.4623 (4)	0.8517 (6)	5.8 (5)
N 7	0.4169 (7)	0.3154 (4)	0.8322 (5)	5.4 (5)
N 8	0.1260 (9)	0.1217 (4)	0.6054 (6)	8.0 (7)
C 1	0.3460 (9)	0.4869 (5)	0.7386 (7)	5.7 (7)
C 2	0.3924 (10)	0.5246 (5)	0.6968 (8)	6.7 (7)
C 3	0.4241 (11)	0.5120 (6)	0.6283 (8)	8.2 (8)
C 4	0.4068 (10)	0.4607 (6)	0.5989 (7)	6.9 (8)
C 5	0.3575 (8)	0.4230 (5)	0.6428 (7)	5.8 (7)
C 6	0.3341 (9)	0.3686 (5)	0.6170 (7)	5.9 (7)
C 7	0.2669 (10)	0.2865 (5)	0.6289 (7)	5.8 (7)
C 8	0.1591 (10)	0.2727 (5)	0.6435 (7)	5.7 (7)
C 9	0.1249 (8)	0.2414 (4)	0.7626 (7)	4.9 (6)
C10	0.1175 (8)	0.2460 (5)	0.8457 (7)	5.2 (6)
C11	0.0810 (9)	0.2041 (5)	0.8887 (7)	5.9 (7)
C12	0.0758 (10)	0.2116 (5)	0.9644 (8)	7.4 (8)
C13	0.1099 (10)	0.2579 (6)	0.9973 (8)	6.6 (7)
C14	0.1482 (8)	0.2949 (5)	0.9491 (7)	5.3 (7)
C15	0.1921 (9)	0.3458 (6)	0.9817 (7)	6.4 (7)
C16	0.2812 (9)	0.4252 (5)	0.9768 (7)	6.6 (7)
C17	0.2441 (10)	0.4715 (6)	0.9292 (8)	7.5 (8)
C18	0.3135 (9)	0.4976 (5)	0.8163 (8)	6.5 (8)
C19	0.0742 (16)	0.5180 (7)	0.6568 (13)	15.3 (16)
C20	0.0876 (14)	0.4056 (8)	0.5064 (9)	11.6 (13)
OW 1	0.0712 (14)	0.3255 (7)	0.1703 (10)	7.4 (5)
OW 2	0.8697 (16)	0.3655 (9)	0.1842 (12)	10.2 (6)
OW 3	0.222 (3)	0.3695 (13)	0.1828 (18)	18.2 (11)

Beq is the mean of the principal axes of the thermal ellipsoid for atoms refined anisotropically. For OW1, OW2 and OW3, Beq = Biso. These three atoms have partial occupancies of 0.5.

Table 2.3.5 Bond Distances (Å) of Structure B.

Ce-O(1)	2.415 (8)	N(2)-C(6)	1.278 (16)
Ce-O(2)	2.400 (8)	N(2)-C(7)	1.437 (15)
Ce-O(3)	2.678 (7)	N(3)-C(8)	1.447 (15)
Ce-O(4)	2.632 (8)	N(3)-C(9)	1.248 (14)
Ce-N(1)	2.703 (9)	N(4)-C(10)	1.316 (15)
Ce-N(2)	2.657 (9)	N(4)-C(14)	1.303 (15)
Ce-N(3)	2.663 (8)	N(5)-C(15)	1.265 (16)
Ce-N(4)	2.703 (9)	N(5)-C(16)	1.471 (15)
Ce-N(6)	2.694 (9)	N(6)-C(17)	1.455 (17)
P-O(1)	1.447 (8)	N(6)-C(18)	1.276 (16)
P-O(2) a	1.432 (8)	C(1)-C(2)	1.386 (18)
P-O(6)	1.549 (10)	C(1)-C(18)	1.501 (20)
P-O(7)	1.567 (11)	C(2)-C(3)	1.356 (22)
O(2)-Pa	1.432 (8)	C(3)-C(4)	1.412 (21)
O(3)-N(7)	1.250 (13)	C(4)-C(5)	1.426 (17)
O(4)-N(7)	1.254 (12)	C(5)-C(6)	1.477 (19)
O(5)-N(7)	1.219 (12)	C(7)-C(8)	1.539 (18)
O(6)-C(19)	1.303 (20)	C(9)-C(10)	1.491 (17)
O(7)-C(20)	1.276 (19)	C(10)-C(11)	1.418 (17)
O(8)-N(8)	1.236 (18)	C(11)-C(12)	1.364 (20)
O(9)-N(8)	1.224 (17)	C(12)-C(13)	1.376 (20)
O(10)-N(8)	1.179 (14)	C(13)-C(14)	1.392 (18)
N(1)-C(1)	1.389 (15)	C(14)-C(15)	1.518 (18)
N(1)-C(5)	1.356 (16)	C(16)-C(17)	1.509 (22)

Table 2.3.6 Bond Angles (°) of Structure B.

O(1)-Ce-O(2)	74.5(3)	Ce-N(1)-C(1)	120.4(8)
O(1)-Ce-O(3)	137.1(3)	Ce-N(1)-C(5)	120.9(7)
O(1)-Ce-O(4)	135.4(3)	C(1)-N(1)-C(5)	118.6(10)
O(1)-Ce-N(1)	70.6(3)	Ce-N(2)-C(6)	123.9(8)
O(1)-Ce-N(2)	69.0(3)	Ce-N(2)-C(7)	121.2(7)
O(1)-Ce-N(3)	78.3(3)	C(6)-N(2)-C(7)	114.4(10)
O(1)-Ce-N(4)	121.6(3)	Ce-N(3)-C(8)	118.3(6)
O(1)-Ce-N(6)	97.7(3)	Ce-N(3)-C(9)	120.7(7)
O(2)-Ce-O(3)	137.1(3)	C(8)-N(3)-C(9)	119.9(9)
O(2)-Ce-O(4)	137.3(3)	Ce-N(4)-C(10)	120.3(7)
O(2)-Ce-N(1)	119.0(3)	Ce-N(4)-C(14)	123.0(7)
O(2)-Ce-N(2)	141.2(3)	C(10)-N(4)-C(14)	116.7(10)
O(2)-Ce-N(3)	99.1(3)	C(15)-N(5)-C(16)	118.1(10)
O(2)-Ce-N(4)	72.9(3)	Ce-N(6)-C(17)	117.9(8)
O(2)-Ce-N(6)	76.2(3)	Ce-N(6)-C(18)	122.0(8)
O(3)-Ce-O(4)	47.55(24)	C(17)-N(6)-C(18)	120.0(10)
O(3)-Ce-N(1)	68.0(3)	O(3)-N(7)-O(4)	117.5(9)
O(3)-Ce-N(2)	81.0(3)	O(3)-N(7)-O(5)	120.5(10)
O(3)-Ce-N(3)	113.5(3)	O(4)-N(7)-O(5)	121.9(10)
O(3)-Ce-N(4)	98.6(3)	O(8)-N(8)-O(9)	112.0(12)
O(3)-Ce-N(6)	71.9(3)	O(8)-N(8)-O(10)	122.7(13)
O(4)-Ce-N(1)	101.7(3)	O(9)-N(8)-O(10)	125.2(14)
O(4)-Ce-N(2)	69.6(3)	N(1)-C(1)-C(2)	122.0(12)
O(4)-Ce-N(3)	67.9(3)	N(1)-C(1)-C(18)	115.3(10)
O(4)-Ce-N(4)	65.2(3)	C(2)-C(1)-C(18)	122.8(11)
O(4)-Ce-N(6)	117.4(3)	C(1)-C(2)-C(3)	120.1(12)
N(1)-Ce-N(2)	60.1(3)	C(2)-C(3)-C(4)	119.6(11)
N(1)-Ce-N(3)	120.0(3)	C(3)-C(4)-C(5)	119.0(13)
N(1)-Ce-N(4)	166.1(3)	N(1)-C(5)-C(4)	120.6(12)
N(1)-Ce-N(6)	61.2(3)	N(1)-C(5)-C(6)	115.9(11)
N(2)-Ce-N(3)	61.1(3)	C(4)-C(5)-C(6)	123.5(12)
N(2)-Ce-N(4)	115.9(3)	N(2)-C(6)-C(5)	118.8(11)
N(2)-Ce-N(6)	121.0(3)	N(2)-C(7)-C(8)	108.2(9)
N(3)-Ce-N(4)	61.0(3)	N(3)-C(8)-C(7)	107.2(9)
N(3)-Ce-N(6)	174.6(3)	N(3)-C(9)-C(10)	121.8(10)
N(4)-Ce-N(6)	119.2(3)	N(4)-C(10)-C(9)	115.5(10)
O(1)-P-O(2) a	118.9(5)	N(4)-C(10)-C(11)	122.8(11)
O(1)-P-O(6)	114.7(6)	C(9)-C(10)-C(11)	121.6(11)
O(1)-P-O(7)	112.0(7)	C(10)-C(11)-C(12)	118.1(12)
O(2) a-P-O(6)	107.1(6)	C(11)-C(12)-C(13)	119.9(12)
O(2) a-P-O(7)	101.6(7)	C(12)-C(13)-C(14)	116.1(12)
O(6)-P-O(7)	100.2(8)	N(4)-C(14)-C(13)	126.3(12)
Ce-O(1)-P	155.5(6)	N(4)-C(14)-C(15)	114.4(10)
Ce-O(2)-Pa	174.5(6)	C(13)-C(14)-C(15)	119.3(11)
Ce-O(3)-N(7)	96.4(6)	N(5)-C(15)-C(14)	120.8(11)
Ce-O(4)-N(7)	98.5(6)	N(5)-C(16)-C(17)	107.2(10)
P-O(6)-C(19)	130.3(12)	N(6)-C(17)-C(16)	108.5(10)
P-O(7)-C(20)	131.1(13)	N(6)-C(18)-C(1)	120.6(11)

Atoms flagged 'a' are symmetry equivalents

O(2) a	-0.06628	0.39947	0.66223
Pa	-0.02642	0.41933	0.85997

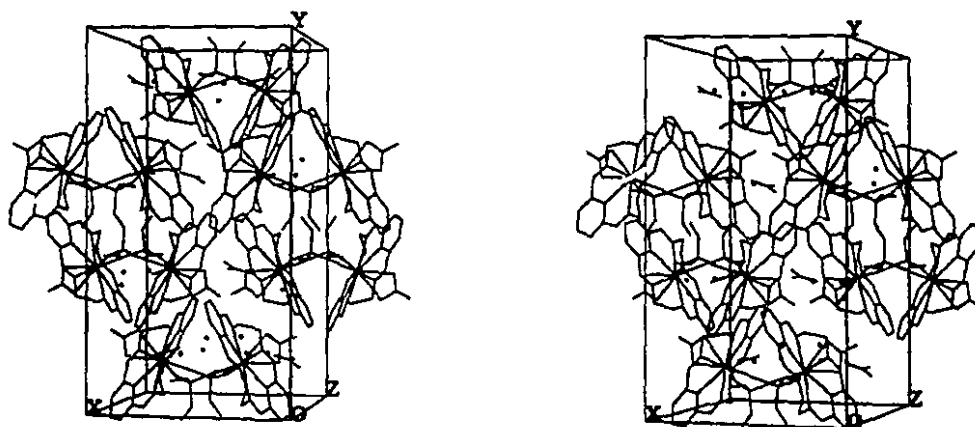


Figure 2.3.4 Packing diagram of structure B.

Chapter 3.

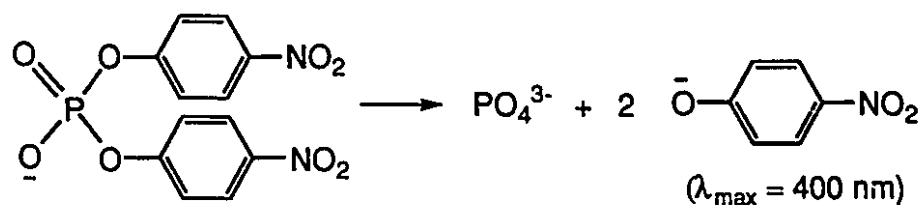
Unusual Behavior in the Ce(III) mediated cleavage of BNPP

3.1. Introduction

Although lanthanide ions are able to rapidly hydrolyze the phosphate diester backbone of RNA they are not nearly as successful at cleaving DNA. Because the deoxyribose sugar lacks the 2'-hydroxyl which acts as an internal nucleophile in the hydrolysis of RNA, DNA is inherently several orders of magnitude less reactive than RNA. Therefore, the 10^7 fold rate enhancement in the cleavage of RNA afforded by the lanthanide ion (Komiyama *et al.*, 1992) is not sufficient to cleave DNA rapidly under physiological conditions.

The enormous stability of the phosphate backbone of DNA ($t_{1/2} = 200$ million years (Chin *et al.*, 1989)) makes it an unsuitable substrate for catalysts which provide less than 10^{10} fold rate enhancement. The much more reactive bis-*p*-nitrophenylphosphate (BNPP) is a phosphate diester which can be hydrolyzed at observable rates and whose hydrolysis can be easily monitored by UV-vis spectroscopy (scheme 3.1). It therefore serves as a useful DNA analog.

Scheme 3.1



bis(p-nitrophenyl)phosphate (BNPP)

In this chapter, the effect of lanthanide ions on the rate of cleavage of BNPP is studied. In all of the cases studied, with the exception of Ce(III), the presence of the lanthanide ions provides five to six orders of magnitude rate enhancement in the cleavage of BNPP (Table 3.1). However, in the case of Ce(III), unusual and unexpected behavior is observed. While the cause of this unusual behavior is still not well understood, exploration of the mechanism of this reaction has led to several interesting discoveries which represent the bulk of the work presented in this thesis. For this reason, the Ce(III) results are presented here in some detail even though some of the results remain enigmatic and some of the proposed explanations are still tentative.

3.2. The effect of lanthanide ions on the hydrolysis of BNPP

Table 3.1 shows the observed pseudo first-order rate constants for the hydrolysis of BNPP in the presence of various lanthanide ions. The effect of the lanthanide ions on the rate of cleavage for BNPP is significant but still very far short of the twelve orders of magnitude required to cleave unactivated phosphate diesters such as DNA in minutes.

Table 3.1 The Effect of LnCl_3 (3.0 mM) on the Rate of Cleavage of BNPP (5×10^{-5} M) at pH 7.5 (50 mM N-ethylmorpholine), 20 °C.

catalyst	k_{obs} (s^{-1})	relative rate
none ^a	1.10×10^{-11}	1.00
La	$2.61 \pm 0.2 \times 10^{-6}$	2.3×10^5
Pr	$1.27 \pm 0.1 \times 10^{-5}$	1.2×10^6
Nd	$1.59 \pm 0.2 \times 10^{-5}$	1.4×10^6
Tb	$9.61 \pm 0.9 \times 10^{-6}$	8.7×10^5
Gd	$1.76 \pm 0.2 \times 10^{-5}$	1.6×10^6
Yb	$6.84 \pm 0.7 \times 10^{-5}$	6.2×10^6

^a(Chin *et al.*, 1989)

3.3. The unusual case of Ce(III)

The disappointing results obtained using lanthanide ions to cleave DNA analogs might have signaled the end of the story of lanthanide ions in the development of an artificial DNase had it not been for the somewhat serendipitous discovery of unusual behavior in the case of Ce(III). Like the other lanthanide ions, Ce(III) is not very effective at cleaving BNPP; however, it was discovered that if one monitors the reaction over a period of several hours, the initial slow stage of the reaction is followed by a sudden burst of activity where the BNPP is rapidly cleaved, releasing both equivalents of *p*-nitrophenoxide. A typical absorbance vs. time plot for the Ce(III) mediated cleavage of BNPP is shown in Figure 3.1

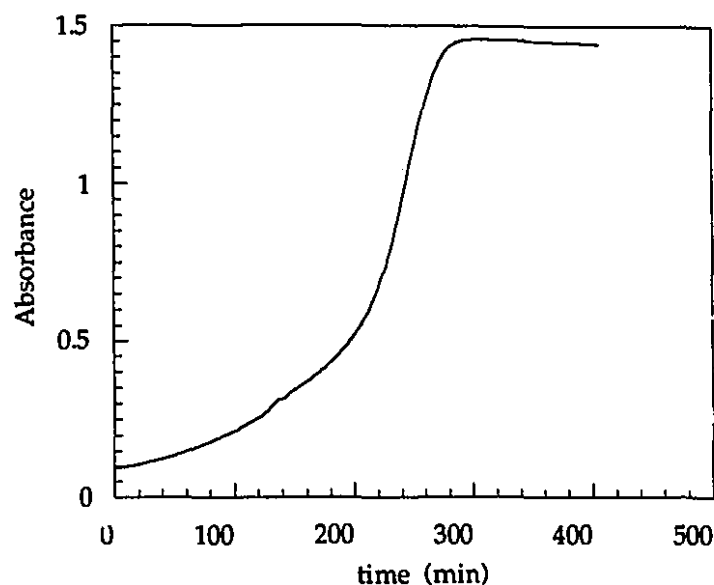


Figure 3.1 Absorbance ($\lambda=400$ nm) vs. time plot of CeCl_3 (10 mM) mediated cleavage of BNPP (5×10^{-5} M) in 0.1 M HEPES buffer at pH 7.52, 20 °C.

It was confirmed that the dramatic change in absorbance was indeed due to the formation of the *p*-nitrophenoxide ion by the good agreement between the UV-vis spectrum obtained at the end of the kinetic run with the spectrum of an authentic sample of *p*-nitrophenoxide. The fact that phosphate diester cleavage was actually being observed was further confirmed by testing a variety of other phosphate diester substrates which were also rapidly cleaved by cerium (Chapter 4).

The unusual kinetics in the case of Ce(III) indicate that the mechanism is complex; however, the steep part of the kinetic curve (Figure 3.1) represents very rapid BNPP cleavage and therefore merited further examination.

The S-shaped kinetic curve indicates that the initially unreactive system slowly evolves into a much more reactive system which rapidly and suddenly cleaves the BNPP. This transformation from unreactive to reactive

species most likely involves an interaction between the Ce(III) and the BNPP and/or its hydrolysis products, or an independent interaction between Ce(III) and the solvent or buffer. In other words, the two most likely explanations of the S-shaped kinetic curve are:

1. One of the products of BNPP hydrolysis catalyzes the Ce(III) mediated cleavage of BNPP in an autocatalytic process.
2. The Ce(III) ion slowly forms an active complex with the solvent or buffer independent of the presence of the BNPP. After an induction period wherein the active complex is formed, the BNPP is suddenly and rapidly cleaved.

The first hypothesis was ruled out by adding *p*-nitrophenol, *p*-nitrophenylphosphate and inorganic phosphate to the reaction mixture containing Ce(III) and BNPP. It was found that adding any of the BNPP hydrolysis products to the reaction mixture had no effect on the observed rate of BNPP cleavage by Ce(III).

The second hypothesis was supported by the observation that the duration of the initial unreactive stage (induction period) and the subsequent generation of the active species is independent of the presence of the substrate. It was found that if the BNPP is added to the reaction mixture three hours after mixing the Ce(III) salt with the buffer then the initial induction period is three hours shorter than normally observed. Furthermore, it was found that the longer the delay between mixing the Ce(III) with the buffer and the addition of BNPP, the more reactive the system becomes (Figure 3.2 and Table 3.2) until a certain maximum reactivity is reached. Clearly, the Ce(III) is interacting with the buffer or something other than the substrate to slowly produce a reactive Ce(III) species which is capable of rapid hydrolysis of BNPP.

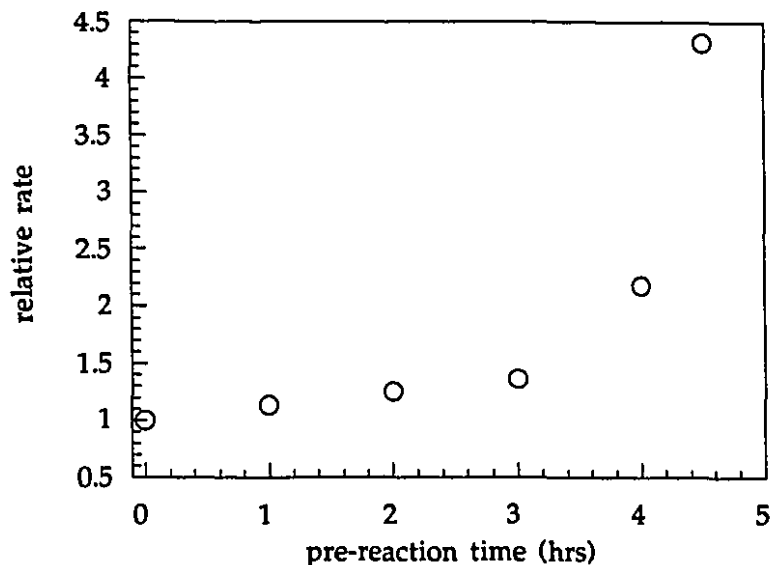


Figure 3.2 The effect of pre-reaction delay between time of mixing CeCl_3 (20 mM) with the buffer (50 mM N-ethylmorpholine, pH 7.5) and the addition of the BNPP (5×10^{-5} M) on the rate of BNPP hydrolysis measured at the inflection point where the rate of BNPP cleavage is greatest (see Figure 3.1) at 20 °C.

Table 3.2 The Relative Rates of Reaction for BNPP Hydrolysis by CeCl_3 after a Pre-Reaction Delay Between Mixing the CeCl_3 (20 mM) with the Buffer (50 mM N-ethylmorpholine, pH 7.5) and the Addition of the BNPP (5×10^{-5} M) at 20 °C.

pre-reaction delay (hrs)	rate (Abs/sec)	relative rate
0.0	0.0209 ± 0.002	1.00
1.0	0.0237 ± 0.002	1.13
2.0	0.0262 ± 0.003	1.25
3.0	0.0285 ± 0.003	1.36
4.0	0.0456 ± 0.005	2.18
4.5	0.0902 ± 0.009	4.32

3.4. Hydroxide consumption in the formation of the active species.

In order to determine if hydroxide ion is consumed in the formation of the active form of the Ce(III), the uptake of NaOH was monitored using the pH-stat technique. The pH was maintained constant by the addition of small amounts of 0.1015 M NaOH titrant. Figure 3.5 shows the amount of NaOH added as a function of time in order to maintain the pH of a 10 mM CeCl₃ solution constant at pH 7.77. The consumption of hydroxide ion is initially very slow but after a certain induction period the rate of sodium hydroxide consumption increases rapidly and two equivalents of sodium hydroxide are quickly consumed. If BNPP is added to the Ce(III) solution immediately after the consumption of the two equivalents of NaOH, the BNPP is immediately cleaved and turns the solution yellow, indicating that the active cerium species has been formed.

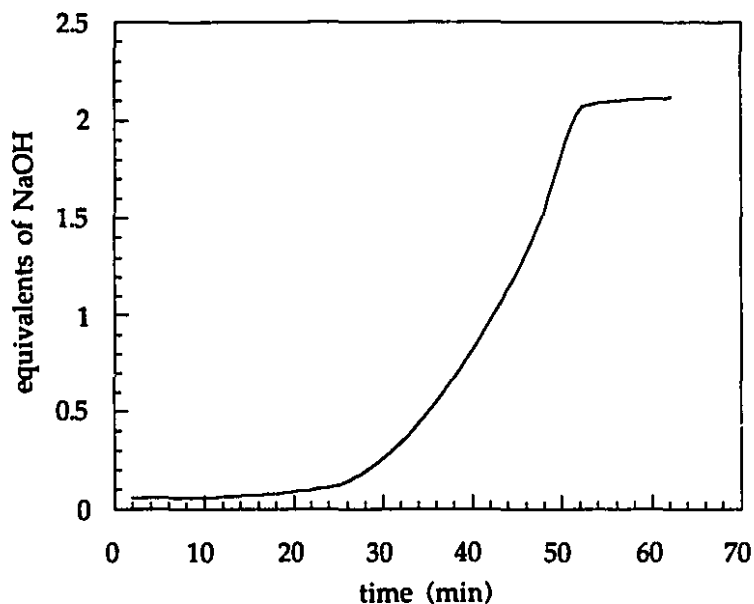


Figure 3.3 Equivalents of NaOH (0.1015M) added to 5 mL 10 mM CeCl₃ in order to maintain the pH constant at 7.77 as a function of time at 20 °C.

The similarity in the behavior of the hydroxide consumption (Figure 3.3) and the rate of BNPP cleavage (Figure 3.1) strongly suggest that the formation of the active cerium species can be monitored by the consumption of hydroxide ion and that two equivalents of hydroxide are required to form the active species from the Ce(III).

Having recognized that two equivalents of hydroxide ion per equivalent of Ce(III) are required to generate the active species, I discovered that by simply adding two equivalents of a concentrated (1.0 M) sodium hydroxide solution to a prepared Ce(III) solution the active species could be immediately generated without any observable induction period. After the addition of two equivalents of NaOH to 20 mM Ce(III), the pH of the resulting solution is initially 8.2 and slowly drops below pH 7 over a period of several hours. The pH does not change appreciably in the first hour after mixing the Ce(III) and hydroxide and this procedure provides a convenient way of preparing the active cerium species with no induction period, thus making it possible to measure the rate of reaction of the active species with a number of different phosphate diester substrates (described in the next chapter).

When the active cerium species is generated immediately by combining the Ce(III) with two equivalents of NaOH, the BNPP is cleaved so rapidly that the stopped-flow technique is needed to measure the rate constant. When a solution of $\text{Ce}(\text{ClO}_4)_3$ (20 mM) and NaOH (40 mM) (pH adjusted to 7.0) is mixed 1:1 with BNPP (1×10^{-4} M) in the stopped-flow apparatus at 20 °C, the pseudo first-order rate constant for BNPP cleavage is 1.6 s^{-1} . This is 10^{11} times greater than that observed in the absence of any catalyst under the same conditions ($1.0 \times 10^{-11} \text{ s}^{-1}$).

The initial pH of 8.2 upon combination of 20 mM Ce(III) with two equivalents of NaOH is consistent with the potentiometric titration of 20 mM Ce(III) (Figure 3.4) where two equivalents of hydroxide are consumed at pH 8.2.

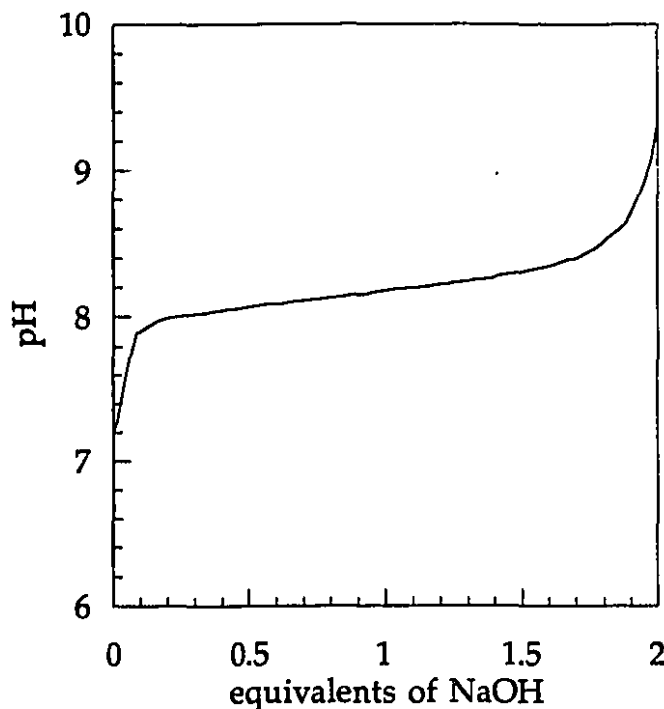


Figure 3.4 Potentiometric titration of 20 mM Ce(III) at 20 °C.

There is insufficient data to identify the structure of the active cerium species. However, it is clear from the pH-stat data and the potentiometric titration that two equivalents of hydroxide ion per equivalent of cerium ion are required to form the active species. It must therefore have a 2:1 stoichiometry ($\text{Ce}_x(\text{OH})_{2x}$).

3.5. Oxygen Dependence

None of the other lanthanide ions tested (Table 3.1) show the same burst in BNPP hydrolysis activity observed with the cerium ion. This

observation coupled with the knowledge that cerium is the only member of the lanthanide series which can form a stable tetravalent ion under our reaction conditions suggests that the rapid cerium mediated cleavage of BNPP proceeds via an oxidative mechanism rather than a hydrolytic one. This hypothesis is supported by the unusual oxygen dependence of the Ce(III) mediated cleavage of BNPP.

The unusual "s-shaped" kinetic plot (Figure 3.1) observed in the Ce(III) promoted cleavage of BNPP is observed only in the presence of molecular oxygen. When oxygen is removed from the reaction medium by first degassing the buffer by bubbling nitrogen gas through the solution for 1-2 hours, no burst in activity is observed and Ce(III) shows the same activity for BNPP hydrolysis as the other lanthanide ions.

Rapid generation of the active species by combining Ce(III) with two equivalents of NaOH in the presence of molecular oxygen leads to 11 orders of magnitude rate enhancement in the cleavage of BNPP at pH 7.0 ($k_{\text{obs}}=1.6 \text{ sec}^{-1}$). When the same reaction is performed in the absence of molecular oxygen the pseudo first-order rate constant for BNPP cleavage, $5.3 \times 10^{-6} \text{ s}^{-1}$, is comparable to that observed for the other lanthanide ions (Table 3.1). This represents a 3×10^5 fold increase in the rate of BNPP cleavage due to the cooperativity between Ce(III) and molecular oxygen. It is clear that molecular oxygen is essential for the exceptional rate of BNPP cleavage observed with Ce(III).

3.6. Effect of pH and [Ce(III)] on the duration of the lag time.

In an effort to better understand the reason for the induction period and the nature of the reactive species generated after several hours, the effect of pH and Ce(III) and concentration on the reaction was determined. The

absorbance vs. time plots for the Ce(III) mediated cleavage of BNPP as a function of pH and Ce(III) concentration are shown in Figures 3.5 and 3.6 respectively. These results indicate that the length of the induction period decreases with increasing pH and Ce(III) concentration.

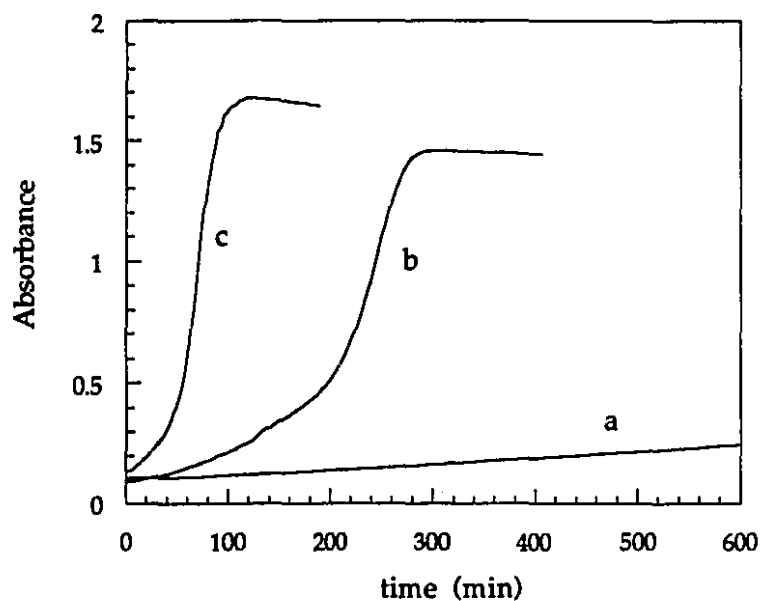


Figure 3.5 Effect of pH on induction period. Absorbance ($\lambda=400$ nm) as a function of time for 5.0×10^{-5} M BNPP in 0.1 M HEPES buffer, 10 mM CeCl_3 , 20 °C at (a) pH 7.25; (b) pH 7.52; (c) pH 7.77.

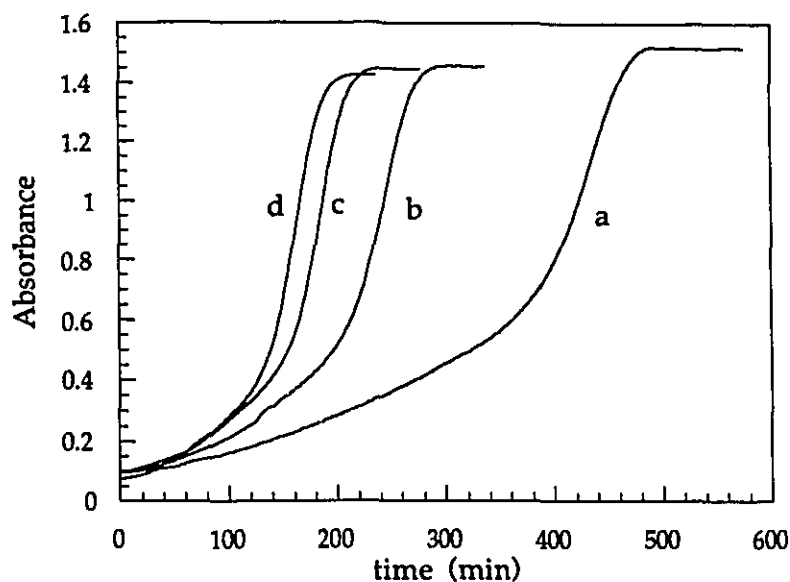


Figure 3.6 Effect of [Ce(III)] on induction period. Absorbance ($\lambda=400$ nm) as a function of time for 5.0×10^{-5} M BNPP in 0.1 M HEPES buffer, pH 7.52, 20° C in the presence of: (a) 5 mM CeCl_3 ; (b) 10 mM CeCl_3 ; (c) 15 mM CeCl_3 ; (d) 20 mM CeCl_3 .

3.7. UV-vis observation of the active species.

The formation of the active species can be observed not only by the rate of BNPP cleavage or release of protons but also directly by UV-vis spectroscopy. When two equivalents of NaOH are added to a solution of 1 mM $\text{Ce}(\text{NO}_3)_3$ a new absorbance maximum appears with a $\lambda_{\text{max}}=294$ nm (Figure 3.7) over a period of 5-10 minutes.

When the absorbance at 294 nm of a buffered 10 mM solution of $\text{Ce}(\text{ClO}_4)_3$ without BNPP is monitored over a period of several hours, the absorbance initially grows slowly until, at a certain point, it increases suddenly and rapidly in a manner reminiscent of the uptake of hydroxide ion (Figure 3.3) and the rate of BNPP hydrolysis (Figure 3.1). Furthermore, the length of the initial induction period shows the same pH dependence as the

pH dependence of the BNPP cleavage (Figure 3.5). This strongly suggests the active species in the cleavage of BNPP absorbs in the UV with a $\lambda_{\text{max}}=294$ nm.

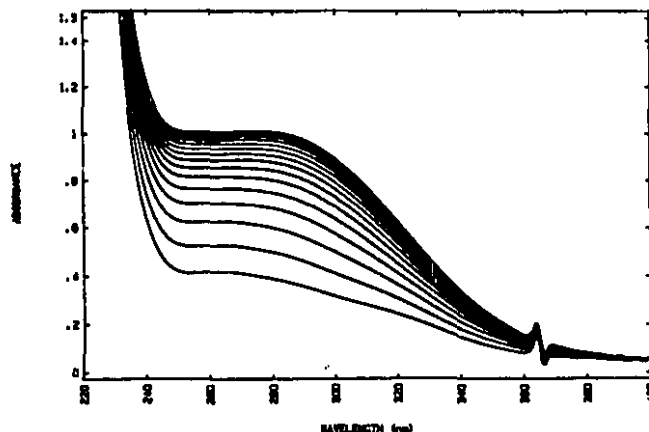


Figure 3.7 UV-vis spectra of $\text{Ce}(\text{NO}_3)_3$ (0.5 mM) + NaOH (1.0 mM) at 25 °C. Spectra recorded every 40 seconds.

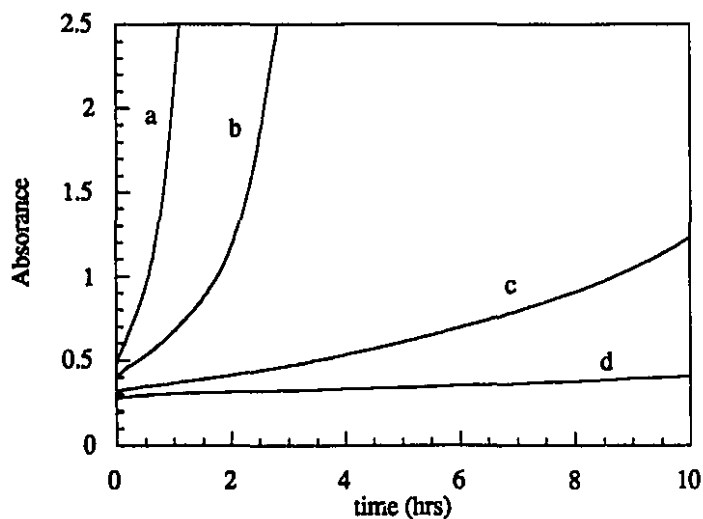


Figure 3.8 Absorbance (294 nm) vs. time for Ce(III) (10 mM) at 25 °C in 0.1 M HEPES buffer at (a) pH 7.75; (b) pH 7.50; (c) pH 7.25; (d) pH 7.00.

The UV-vis spectrum of the active species ($\lambda_{\text{max}}=294$ nm) generated from the combination of Ce(III), NaOH and molecular oxygen (Figure 3.9b) closely resembles the UV-vis spectrum of Ce(IV) (Figure 3.9c). This

resemblance suggests that the active species is in fact a Ce(IV) species generated from the *in situ* oxidation of Ce(III) by molecular oxygen to produce either Ce(IV) and superoxide, or two equivalents of Ce(IV) and hydrogen peroxide.

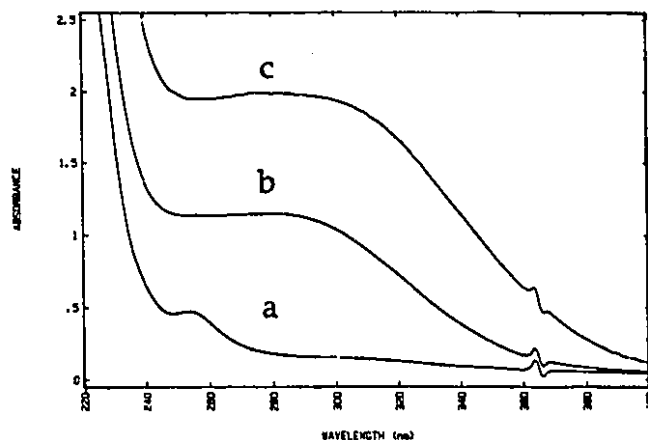
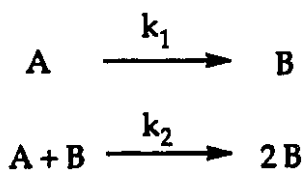


Figure 3.9 Electronic spectra of (a) 0.5 mM Ce(NO₃)₃; (b) 0.5 mM Ce(NO₃)₃ + 1.0 mM NaOH after 20 min; (c) 0.5 mM (NH₄)₂Ce(NO₃)₆ + 1.0 mM NaOH.

3.8. Theoretical explanation of the induction period.

The potentiometric titration and the pH-stat data suggest that the active form of the catalyst is a Ce_x(OH)_{2x} complex but it does not explain why at pH's near neutrality this species is formed only after a long induction period. The "S-shaped" curves shown in Figures 3.9 and 3.10 are reminiscent of the reaction kinetics observed for autocatalytic reactions where the product catalyzes its own formation. The simplest scheme consistent with our data is shown in scheme 3.2.

Scheme 3.2 First-order autocatalytic process



In scheme 3.2, the production of B is governed by two processes, the spontaneous conversion of A to B (k_1) and the conversion of A to B catalyzed by B (k_2). If at time=0 only A is present then B is initially produced only through the uncatalyzed pathway (k_1) which would give rise to the slow induction period. When B accumulates sufficiently that the B assisted pathway becomes predominant, the reaction becomes faster and faster as more B is produced. This produces the sudden and catastrophic conversion of A to B and the "S-shaped" reaction curve.

The rate equation (3.1) derived from scheme 3.2 can be integrated and rearranged to give the form shown in (3.2). The full derivation of (3.2) from (3.1) is given in Appendix 3.1.

$$-d[A]/dt = k_1[A] + k_2[A][B] \quad (3.1)$$

$$[A] = \frac{[A]_0 u e^{-ut}}{k_1 + k_2[A]_0 e^{-ut}} \quad \text{where } u = k_1 + k_2[A]_0 \quad (3.2)$$

Using (3.2), the concentration of A and B can be calculated as a function of time for any values of k_1 and k_2 . Figures 3.10 and 3.11 illustrate the effect of changing values of k_1 and k_2 on the calculated concentration of product (B) vs. time.

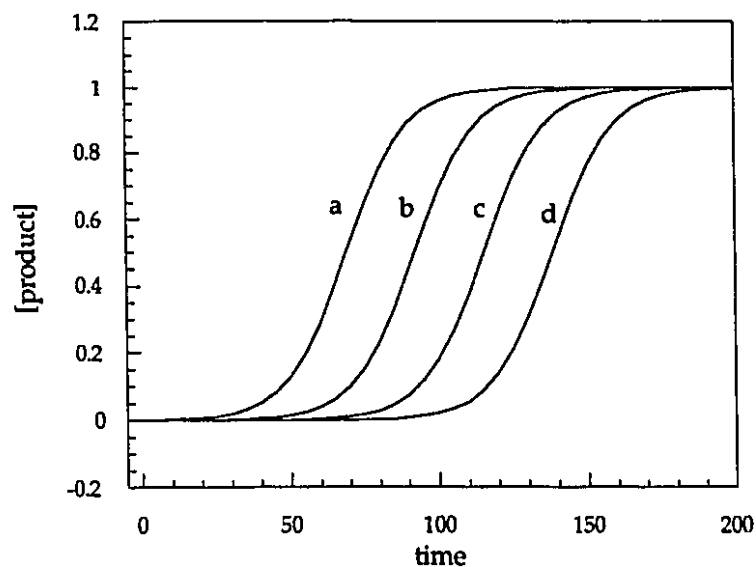


Figure 3.10 Effect of k_1 on the concentration of product (B) as a function of time calculated according to (3.2) where $k_2=0.1$ and $k_1 =$ (a) 10^{-4} ; (b) 10^{-5} ; (c) 10^{-6} ; (d) 10^{-7} .

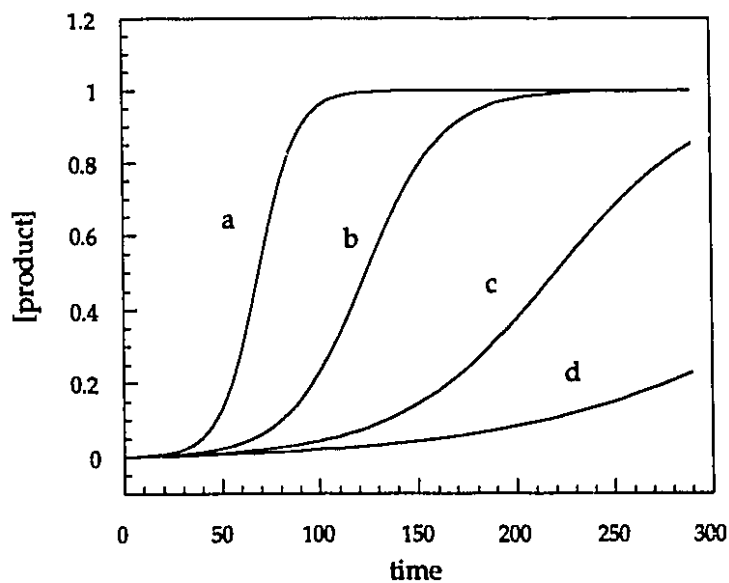


Figure 3.11 Effect of k_2 on the concentration of product (B) as a function of time calculated according to (3.2) where $k_1 = 1.0 \times 10^{-4}$ and $k_2 =$ (a) 0.1; (b) 0.05; (c) 0.025; (d) 0.0125.

The similarity between the effect of changing values of k_1 on the calculated curves shown in figure 3.10 and the effect of pH and cerium concentration on the observed curves shown in figures 3.5 and 3.6 suggest that the observed behavior is consistent with an autocatalytic process like that of scheme 3.2 and that k_1 and k_2 are dependent upon pH and Ce(III) concentration.

3.9. Conclusions

The mechanism of the cerium mediated cleavage of BNPP in the presence of molecular oxygen is clearly very complex; however, the experiments described in this chapter have revealed several important details about the reaction. This information has led to the discovery of conditions under which other phosphate diesters such as DNA itself can be rapidly and efficiently cleaved with no destruction of the deoxyribose sugar (cf. chapter 4). These experiments have also shed light on some aspects of the mechanism which may eventually lead to a more detailed elucidation of the mechanism and further application of the impressive DNA cleavage activity of this system.

The experiments described in this chapter have revealed the following information about the remarkable cerium mediated cleavage of BNPP:

- Ce(III) is the only one of the lanthanide ions tested which shows a sudden burst in activity in the cleavage of BNPP.
- In the absence of molecular oxygen, Ce(III) behaves like the other lanthanide ions and shows no burst of BNPP cleavage activity.

- The sudden burst in BNPP cleavage activity is caused by the slow generation of an active form of cerium from the interaction of Ce(III) with molecular oxygen and two equivalents of hydroxide ions.
- The combination of Ce(III) with two equivalents of NaOH in the presence of molecular oxygen leads to the rapid generation of the active species with no induction period.
- The generation of the active form of the catalyst can be monitored by UV-vis spectroscopy ($\lambda_{\text{max}}=290$ nm) or by the consumption of hydroxide ions.
- The electronic spectrum of the active Ce(III)•O₂ complex is very similar to that of Ce(IV) ((NH₄)Ce(NO₃)₆).
- The rate of formation of the active species is dependent on the concentration of cerium and hydroxide ion.
- The "s-shaped" kinetic plots observed with Ce(III) in the cleavage of BNPP is due to the concentration of the active form of the catalyst whose formation also follows an "s-shaped" kinetic plot. The "s-shape" is most likely reflective of an autocatalytic system wherein the product catalyzes its own formation.

From a mechanistic point of view, the most significant observation outlined above is the oxygen dependence of the reaction. The oxygen dependence of the cerium reactions seems to confirm the hypothesis that the

extraordinary cleavage of BNPP by cerium proceeds via an oxidative mechanism; however, it is difficult to imagine an oxidative mechanism analogous to those previously proposed for DNA cleavage (cf. section 1.3) which could be applied to the cleavage of BNPP. Furthermore, the UV-vis spectrum of the products indicate complete hydrolysis of BNPP to release the expected two equivalents of *p*-nitrophenoxide ions with no apparent oxidation of the leaving groups. Product analysis by ^{31}P nmr also indicate that inorganic phosphate is the sole phosphorus containing product detected at the end of the reaction. A similar analysis of the products of DNA cleavage described in the next chapter also indicate that only the products expected from hydrolytic cleavage are found at the end of the reaction. Thus, while the oxygen dependence is suggestive of an oxidative mechanism, analysis of the products suggest only overall hydrolytic cleavage.

The oxygen dependence of the reaction with cerium, which is the only lanthanide which can be oxidized to the tetravalent state under our reaction conditions, suggests that the reaction may involve the activation of molecular oxygen by Ce(III). This hypothesis is supported by the observation that the electronic spectrum of the active species generated from Ce(III) and O_2 closely resembles that of Ce(IV).

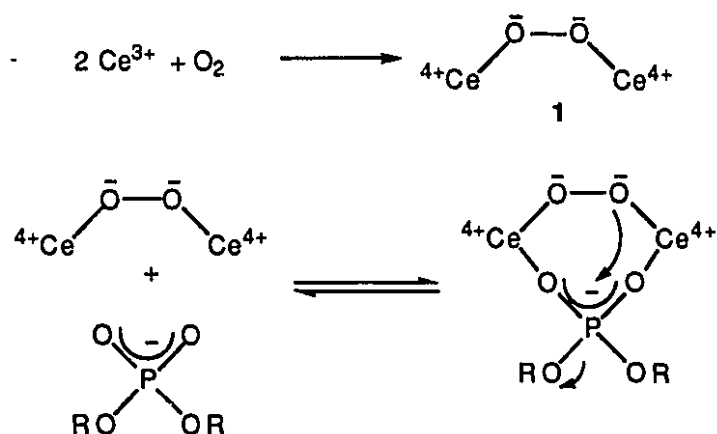
The reduction of molecular oxygen to superoxide or peroxide by Ce(III) would produce activated oxygen species which could bring about the cleavage of phosphate diesters by nucleophilic attack upon phosphorus to give hydrolytic products rather than abstracting a hydrogen atom to give the products expected from oxidative cleavage.

In order to test this hypothesis, I looked for cooperativity between La(III) and superoxide and hydrogen peroxide. The combination of $\text{La}(\text{ClO}_4)_3$ and potassium superoxide (KO_2) does not result in the rapid cleavage of

BNPP. However, the combination of $\text{La}(\text{ClO}_4)_3$ and hydrogen peroxide produces a very reactive complex for the hydrolysis of BNPP (described in chapter 5).

From the oxygen dependence of the cerium mediated cleavage of BNPP described in this chapter and the $\text{La}(\text{III})\cdot$ peroxide cooperativity described in chapter 5 a simple mechanistic scheme can be proposed.

Scheme 3.3



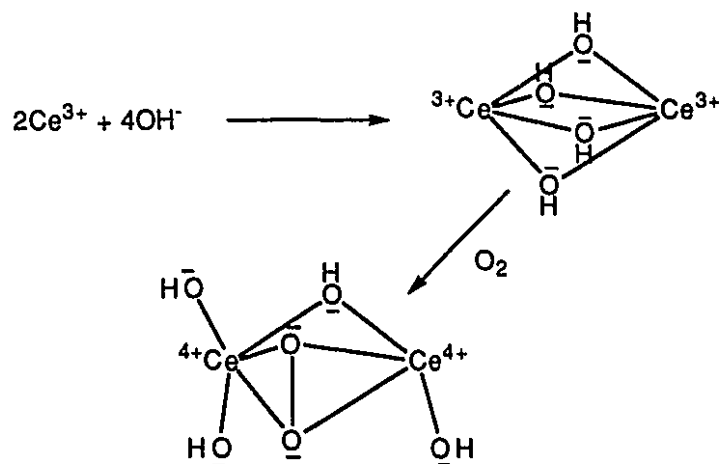
In the first step, an electron transfer from two $\text{Ce}(\text{III})$ ions to a coordinated molecule of molecular oxygen produces two $\text{Ce}(\text{IV})$ ions coordinated to peroxide dianion (1). In the second step, coordination of the phosphate diester to either one or both of the $\text{Ce}(\text{IV})$ ions provides Lewis Acid activation of the coordinated substrate (the 4+ charge of the $\text{Ce}(\text{IV})$ would make it a more effective Lewis Acid than $\text{Ce}(\text{III})$). In the third step, the coordinated peroxide acts as a nucleophile and attacks the coordinated phosphate diester followed by expulsion of the leaving group. The peroxyphosphate monoester would then have to be reduced to the phosphate monoester by peroxide or by $\text{Ce}(\text{III})$. The phosphate monoester could then

also be cleaved in the same way. This proposed mechanism combines the added Lewis Acidity of the Ce(IV) ion with the proximity of a strong nucleophile to explain the oxygen dependence and the enormous difference in reactivity relative to the other lanthanides which cannot be oxidized to the tetravalent state.

The complex "s-shaped" kinetics described in this chapter are most likely due to the rate limiting autocatalytic formation of the reactive Ce(IV) peroxide complex (1) (scheme 3.3). There is insufficient data to determine the structure of this reactive combination of Ce(IV) and peroxide; however, it is most likely much more complex than the simplified model shown in scheme 3.3. The pH-stat experiments and the studies on the effect of pH on the induction period indicate that the formation of the reactive complex involves the consumption of two equivalents of hydroxide ion per cerium ion and that its rate of formation is pH dependent. One possible mechanism which accounts for the hydroxide requirement involves the formation of a cerium hydroxide cluster, the simplest of which is the dimer $[(\text{Ce}(\text{OH})_2)_2]^{2+}$. By bringing two Ce(III) ions into close proximity, the formation of the cerium hydroxide cluster facilitates the addition of molecular oxygen to the two Ce(III) ions resulting in the two-electron transfer to produce the reactive complex.

With the available data it is not possible to discern the structure of the reactive ceric peroxide complex or the cerium hydroxide cluster; however, most likely some or all of the hydroxide ions act as bridging ligands and, once formed, the peroxide would also likely act a bridging ligand. One possible scenario is shown in Scheme 3.4.

Scheme 3.4



The peroxide dianion may bridge between the two Ce(IV) ions either in a μ -1,2 fashion as depicted in Scheme 3.3 or in a μ - η^2 : η^2 fashion as shown in Scheme 3.4. Although there is insufficient data to discern between the two structures, an X-ray structure obtained by Xu (Xu *et al.*, 1988) indicates that lanthanide ions can bind peroxide in a μ_3 - η^2 : η^2 fashion. Curiously, no hydrogen peroxide was added to the system in growing the crystals. The SmCl_3 salt was simply crystallized from THF. The authors assume that the peroxide was generated *in situ* from the reduction of atmospheric oxygen by some other unknown component of the system (Xu *et al.*, 1988). The structure contains four lanthanide ions bridged by two peroxide anions (μ - η^2 : η^2).

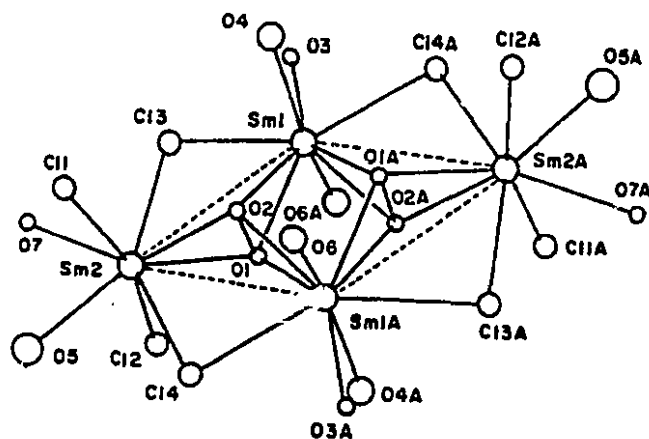


Figure 3.12 X-ray structure of $\text{Sm}_4\text{O}_4\text{Cl}_8(\text{THF})_6(\text{H}_2\text{O})_6$ from (Xu *et al.*, 1988).

If one exchanges OH^- for Cl^- and Ce(IV) for Sm(III) in the X-ray structure shown in Figure 3.12 one would have the appropriate stoichiometry of Ce, peroxide and hydroxide (2:1:2) predicted by the observation that two hydroxides per Ce are required and two Ce(III) are needed to reduce molecular oxygen to peroxide. In fact, this structure is essentially a dimer of the structure for the active complex depicted in Scheme 3.4. Both structures could represent the active ceric peroxide complex and be consistent with the data. It may be that a structure containing only two Ce(IV) like the one shown in Scheme 3.4 is the active form but that once formed it can assist in the formation of other such complexes by forming a larger complex like that shown in Figure 3.12 which can then dissociate giving two of the active dimers. This type of assistance in the formation of the active species could explain the autocatalytic behavior.

Investigation of the complex mechanism of the cerium mediated cleavage of BNPP has led to the proposal of novel mechanism involving the autocatalytic formation of a reactive ceric peroxide species which provides

both Lewis Acid activation and a metal bound peroxide nucleophile to bring about the rapid net hydrolytic cleavage of a coordinated phosphate diester.

This investigation has also led to several other interesting and significant results. By quickly generating the active species by adding two equivalents of NaOH to Ce(III) in the presence of atmospheric oxygen the cleavage of other less activated phosphate diesters, including DNA itself, have been investigated (chapter 4). In order to test the proposed mechanism involving the generation of nucleophilic peroxide *in situ*, cooperativity between La(III) and hydrogen peroxide has also been investigated (chapter 5).

3.10. Experimental

3.10.1. Chemicals

BNPP (sodium salt) was purchased from Sigma Chemical Company. N-ethyl morpholine and $(\text{NH}_4)_2\text{Ce}(\text{NO}_3)_6$ was purchased from Aldrich Chemical Co..

3.10.2. UV-vis spectroscopy

The cleavage of BNPP was monitored by following the increase in absorbance at 400 nm due to the formation of the *p*-nitrophenoxide ion. The pseudo first-order rate constants for BNPP cleavage in the presence of lanthanide(III) salts listed in Table 3.1 were calculated from the initial rate of reaction calculated measured during the first 10% of the reaction. The rate constants were calculated assuming that both equivalents of *p*-nitrophenoxide were released.

The effect of pre-reaction delay prior to the addition of substrate on the rate of BNPP cleavage was determined by taking 2 mL aliquots of the buffered (50 mM N-ethylmorpholine pH 7.5) CeCl_3 (20 mM) solution at designated times and combining it with 10 μL of a 10 mM solution of BNPP in a UV cell. The rate of reaction was calculated from the slope of the absorbance vs. time line at the steepest point. The solutions were all made up in distilled water without degassing.

3.10.3. pH-stat

The rate of hydroxide consumption by Ce(III) in the formation of the active species (Section 3.4) was monitored by the pH-stat method. The pH of the Ce(III) solution (5 mL 10 mM CeCl_3) was maintained at pH 7.77 by the addition of NaOH (0.1015 M) controlled by Radiometer ABU80 autoburette

and TTT80 titrator equipped with a REA 270 pH-stat attachment. The volume of hydroxide added vs. time plot was taken from the strip chart recorder and scanned using Ofoto scanner attached to a Macintosh Quadra 700 computer. The scanned image was converted to cartesian coordinates using the Flexitrace software and was plotted using the Kaleidagraph software.

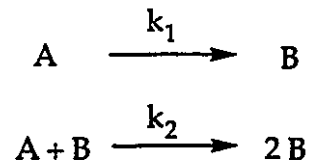
3.10.4. Titrations

The potentiometric titration of $\text{Ce}(\text{ClO}_4)_3$ (5 mL 20 mM) was performed using the Radiometer ABU80 autoburette and TTT80 titrator. The titration was done at room temperature (20 °C) using 1.0 M NaOH as titrant with a constant flow of nitrogen gas blown through the titration vessel. The titration curve was transferred from the chart recorder to a Macintosh computer using the method described previously for the pH-stat experiments.

3.10.5. UV-vis observation of the active species.

The change in the UV-vis spectrum of the $\text{Ce}(\text{NO}_3)_3$ (0.5 mM) after the addition of two equivalents of NaOH was monitored using a Hewlett-Packard 8451A diode array spectrophotometer. The UV-vis scans were taken at 40 second intervals and stored in memory. At the end of the kinetic run, the spectra were recalled from memory and plotted. The spectra were all taken at 20 °C.

Appendix 3.1 Derivation of (3.2)



$$-d[A]/dt = k_1[A] + k_2[A][B] \quad (3.1.1)$$

if we define $x=[A]$ and $[A]_0=A_0$ then (3.1.1) becomes

$$-dx / dt = k_1x + k_2x(A_0 - x) \quad (3.1.2)$$

upon integration

$$\int \frac{dx}{x(k_1 + k_2(A_0 - x))} = -\int dt \quad (3.1.3)$$

integration by partial fractions

$$\frac{1}{u} \int \frac{dx}{x} + \frac{1}{u} \int \frac{k_2 dx}{(u - k_2 x)} = -\int dt \quad (3.1.4)$$

where $u=k_1+k_2A_0$

integration gives

$$\frac{1}{u} \ln \left(\frac{xc}{u - k_2 x} \right) = -t \quad (3.1.5)$$

at $t=0$ $x=A_0$

$$\frac{1}{u} \ln \left(\frac{A_0 c}{k_1} \right) = 0 \quad \text{therefore } c=k_1/A_0 \quad (3.1.6)$$

substituting c into (3.1.5)

$$\frac{1}{u} \ln \left(\frac{xk_1}{(u - k_2x)A_0} \right) = -t \quad (3.1.7)$$

raising both sides of (3.1.7) to the power of e

$$\frac{xk_1}{(u - k_2x)A_0} = e^{-ut} \quad (3.1.8)$$

rearranging (3.1.8)

$$x = A = \frac{A_0 u e^{-ut}}{k_1 + k_2 A_0 e^{-ut}} \quad (3.1.9)$$

where $u = k_1 + k_2 A_0$

Chapter 4

Ce(III) + DNA analogs

4.1. Introduction

In the previous chapter, the remarkably rapid cleavage of BNPP by Ce(III) and oxygen was described. While the eleven orders of magnitude rate enhancement observed for the Ce(III)•O₂ mediated cleavage of BNPP is several orders of magnitude greater than that observed with even the most efficient transition metal ion complexes, the true test of the system is whether or not the same rate enhancement is possible with phosphate diesters containing poor leaving groups such as bis-alkyl phosphates or DNA itself. In this chapter the effect of Ce(III)•O₂ on less activated phosphate diesters and ultimately a DNA dinucleotide is examined.

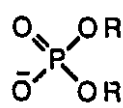
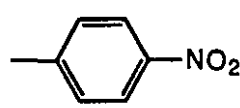
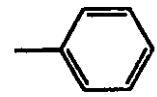
	R	name	pK _a (leaving group)
		BNPP	7.15
		DPP	9.99
	—CH ₃	DMP	15.5
	2'-deoxyadenosine	dApdA	13.0

Figure 4.1 Phosphate diesters studied and the pK_as of the conjugate acids of the leaving groups

4.2. Results and discussion

4.2.1. Dimethyl Phosphate (DMP)

Dimethyl phosphate (DMP) is a phosphate diester with a very poor leaving group. It is hydrolyzed by hydroxide ion at a rate three million times slower than BNPP and is actually less reactive than DNA itself (Chin *et al.*, 1989). The only Co(III) complex shown to hydrolyze DMP under mild conditions does so with a half-life of 40 days at 60° C at pD 6.3 (Kim & Chin, 1992).

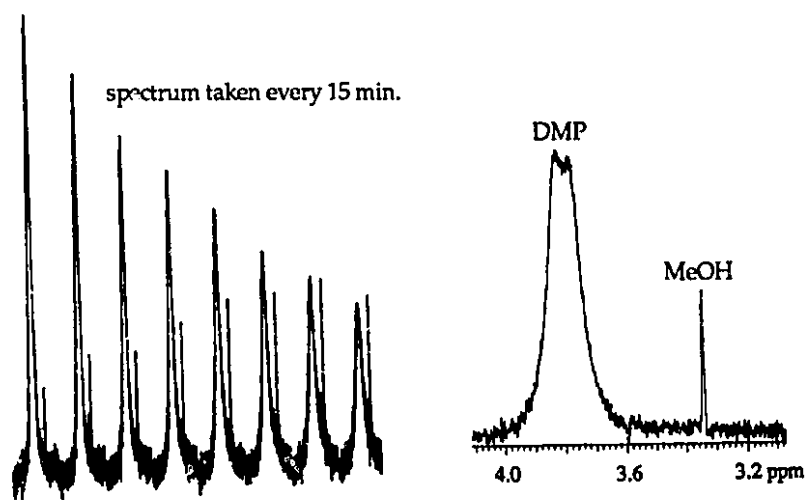


Figure 4.2 Horizontally stacked ¹H nmr spectra (taken every 15 minutes) showing the hydrolysis of DMP to produce methanol in the presence of 20 mM CeCl₃ at pD 8.2 and 25° C.

The cleavage of DMP can be monitored by ¹H nmr spectroscopy. In the presence of 20 mM CeCl₃ at pH 8.2 the signal due to DMP (normally a doublet) at $\delta=3.8$ ppm is broadened by the presence of the paramagnetic Ce(III) ion but its disappearance can be easily monitored as well as the accompanying increase in the signal ($\delta=3.34$ ppm) due to the formation of methanol. Figure 4.2 shows a series of horizontally stacked nmr spectra taken every 15 minutes at room temperature. The observed first-order rate constant for the Ce(III)

mediated cleavage can be calculated from the slope of the $\ln([DMP]/[DMP]_0)$ vs. time plot (Figure 4.3).

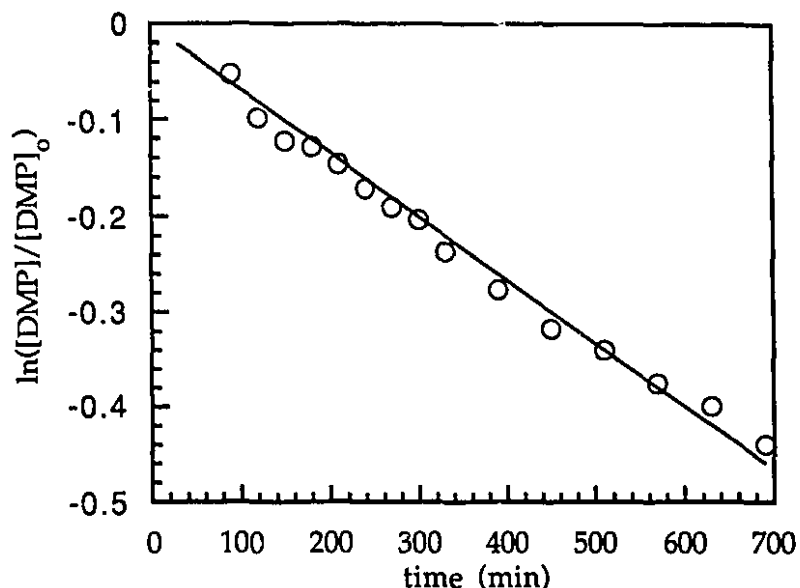


Figure 4.3 First-order linear plot showing the rate of conversion of DMP (5 mM) to methanol mediated by 20 mM $CeCl_3$ at pH 8.2, 25° C.

The pseudo first-order rate constant for DMP cleavage in the presence of 20 mM $CeCl_3$ at pH 8.2 and 25 °C calculated from the plot shown in Figure 4.3 is $1.1 \pm 0.1 \times 10^{-5} s^{-1}$. This is approximately 12 orders of magnitude greater the estimated pseudo-first order rate constant for the hydroxide mediated cleavage of DMP ($7 \times 10^{-18} s^{-1}$) under the same conditions (Chin *et al.*, 1989). The 10^{12} fold rate enhancement in the cleavage of DMP with the $Ce(III) \cdot O_2$ system that it is as effective for unactivated phosphate diesters as for activated phosphate diesters. It is also much more efficient than even the fastest transition metal ion catalysts developed to date which provide only 10 orders of magnitude rate enhancement (Kim & Chin, 1992).

4.2.2. Diphenyl Phosphate

Diphenyl phosphate (DPP) is a phosphate diester with a leaving group pK_a intermediate between those of BNPP and DMP. The hydrolysis of DPP can be monitored by HPLC. A series of HPLC chromatograms taken at five minute intervals after the addition of 20 mM Ce(III) (Figure 4.4) shows the rapid conversion of DPP to phenol with very little accumulation of the phenylphosphate intermediate at 25 °C, pH 8.2. The integration of the peaks due to DPP, phenol (PhOH) and phenyl phosphate (PP) are shown in Figure 4.5. From the non-linear least squares fit of the first-order rate equation to the decrease in the concentration of DPP the first-order rate constant for the hydrolysis of DPP is $0.078 \pm 0.002 \text{ min}^{-1}$. This represents approximately 10 orders of magnitude rate enhancement in the cleavage of DPP.

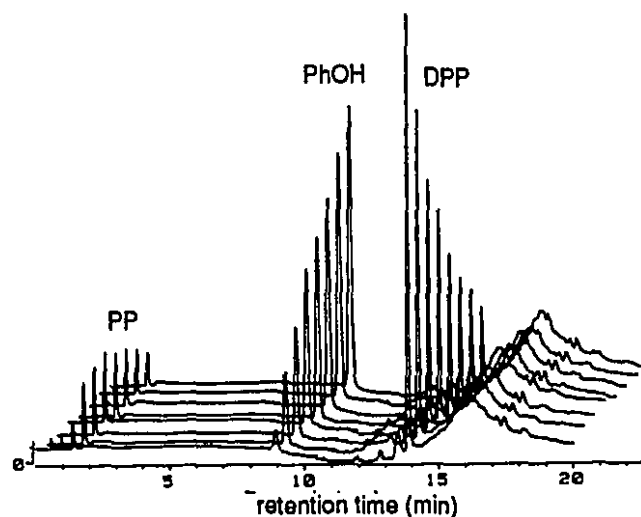


Figure 4.4 Stacked HPLC chromatograms showing the conversion of DPP to phenol and phenyl phosphate by $\text{Ce}(\text{ClO}_4)_3$ (20 mM), pH 8.2 at 25 °C. Chromatograms are taken of the reaction mixture at 5-min intervals from 0 to 30 minutes after mixing of the reactants.

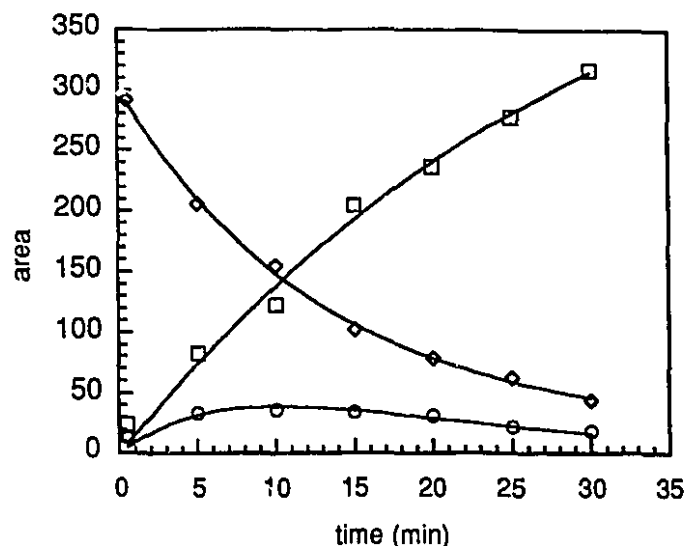


Figure 4.5 Kinetic plot showing the distribution of products as a function of time for the cleavage of DPP by $\text{Ce}(\text{ClO}_4)_3$ (20 mM), pH 8.2 at 25 °C.

4.2.3. dApdA cleavage by $\text{Ce}(\text{III})\cdot\text{O}_2$

The rapid cleavage of DMP and DPP by $\text{Ce}(\text{III})$ demonstrate that the $\text{Ce}(\text{III})\cdot\text{O}_2$ system is very effective at promoting the cleavage of not only activated but also inactivated phosphate diesters. The key remaining question is whether or not this enormous reactivity can be used to cleave the phosphate diester backbone of DNA. Observable hydrolysis of DMP does not necessarily imply that the same catalyst will be effective at hydrolyzing DNA. The $\text{Co}(\text{III})$ complex used to hydrolyze DMP (Kim & Chin, 1992) is not an effective reagent for hydrolyzing DNA since it also promotes depurination which competes with hydrolysis of the phosphate diester and leads to a mixture of products (Kim, unpublished results).

In order to study the effect of $\text{Ce}(\text{III})\cdot\text{O}_2$ on DNA, we studied its effect on a DNA dinucleotide. Conversion of the dinucleotide dApdA (2'-deoxyadenyl(3'-5')-2'-deoxyadenosine) to dA (2'-deoxyadenosine) was monitored by HPLC (Figure 4.6). As is apparent from Figure 4.6, the dApdA is

cleanly converted to dA with very little accumulation of the monophosphate intermediates and with no evidence of depurination (authentic adenine is eluted at 2.54 minutes). The pseudo first-order rate constant of dApdA cleavage in the presence of 20 mM $\text{Ce}(\text{ClO}_4)_3$ at pH 8.2 and 37° C was obtained by following the initial rate of decrease in the concentration of dApdA ($k_{\text{obs}} = 6.8 \pm 0.1 \times 10^{-3} \text{ min}^{-1}$). Thus, the presence of 20 mM Ce(III) effectively reduced the half-life of the phosphate diester backbone of DNA from an estimated 10 million years (pH 8.2, 37° C) to approximately 2 hours.

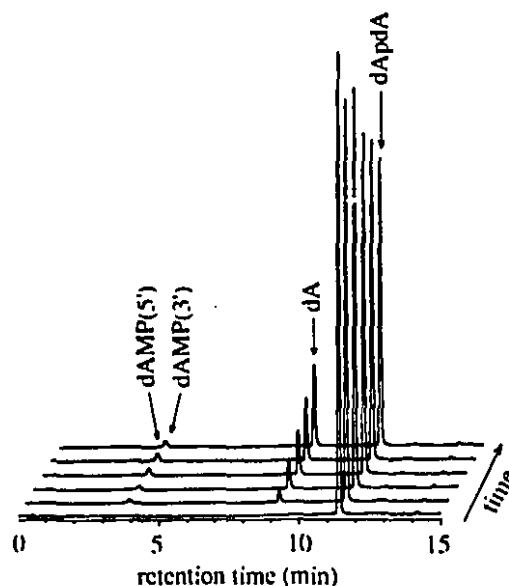


Figure 4.6 HPLC chromatograms showing the cleavage of dApdA (1 mM) by $\text{Ce}(\text{ClO}_4)_3$ (20 mM), pH 8.2 at 37 °C. Chromatograms are taken of the reaction mixture quenched at 10-min intervals from 0 to 50 minutes after mixing of the reactants.

4.2.4. Linear Free Energy Relationship.

Having studied the effect of Ce(III) on the rate of cleavage of a number of different phosphate diesters with a wide range of reactivities allows for the examination of the relationship between the rate of reaction and the pK_a of the leaving group. As shown in Figure 4.7 there is a linear relationship

between $\log(k_{\text{obs}})$ and the pK_a of the leaving group which parallels the linear free energy relationship previously observed for the rate of hydroxide ion catalyzed rate of reaction.

The linear correlation between rate of reaction and leaving group acidity over such a wide range of reactivity supports the use of activated esters such as BNPP as DNA analogs. There is no indication of a change in mechanism or rate determining step as the leaving group is altered. The similar slope of the hydroxide catalyzed process (slope = -0.76) and the Ce(III) mediated process (slope = -0.61) suggests that the mechanism of the two processes are analogous.

The linear free energy relationship observed with Ce(III) is inconsistent with an oxidative cleavage mechanism which involves hydrogen abstraction from the leaving group leading ultimately to cleavage. The phosphate diesters studied are structurally quite different and the rate of hydrogen abstraction would be most unlikely to correlate well with the pK_a of the leaving group.

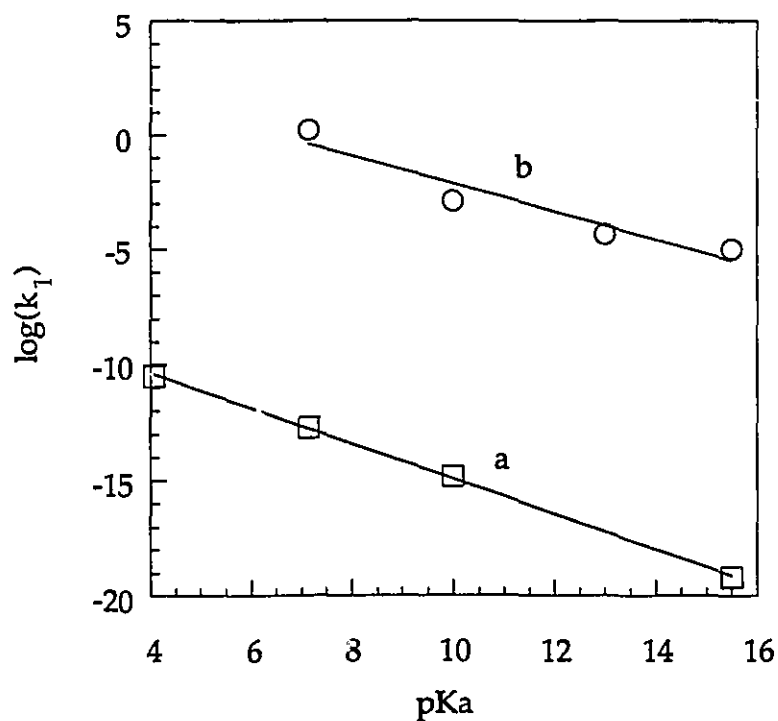


Figure 4.7 Linear free-energy relationship between the pseudo first-order rate constant for hydrolysis of phosphate diesters at 25° C, pH 8.2 and the pK_a of the conjugate acid of the leaving group (a) the hydroxide catalyzed; (b) the Ce(III) (20 mM) catalyzed.

Table 4.1 First-Order Rate Constants for the Hydroxide Catalyzed and Ce(III) Mediated Cleavage of Phosphate Diesters at 25° C, pH 8.2.

pK _a	hydroxide		Ce(III)	
	k (s ⁻¹)	log(k)	k (s ⁻¹)	log(k)
15.5	6.80 × 10 ⁻¹⁸	-17.2	1.10 ± .1 × 10 ⁻⁵	-4.96
13.0			4.60 ± .05 × 10 ⁻⁵	-4.34
9.99	1.57 × 10 ⁻¹³	-12.8	1.30 ± .03 × 10 ⁻³	-2.89
7.15	2.00 × 10 ⁻¹¹	-10.7	1.60 ± .1	0.204
4.07	3.20 × 10 ⁻⁹	-8.49		

4.2.5. Product analysis of dApdA cleavage

The rapid cleavage of dApdA shows the same oxygen dependence observed in the cleavage of BNPP (Figure 4.8). This oxygen dependence suggests that the observed cleavage is due to some kind of oxidative process as opposed to hydrolytic. However, detailed analysis of the products of this reaction reveal that only the products expected from hydrolytic cleavage are produced.

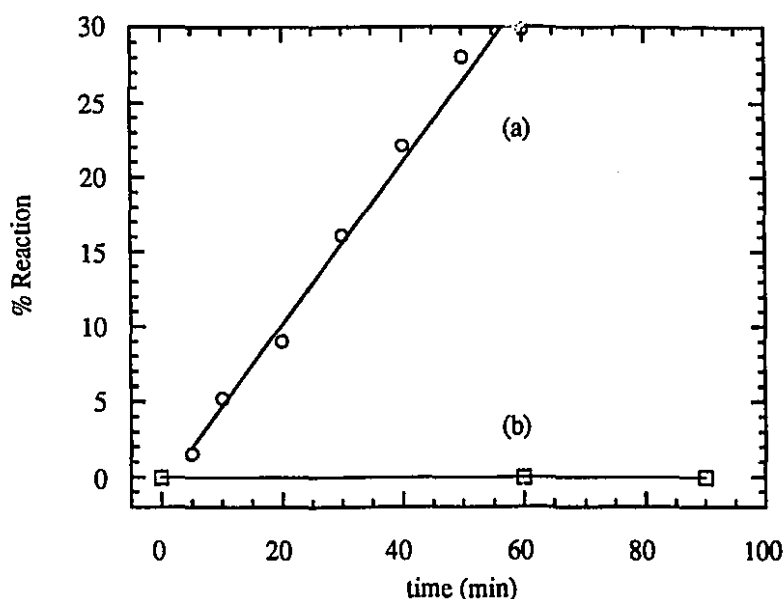


Figure 4.8 Kinetic plot showing the rate of dApdA (1 mM) cleaved by $\text{Ce}(\text{ClO}_4)_3$ (20 mM), pH 8.2 at 37 °C: (a) in the presence of atmospheric oxygen; (b) after degassing with nitrogen gas.

As discussed earlier (cf. Section 1.3), although the mechanism of oxidative cleavage of DNA is still under investigation, in all cases, the reaction involves oxidation of a deoxyribose sugar and loss of the base. Meanwhile hydrolytic cleavage produces only the two strands with both

terminal nucleosides intact and one end possessing the phosphate monoester. The HPLC chromatograms (Figure 4.6) used to detect the cleavage of dApdA by $Ce(III)\cdot O_2$ show no evidence of the formation of adenine or any furanone derivatives. Furthermore, from the integration of the peaks it can be seen that all of the dApdA is converted to dA or dAMP with no loss of material due to the formation of undetected products.

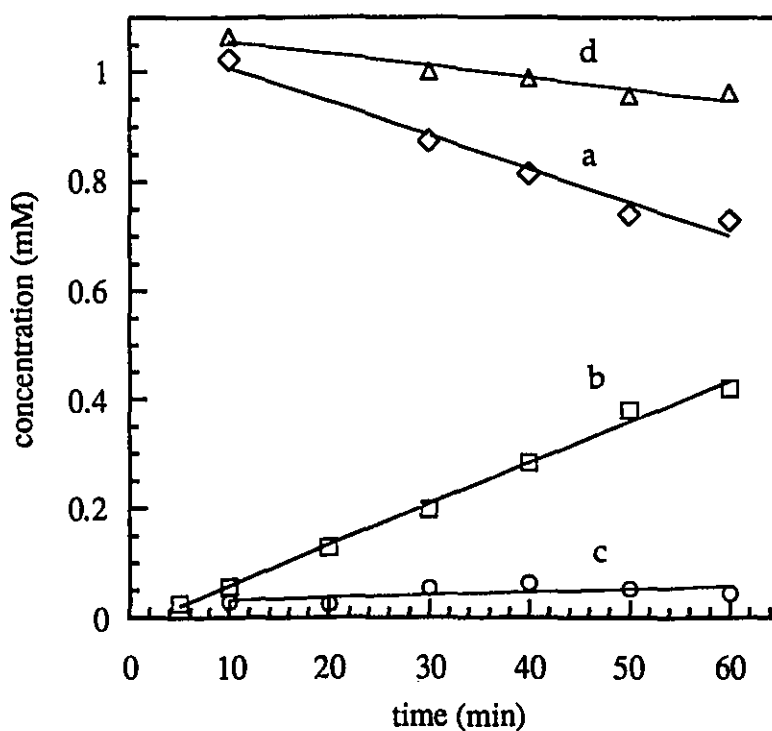


Figure 4.9 Kinetic plot showing the concentrations of: (a) dApdA; (b) dA; (c) dAMP and (d) $dApdA + (dA + dAMP)/2$ as a function of time in the cleavage of dApdA (1 mM) by $Ce(ClO_4)_3$ (20 mM), pH 8.2, 37 °C.

The phosphorous containing products can be detected by ^{31}P nmr spectroscopy. During the course of the reaction, signals due to dApdA, dAMP and inorganic phosphate can be detected and at the end of the reaction only inorganic phosphate is detected (Figure 4.10). No other phosphorous

containing species are detected during the reaction.

It is clear from analysis of the products that in the presence of Ce(III) and molecular oxygen, the DNA dinucleotide dApdA is cleanly and efficiently converted to dA and inorganic phosphate with no sign of the products expected from oxidative cleavage.

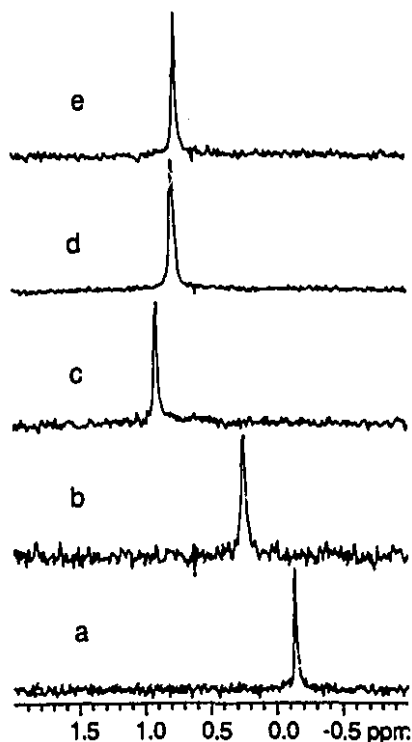


Figure 4.10 ^{31}P nmr spectra showing the products of dApdA cleavage by $\text{Ce(III)} \cdot \text{O}_2$. ^{31}P nmr spectra of authentic samples of: a) dApdA; b) 3'-dAMP; c) 5'-dAMP; d) Na_3PO_4 ; e) products of the reaction of 1 mM dApdA with 20 mM $\text{Ce(ClO}_4)_3$ at pH 8.2 after 24 hours at 37 °C. The inorganic phosphate product was released from the CePO_4 precipitate by saturating the solution with 2,6-pyridinedicarboxylic acid. All samples were prepared in D_2O saturated with 2,6-pyridinedicarboxylic acid. Chemical shifts are referenced to 85% H_3PO_4 .

4.3. Conclusion

The rapid conversion of dApdA to dA in the presence of Ce(III) and molecular oxygen with a half-life of only two hours at 37° C at pH 8.2 represents the first example of net hydrolytic cleavage of relaxed DNA (for an example of supercoiled plasmid DNA cleavage see (Basile *et al.*, 1987)) by a simple metal ion catalyst under mild conditions. The oxygen dependence of the reaction and the clean conversion of dApdA to dA and inorganic phosphate with no indication of the formation of any products normally expected from oxidative cleavage are consistent with the Ce(IV)•peroxide mechanism proposed in the previous chapter. The similar rate enhancements achieved with cerium for other structurally different phosphate diesters further supports the hypothesis that the reaction is occurring through attack at phosphorus not at oxygen or at other parts of the leaving group. In order to further test the hypothesis that the remarkably rapid cleavage of phosphate diesters with Ce(III) is due to the *in situ* generation of hydrogen peroxide and Ce(IV), cooperativity between La(III) and hydrogen peroxide was investigated and is presented in the next chapter.

4.4. Experimental

4.4.1. Chemicals

Sodium diphenyl phosphate (DPP) was purchased from Aldrich Chemical Co.. dApdA (sodium salt) was purchased from Sigma Chemical Co.. Dimethyl phosphate (DMP) was synthesized by the cleavage of trimethyl phosphate using sodium iodide in acetone.

4.4.2. DMP cleavage

The conversion of DMP to methanol was monitored by ^1H nmr spectroscopy. In a typical run, 100 μL of 0.1 M CeCl_3 and 20 μL of 1.0 M NaOH are mixed together with 0.33 mL of D_2O in a nmr tube. The white precipitate initially formed upon mixing disappears over a period of 1-5 minutes to give a clear solution with a slightly purple tinge and a pD of 8.2. At this point, 50 μL of 0.1 M DMP is added to begin the reaction. NMR spectra were recorded using a Varian XL-300 spectrometer. All chemical shifts are reported with reference to TMS. The pseudo first-order rate constant for the cleavage of DMP was calculated from the initial rate of disappearance of the DMP signal.

4.4.3. Diphenyl phosphate cleavage

The $\text{Ce(III)} \cdot \text{O}_2$ mediated cleavage of diphenyl phosphate was monitored by HPLC using a Hewlett Packard 1090 series II Liquid Chromatograph. In a typical run, 222 μmoles (121.5 mg) of $\text{Ce}(\text{ClO}_4)_3 \cdot 6\text{H}_2\text{O}$ was dissolved in 9.5 mL of water and 0.444 mL of 1.0 M NaOH was added with stirring. Once the initial precipitate had dissolved to give the clear purple solution with a pH of 8.2, 4.5 mL of this solution was mixed with 0.5 mL of 10 mM DPP. At five minute intervals, 50 μL aliquots of the reaction solution were mixed with 50 μL of 0.2 M inorganic phosphate (pH 5.5). The

cerium phosphate precipitate was spun down for 3 minutes at 13200 rpm. 1 μ L of the supernatant was then injected onto a C-18 reversed phase column (5- μ m Hypersil maintained at 40 °C) and eluted for 5 min with $\text{NH}_4\text{H}_2\text{PO}_4$ (0.2 M pH 5.5) followed by a 0-100% linear gradient of $\text{NH}_4\text{H}_2\text{PO}_4$ (0.2 M pH 5.5) and methanol/water (3:2) solutions over 10 minutes with a flow rate of 0.5 mL/min. The retention times of DPP (13.86 min), phenol (8.93 min) and phenyl phosphate (1.38 min) were all determined by injecting authentic samples of each compound.

4.4.4. dApdA cleavage

The cleavage of dApdA was monitored by HPLC using the same equipment and method described above for the cleavage of DPP. The only major difference was the solvent gradient used. The dApdA reaction mixture was injected on the column and eluted for 5 min with $\text{NH}_4\text{H}_2\text{PO}_4$ (0.2 M pH 5.5) followed by a 0-50% linear gradient of $\text{NH}_4\text{H}_2\text{PO}_4$ (0.2 M pH 5.5) and methanol/water (3:2) solutions over 10 minutes with a flow rate of 0.5 mL/min. The retention times of dApdA (11.40 min), 3'-dAMP (3.54 min), 5'-dAMP (3.73 min), dA (9.06 min) and adenine (2.54 min) were all determined by eluting authentic samples of each.

Chapter 5.

Cooperativity between La(III) and Hydrogen Peroxide in Phosphate Diester Cleavage

5.1. Introduction

The cooperativity between Ce(III) and molecular oxygen in the net hydrolytic cleavage of phosphate diesters described in chapters 2 and 3 suggest that a reduced form of molecular oxygen such as hydrogen peroxide or superoxide might be involved as a nucleophile in the cleavage of phosphate diesters. If hydrogen peroxide, formed from the combination of two equivalents of Ce(III) and molecular oxygen, is acting as a nucleophile in the Ce(III)•O₂ cleavage of DNA then one might expect to observe cooperativity between hydrogen peroxide and other lanthanide ions, such as La(III) in the cleavage of DNA analogs such as BNPP.

Although the possibility of cooperativity between lanthanide ions and hydrogen peroxide was mainly suggested by the observed cooperativity between Ce(III) and molecular oxygen, there are other reasons to believe that the addition of hydrogen peroxide could convert the lanthanide ions, already known to be effect reagents for the cleavage of RNA, into reagents capable of DNA hydrolysis as well.

Studies of *cis*-diaqua cobalt complexes have shown that the combination of Lewis Acid activation and intramolecular metal-hydroxide

nucleophilic attack results in 10^8 to 10^{10} fold rate enhancement in the hydrolysis of activated and unactivated phosphate diesters (Chin, 1991; Kim & Chin, 1992). In general, simple Lewis Acid activation by Co(III) gives two to three orders of magnitude rate enhancement for hydrolyzing phosphate diesters (Hendry & Sargeson, 1990) which suggests that the intramolecular nucleophile is responsible for the additional 10^6 - 10^8 fold rate enhancement.

The inability of La(III) to cleave DNA rapidly suggests that it does not possess a well placed metal hydroxide to act as an intramolecular nucleophile. The impressive effect of such a nucleophile in the *cis*-diaqua cobalt system suggests that if a suitable nucleophile could be incorporated into the La(III) system its effectiveness at cleaving DNA analogs could be drastically improved. In this chapter, the effectiveness of this strategy has been tested by combining the Lewis Acidity of La(III) with the nucleophilicity of hydrogen peroxide.

The hydrogen peroxide anion is known to be a strong nucleophile for a wide variety of substrates (Edwards & Pearson, 1962). Although the mechanistic explanation for the α -effect is not well understood, it has long been observed that nucleophilic groups with an electronegative atom containing one or more pairs of unshared electrons adjacent to the nucleophilic atom are unexpectedly strong nucleophiles. Examples of nucleophiles displaying this effect include hydrazine, hydroxylamine, hydroxamic acids, the anions of peroxides and hydrogen peroxide, hypochlorite ion and oxime anions.

In addition to being a good nucleophile, it is also quite likely that the peroxide anion is a good ligand for the oxophilic La(III) and would therefore bind well to the metal ion and make a cooperative interaction between the La(III) and hydrogen peroxide more likely.

The combination of metal ions and hydrogen peroxide to produce a nucleophilic peroxide is perhaps unexpected since peroxidase enzymes and model systems designed to mimic these enzymes involve a peroxide coordinated to metal ions where the peroxide acts as an electrophile (Tyeklar & Karlin, 1989). However, there have been some recent surprising results which demonstrate that a metal coordinated peroxide can also act as a nucleophile and bring about the cleavage of biopolymers.

Rana and Meares (1990; 1991a) discovered that cooperativity between an Fe•EDTA complex and hydrogen peroxide resulted not in the expected oxidative cleavage but in site specific hydrolytic cleavage of the amide linkage of a protein. Labeled oxygen experiments revealed that oxygen from the hydrogen peroxide was incorporated into the carboxylate terminus of the peptide fragment suggesting that the peroxide acted as a nucleophile (Rana & Meares, 1991).

During the course of a footprinting experiment using Fe•EDTA and HOOH to effect oxidative cleavage of exposed parts of the target DNA strand, Kimball *et al.* (1993) discovered that cooperativity between Flp recombinase and hydrogen peroxide resulted in the site specific hydrolytic cleavage of DNA. They proposed that the enzyme assists in the nucleophilic attack of hydrogen peroxide upon the phosphate backbone of DNA resulting in the site specific scission of one P-O bond.

These recent findings combined with the results presented in this chapter showing impressive cooperativity between La(III) and HOOH support the hypothesis presented in the chapter 3 where it was proposed that the enormous cooperativity between Ce(III) and molecular oxygen is due to the generation of a ceric peroxide species which rapidly cleaves DNA through nucleophilic attack of the peroxide upon the coordinated substrate. The

La(III) peroxide cooperativity also points to a new approach in the design of artificial nucleases capable of rapid cleavage of DNA without the destruction of the deoxyribose expected from oxidative cleavage.

5.2. Results and Discussion

5.2.1. Lanthanide Ions and Hydrogen Peroxide Cooperativity

The pseudo first-order rate constants for $\text{La}(\text{ClO}_4)_3$ (2 mM) promoted hydrolysis of BNPP (bis(*p*-nitrophenyl)phosphate) with and without hydrogen peroxide at pH 7.0 (50 mM HEPES), 25 °C were determined by monitoring the increase in visible absorbance at 400 nm due to *p*-nitrophenoxide formation. Cleavage of BNPP gave two equivalents of nitrophenol with no significant accumulation of *p*-nitrophenylphosphate. The progress of BNPP cleavage was also monitored by ^{31}P NMR. During the course of the reaction, there are ^{31}P NMR signals corresponding to inorganic phosphate (δ 0.77) and BNPP (δ -10.57) with a weak signal due to *p*-nitrophenylphosphate (δ -1.14). At the end of the reaction, only the signal due to inorganic phosphate remains. As shown in Table 5.1, La(III) (2 mM) alone provides a 3,900 fold increase in the rate of hydrolysis of BNPP while a mixture of La(III) (2 mM) and hydrogen peroxide (20 mM) provides an additional 34,000 fold rate enhancement resulting in a total of 1.3×10^8 fold rate enhancement over the background rate. Hydrogen peroxide (20 mM) alone at the same temperature and pH gave no detectable hydrolysis of BNPP after 24 hrs.

Similar cooperativity between lanthanide ions and hydrogen peroxide was observed for all other lanthanide ions tested (see Table 5.2) with the exception of Ce(III). When hydrogen peroxide was added to a solution of Ce(III) the solution immediately turned red which is most likely due to the

oxidation of Ce(III) to the bright red Ce(IV) ion by hydrogen peroxide. This red color prevented the observation of BNPP hydrolysis by UV-vis spectroscopy; furthermore, the reduction of hydrogen peroxide by Ce(III) produced reactive hydroxyl radicals which resulted in many side reactions.

Table 5.1. Relative Rates of Hydrolysis of BNPP at 25° C in pH 7.0, 50mM HEPES buffer.

catalyst	k_{obs} (s ⁻¹)	relative rate
none ^a	1.1×10^{-11}	1.0
2 mM La(III)	$1.4 \pm 0.05 \times 10^{-7}$	1.3×10^4
2 mM La(III) + 20 mM HOOH	$4.8 \pm 0.02 \times 10^{-3}$	4.4×10^8

^a(Chin *et al.*, 1989)

Table 5.2 Pseudo First-Order Rate Constants for the Cleavage of BNPP by 2 mM Ln(III) in the Presence and Absence of Hydrogen Peroxide at pH 7.0 in 0.1 M HEPES Buffer at 25°C.

Lanthanide ion	k_{obs} (s ⁻¹) no HOOH	k_{obs} (s ⁻¹) 20 mM HOOH
Pr(III)	$5.1 \pm 0.02 \times 10^{-6}$	$7.2 \pm 0.04 \times 10^{-3}$
Nd(III)	$5.3 \pm 0.04 \times 10^{-6}$	$7.2 \pm 0.02 \times 10^{-3}$
Eu(III)	$9.4 \pm 0.03 \times 10^{-6}$	$3.7 \pm 0.08 \times 10^{-3}$

5.2.2. Other Phosphate Diesters

Unfortunately, the eight orders of magnitude rate enhancement observed in the hydrolysis of BNPP using La(III) and hydrogen peroxide could not be extended to much less reactive phosphate diesters. The cleavage of diphenylphosphate proceeds rapidly during the first 30 minutes but slows

down drastically after the first hour (Figure 5.1). It appears that the active form of the La(III)•peroxide complex is unstable and decomposes after 30-50 minutes.

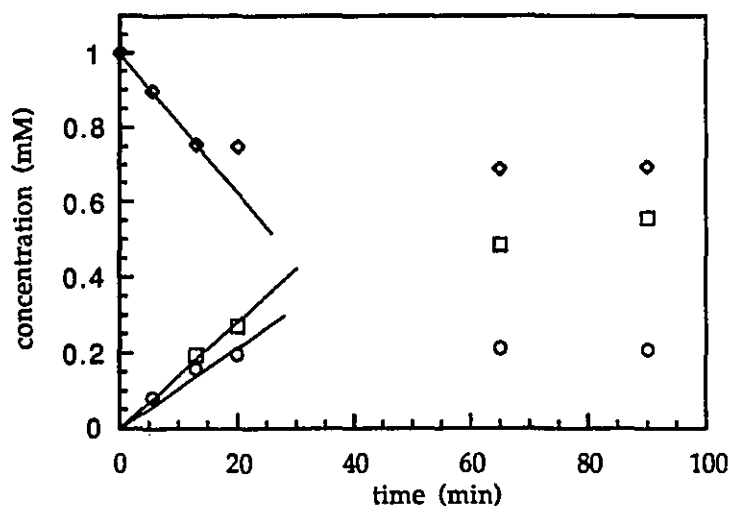


Figure 5.1 Kinetic plot showing the rate of DPP (1 mM) cleavage by La(III) (20 mM) and HOOH (100 mM) at pH 8.0 (0.1 M HEPES) at 25 °C. The diamonds represent DPP; the squares, phenol; the circles, phenylphosphate.

Although the lanthanum peroxide active species is not stable enough to completely cleave DPP it is still able to cleave 2',3'-cAMP. This phosphate diester has poor leaving groups but is much more reactive than dApdA because of ring strain in the phosphorus containing 5-membered ring which makes it much more reactive (Haake & Westheimer, 1961; Thatcher & Kluger, 1989).

In the presence of 5 mM La(ClO₄)₃ alone at pH 8.0 at 25 °C, 2',3'-cAMP is cleaved with a pseudo first-order rate constant of $0.084 \pm 0.006 \text{ min}^{-1}$; while, in the presence of 5 mM La(III) and 50 mM HOOH the rate constant increases to $1.5 \pm 0.1 \text{ min}^{-1}$ (Figure 5.2). This 18-fold increase upon addition of hydrogen peroxide is significantly less than the 34,000 fold increase observed

in the cleavage of BNPP. The relatively small cooperativity between La(III) and HOOH in the ring-opening of 2',3'-cAMP suggests that the hydrogen peroxide might be playing a different role in this case. It may be that the hydrogen peroxide does not act as a nucleophile but rather as a general base assisting the attack of water or the peroxide may simply act as a bridging ligand bringing together two lanthanide ions which then provide double Lewis Acid activation of a doubly coordinated 2',3'-cAMP molecule.

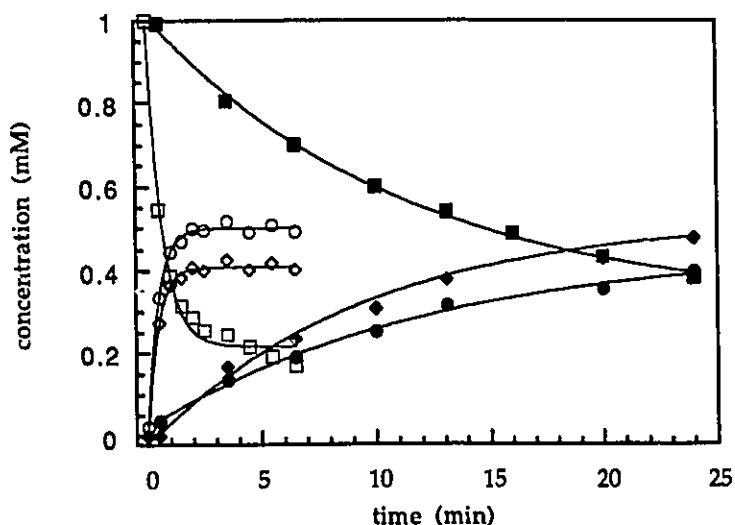


Figure 5.2 Kinetic plot showing the effect of La(III) with and without hydrogen peroxide on the ring opening of 2',3'-cAMP (1 mM) at pH 8.0 (0.1 M HEPES) at 25 °C. The open symbols represent the reaction in the presence of La(III) (5 mM) and hydrogen peroxide (50 mM) while the closed symbols represent the reaction in the presence of La(III) (5 mM) without hydrogen peroxide. The squares represent 2',3'-cAMP; the circles, 2'-AMP; the diamonds, 3'-AMP.

5.2.3. pH Dependence

In order to gain a clearer understanding of the mechanism of this remarkable cooperativity between La(III) and hydrogen peroxide the pH

dependence of the rate of reaction and the effect of added hydrogen peroxide on the potentiometric titration of La(III) were examined and compared.

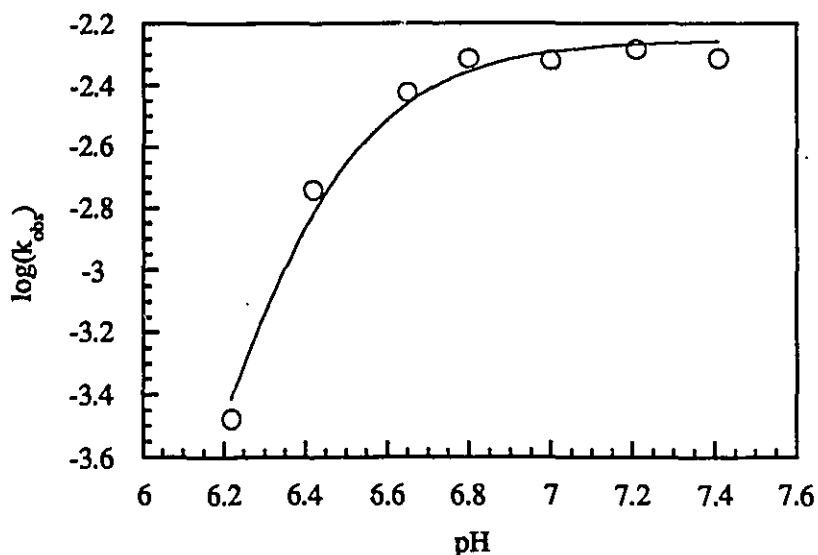


Figure 5.3 pH-rate profile for the La(III)•HOOH mediated cleavage of BNPP. Reactions were performed at 25° C in 0.1 M NaClO₄ in 0.10 M HEPES pH 7.0 buffer. The curve is calculated according to eq. (5.3).

The pH-rate profile of the hydrolysis of BNPP in the presence of both La(III) and hydrogen peroxide (Figure 5.3) indicates a very steep dependence on hydroxide ion in the pH range 6.8-7.2 which then reaches a plateau above pH 7.2.

In the potentiometric titration of La(ClO₄)₃, the hydrolysis of the aqueous La(III) ion gives rise to a sharp equivalence point with a midpoint at pH 9.5 (Figure 5.4a). Although a number of different hydrolysis products are likely formed in this titration (Biedermann & Ciavatta, 1961), at the equivalence point a total of two equivalents of NaOH are consumed per equivalent of La(III).

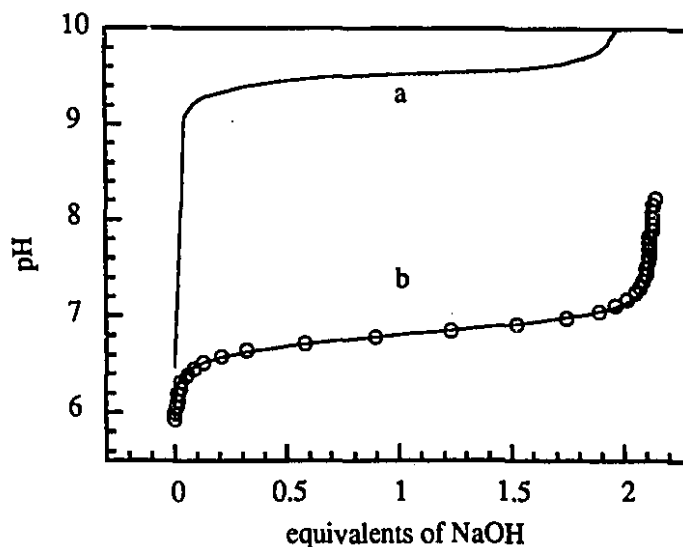


Figure 5.4 Potentiometric titration of $\text{La}(\text{ClO}_4)_3$ (2 mM in 0.1 M NaClO_4) in the a) absence and b) presence of 20 mM HOOH at 25° C. The solid curve is calculated according to (5.6).

In the presence of one equivalent or more of hydrogen peroxide, the equivalence point shifts to lower pH with a midpoint at (pH 6.9) and still consumes two equivalents of base (Fig. 5.4b). The shift to lower pH suggests that it is now the more acidic hydrogen peroxide bound to the $\text{La}(\text{III})$ which is deprotonated. Two equivalents of base are consumed which indicates that both protons of the bound hydrogen peroxide are titrated giving rise to the $\text{La}(\text{III})$ bound peroxide dianion ($\text{La}_x(\text{O}-\text{O})_x$).

The close agreement between the apparent pK_a of the bound peroxide (pK_a 6.9) and the inflection point of the pH-rate profile (pH 6.9) strongly suggests that it is the $\text{La}(\text{III})$ bound peroxide dianion which is the reactive species responsible for the rapid cleavage of the phosphate diester.

The simplest model which is consistent with the pH-rate dependence and the potentiometric titration involves the monomeric $\text{La}(\text{III})$ bound

peroxide dianion (LaO_2)⁺; however, the steepness of both the pH-rate profile and the titration curve suggests that a dimeric form (La_2O_4)²⁺ is the active species (Takasaki & Chin, 1993).

5.2.4. Concentration Dependence

In order to differentiate between these two possible active La(III)•HOOH species (the monomer and dimer), the dependence of the rate of reaction on the concentration of La(III) and hydrogen peroxide was studied (Figures 5.5 & 5.6). The observed second-order dependence of the rate constant on the concentrations of both La(III) and hydrogen peroxide at low concentrations strongly support the proposal that it is a La(III)-peroxide dimer which is the active species.

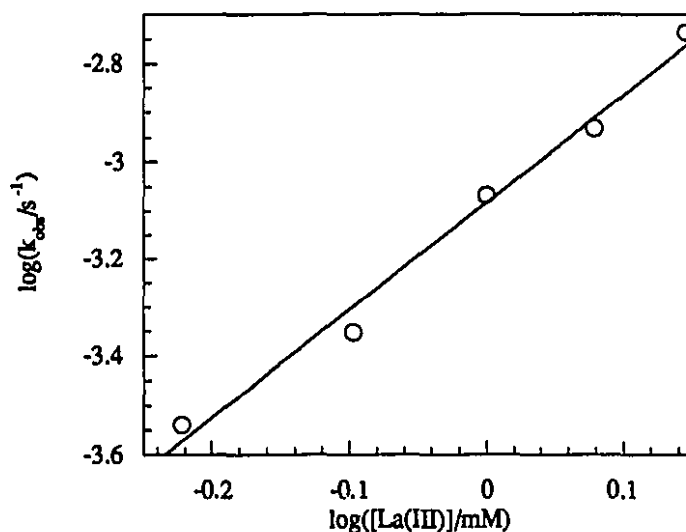


Figure 5.5 Dependence of the log of the pseudo first-order rate constant for the cleavage of BNPP on the log of the concentration of La(III) in the presence of 30 mM hydrogen peroxide at pH 7.0 (0.1 M HEPES) at 25° C (slope=2.2 ± 0.2).

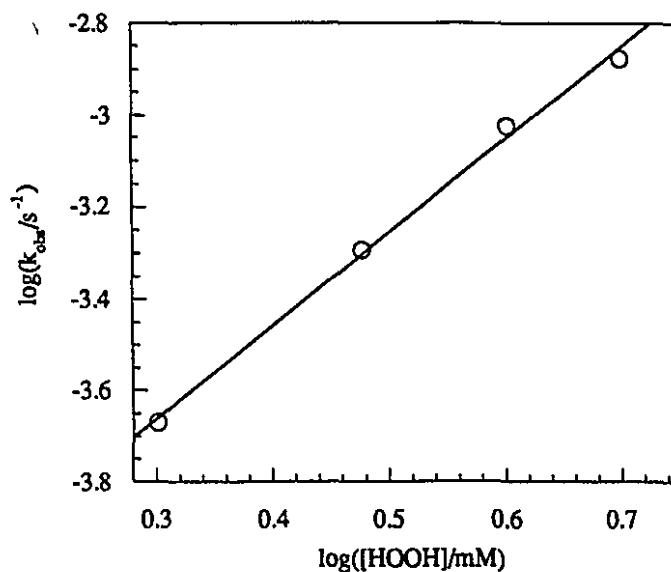
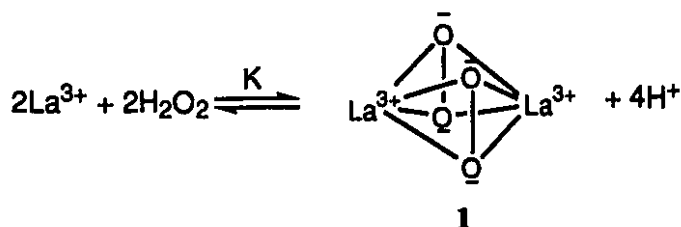


Figure 5.6 Dependence of the log of the pseudo first-order rate constant for the cleavage of BNPP on the log of the concentration of hydrogen peroxide in the presence of 30 mM La(III) at pH 7.0 (0.1 M HEPES) at 25° C (slope=2.02 ± 0.09).

If the La(III)-peroxide dimer is the reactive species responsible for the observed cooperativity between La(III) and hydrogen peroxide then it should be possible to propose a simple mechanistic scheme incorporating the proposed active species which can be used to fit all of the data.

5.2.5. Proposed Mechanism

Scheme 5.1



$$K = \frac{[1][H]^4}{[La]^2[H_2O_2]^2} \quad (5.1)$$

The simplest mechanistic scheme (Scheme 5.1) which fits the titration, pH-rate profile and the concentration dependence data involves the formation of the dimeric La(III)-peroxide complex (1) in a single equilibrium releasing four protons upon binding. (As discussed earlier for the ceric peroxide complex (section 3.9), the La(III) may bind the peroxide in a $\mu\text{-}\eta^2\text{:}\eta^2$ fashion as shown in Scheme 5.1 (1) or in a $\mu\text{-}1,2$ fashion.)

The concentration of free La(III) ($[La]_f$) can be calculated from the total La(III) concentration ($[La]_t$) and that of the active dimer ([1]).

$$[La]_f = [La]_t - 2[1] \quad (5.2)$$

Substitution of (5.2) into (5.1) yields (5.3)

$$K = \frac{[1][H]^4}{([La]_t - 2[1])^2[H_2O_2]^2} \quad (5.3)$$

Rearrangement of (5.3) yields the quadratic equation (5.4)

$$[1]^2 4K[H_2O_2]^2 + [1](-[H]^4 - 4[La]_t K[H_2O_2]^2) + [La]_t^2 K[H_2O_2]^2 = 0 \quad (5.4)$$

(5.4) can be solved for [1] using the quadratic formula to give (5.5).

$$[1] = \frac{[H]^4 + 4[La]_t K[H_2O_2]^2 - [H]^2 \sqrt{[H]^4 + 8[La]_t K[H_2O_2]^2}}{8K[H_2O_2]^2} \quad (5.5)$$

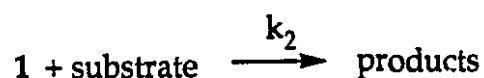
In the potentiometric titration of La(III) in the presence of hydrogen peroxide, four protons are titrated for every equivalent of 1 and so the concentration of added hydroxide ion [OH⁻] should equal four times [1]. Therefore the potentiometric titration data can be fit according to (5.6).

$$[\text{OH}^-] = 4[1] = \frac{[\text{H}]^4 + 4[\text{La}]_t K[\text{H}_2\text{O}_2]^2 - [\text{H}]^2 \sqrt{[\text{H}]^4 + 8[\text{La}]_t K[\text{H}_2\text{O}_2]^2}}{2K[\text{H}_2\text{O}_2]^2} \quad (5.6)$$

Figure 5.4 shows the titration data with the calculated curve fit according to Scheme 5.1 using (5.6) where [OH⁻] is the added titrant and the best fit is obtained with a calculated value of $K=3.6 \times 10^{-22}$ M.

The pH-rate profile data (Figure 5.3 & table 5.3) can also be fit according to Scheme 5.1 if we assume that the reactive La(III)-peroxide dimer (1) reacts with the substrate with a second-order rate constant (k_2) to give the products according to Scheme 5.2.

Scheme 5.2



The rate of reaction can then be expressed as:

$$v = k_2 [1][\text{substrate}] \quad (5.7)$$

If we assume that the concentration of 1 is much greater than the concentration of substrate then the pH-dependence of the observed pseudo-first-order rate constant can be expressed according to (5.8).

$$k_{obs} = k_2[1] = k_2 \frac{[H]^4 + 4[La]_t K [H_2O_2]^2 - [H]^2 \sqrt{[H]^4 + 8[La]_t K [H_2O_2]^2}}{8K[H_2O_2]^2} \quad (5.8)$$

Figure 5.3 shows the pH rate profile of the reaction with the calculated curve fit according to (5.8). The best fit is obtained with calculated values of $k_2=4.1 \text{ M}^{-1}\text{s}^{-1}$ and $K=6.6 \times 10^{-21} \text{ M}$.

As shown in Figures 5.3 and 5.4, the calculated curves fit according to the equations derived from Scheme 5.1 provide a good fit to both the pH rate profile and the potentiometric titration data. Furthermore, the value of the equilibrium constant for formation of the complex (K) obtained from fitting the titration curve ($3.6 \times 10^{-22} \text{ M}$) is in satisfactory agreement with that obtained from fitting the pH-rate profile ($6.6 \times 10^{-21} \text{ M}$).

5.2.6. Substrate Binding

Scheme 5.2 describes the reaction of the active complex 1 with the substrate as a bimolecular reaction (k_2) leading directly to products. This scheme is useful for describing the pH-rate profile as well as the La(III) and hydrogen peroxide concentration data at low concentrations; however, at higher concentrations of La(III) the value of k_{obs} begins to level off (Figure 5.7) which is not predicted by Scheme 5.2. This saturation behavior is consistent with a mechanism which involves the formation of a complex (1.S) between the substrate (BNPP) and the active complex (1) followed by the reaction of the bound substrate (1.S) as shown in Scheme 5.3.

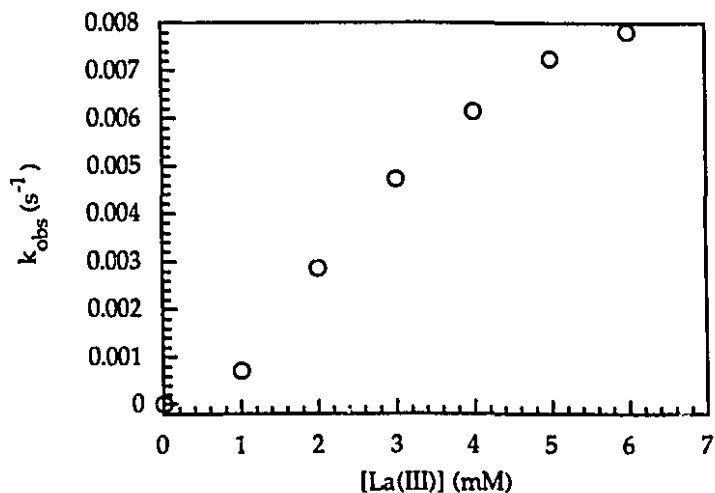
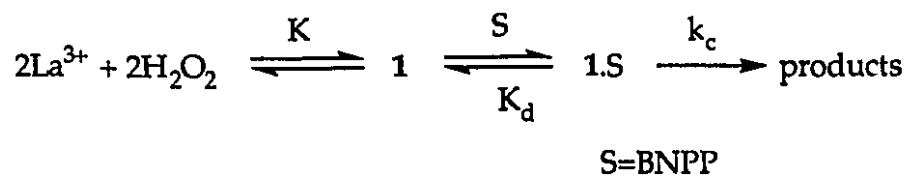


Figure 5.7 Dependence of the pseudo first-order rate constant for the cleavage of BNPP on the concentration of La(III) (0-6 mM) in the presence of 30 mM hydrogen peroxide at pH 7.0 (0.10 M HEPES) at 25° C.

Scheme 5.3



The rate equation (5.9) derived from Scheme 5.3 can be expressed as:

$$v = k_c[\mathbf{1.S}] \quad (5.9)$$

$$K_d = [\mathbf{1}][S] / [\mathbf{1.S}] \quad (5.10)$$

The concentration of substrate ([S]) can be expressed in terms of the total substrate concentration ([S]_T) and the complex ([1.S]).

$$[S] = [S]_T - [1.S] \quad (5.11)$$

Substitution of (5.11) into (5.10) and rearrangement gives (5.12).

$$[1.S] = [1][S]_T / (K_d + [1]) \quad (5.12)$$

Substitution of (5.12) into (5.9) and integration gives (5.13).

$$k_{\text{obs}} = k_c[1] / (K_d + [1]) \quad (5.13)$$

If we assume that the concentration of substrate (5.0×10^{-5} M) is low enough that complexation with **1** is not sufficient to perturb the equilibrium governing the formation of **1** then (5.5) can be used to calculate the concentration of **1** for the experimental total concentrations of La(III). The values for the concentration of **1** listed in Appendix 5.1 Table 5.1.4 were calculated using (5.5). The value of $K = 2.3 \pm 1 \times 10^{-23}$ M was estimated by fitting equation (5.8) to part of the data ($[La(III)] = 0-3$ mM) shown in Table 5.1.4.

When k_{obs} is plotted vs. the concentration of **1** rather than that of La(III), the S-shaped curve (Figure 5.7) is converted to a saturation curve (Figure 5.8) which can be described by (5.13). The non-linear least-squares fit of (5.13) to the data shown in Figure 5.8 yields values of 0.015 ± 0.0002 s⁻¹ and 1.5 ± 0.01 mM respectively for k_c and K_d .

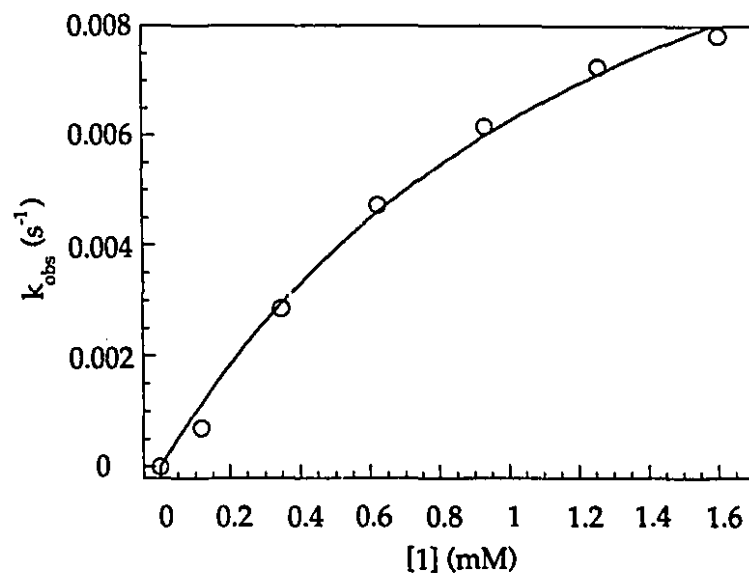


Figure 5.8 The dependence of k_{obs} on the calculated concentration of 1.

The value of 0.015 s^{-1} for the first-order rate constant for the reaction of BNPP bound to 1 is approximately 10^9 times greater than that observed for the hydrolysis of BNPP in the absence of any catalyst. This value is comparable to that observed for *cis*-diaqua cobalt complexes.

The binding of BNPP to 1 ($K_d=1.5 \text{ mM}$) appears to be approximately twelve times stronger than that of the binding of HPNPP to La(III) ($K_d=18.5 \text{ mM}$). The structural differences between BNPP and HPNPP are not likely to cause significant differences in binding to a metal ion so it is more likely that the difference in binding is due to the difference in the structure of 1 as compared to La(III). As discussed chapter 3, there is no evidence of a second-order dependence on Ln(III) concentration in the Ln(III) promoted cleavage of HPNPP and the mechanism most likely involves simple Lewis Acid activation of the substrate through coordination to a single Ln(III) ion. In the case of the dimeric La-peroxide species (1), the arrangement of the two La(III) ions might be such that the phosphate diester can coordinate to both of the

metal ions in a fashion similar to that observed in the crystal structures of CeL₁ with dimethyl phosphate (Figures 2.1 & 2.2). This type of double coordination would likely account for the stronger binding of the substrate to **1**.

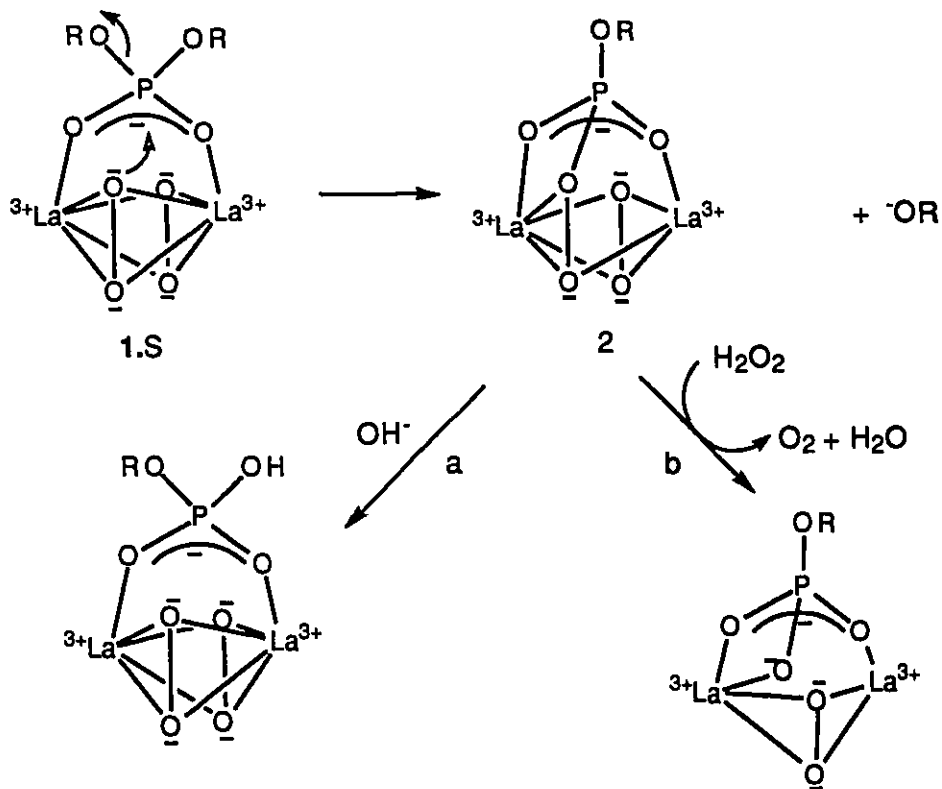
5.3. Proposed Mechanism

The strong Lewis acidity of La(III) is sufficient to cleave RNA rapidly under physiological conditions (Komiya et al., 1992); however, its inability to rapidly cleave DNA or DNA analogs suggests that unlike *cis*-diaqua cobalt complexes, it does not possess a metal hydroxide well positioned for nucleophilic attack upon the phosphorus.

It has long been known that the peroxide anion is a strong nucleophile which can lead to rapid cleavage of phosphate ester bonds. Complexation of hydrogen peroxide with La(III) affords the dianion of this nucleophile at neutral pH, which when combined with the strong Lewis acidity of La(III) should produce an efficient catalyst. This is confirmed by the impressive rate enhancement achieved by combining La(III) and hydrogen peroxide as well as the close agreement between the midpoint of the potentiometric titration and the inflection point of the pH rate profile which suggests that indeed the La(III) bound peroxide dianion is the active form of the catalyst. The fourth order dependence on hydroxide ion below the apparent pK_a of 7.2, the steepness of the titration curve and the second-order dependence of the rate on both the La(III) and hydrogen peroxide concentrations all suggest that the active form of the catalyst is the dimeric [La₂(O-O)₂]²⁺ complex (**1**).

The saturation behavior observed at higher concentrations of **1** (Figure 5.6) is consistent with the formation of a complex of substrate tightly bound to **1**. The strong binding of BNPP to **1** is most likely due to double coordination of the phosphate ester to **1**.

Scheme 5.4



A possible mechanism for 1-catalyzed cleavage of BNPP (Scheme 5.4) involves intramolecular La-peroxide attack on the doubly coordinated phosphate diester (1.S) which then loses the *p*-nitrophenoxide leaving group to give the coordinated peroxyphosphate intermediate 2. The peroxyphosphate 2 may decompose to give the observed hydrolytic products by one of two pathways. Attack by hydroxide ion followed by loss of the peroxide leaving group (path a) or reduction of the peroxyphosphate to phosphate by disproportionation with hydrogen peroxide (path b) (Epstein *et al.*, 1956; Larsson, 1958).

Pathway (a) and (b) were distinguished by ¹⁸O labeling experiments using H₂¹⁸O or H₂¹⁸O₂. In pathway (a), the displacement of peroxide by

hydroxide would lead to incorporation of labeled oxygen into the inorganic phosphate product from labeled water but not from labeled hydrogen peroxide. However, the reduction of the peroxyphosphate by hydrogen peroxide in pathway (b) would lead to incorporation of labeled oxygen into the inorganic phosphate from labeled hydrogen peroxide but not from labeled water.

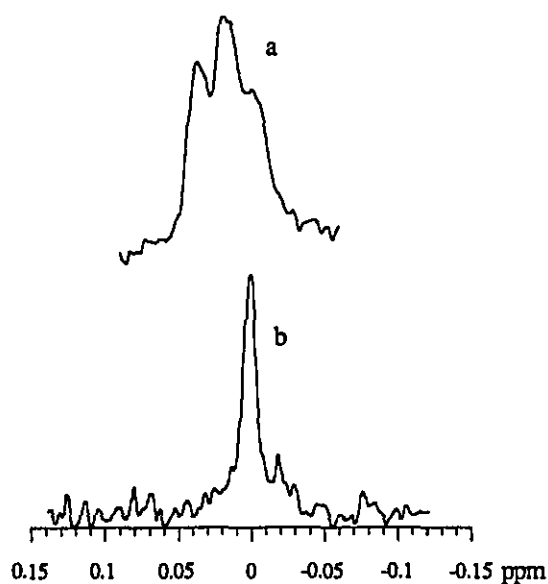


Figure 5.9 ^{31}P nmr spectrum showing the product of BNPP (2 mM) hydrolysis by La(III) (2 mM) and HOOH (50 mM) at pH 7.0 (0.1 M HEPES) (a) using 50% $\text{H}_2^{18}\text{O}_2$ and 50% H_2O_2 in D_2O ; (b) in 50% H_2^{18}O , 50% D_2O . The reaction was quenched after 1 hr. by the addition of an excess of 2,6-pyridine dicarboxylic acid.

The incorporation of ^{18}O into inorganic phosphate can be detected by ^{31}P nmr spectroscopy. Incorporation of ^{18}O into inorganic phosphate results in a 0.02 ppm upfield shift of the phosphate signal (Cohn & Hu, 1978; Lowe & Sproat, 1978). When BNPP (2mM) was allowed to react with La(III) (5 mM) and HOOH (50 mM) for 30 minutes in pH 7.0 buffer (0.1 M HEPES) in 50% H_2^{18}O , 50% D_2O the inorganic phosphate peak appeared as a sharp singlet with only a small peak representing less than 1% of the total area corresponding to

incorporation of one ^{18}O (Figure 5.9a). When the same reaction was performed using 50% $\text{H}_2^{18}\text{O}_2$, 50% H_2O_2 in D_2O , the inorganic phosphate peak appeared as a triplet (Figure 5.9b) with a 1:2:1 ratio of $\text{P}^{16}\text{O}_4^{3-} : \text{P}^{16}\text{O}_3^{18}\text{O} : \text{P}^{16}\text{O}_2^{18}\text{O}_2$ clearly demonstrating incorporation of ^{18}O from $\text{H}_2^{18}\text{O}_2$ into the inorganic phosphate product. The incorporation of two labeled oxygen atoms into the phosphate product and the 1:2:1 ratio of products suggests that both the BNPP and the intermediate *p*-nitrophenylphosphate are cleaved through nucleophilic attack of hydrogen peroxide.

The incorporation of labeled oxygen from the peroxide and the lack of incorporation of labeled oxygen from the solvent into the inorganic phosphate product favors pathway (b) and is consistent with the results obtained in the peroxide catalyzed cleavage of phosphate triesters (Epstein *et al.*, 1956; Larsson, 1958).

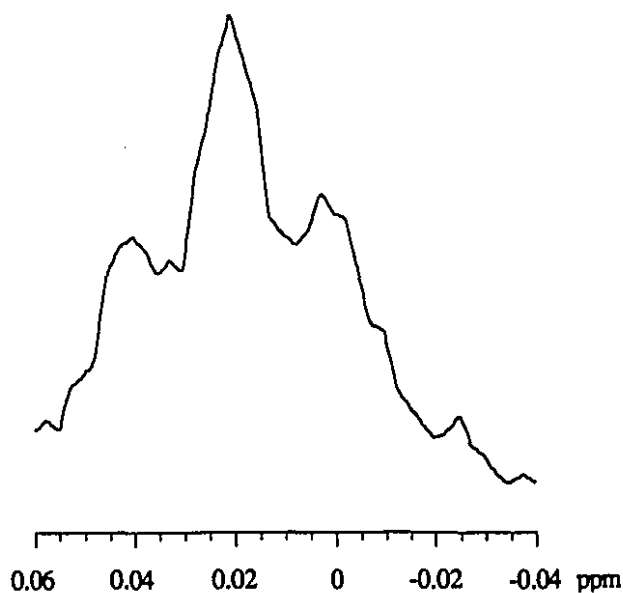


Figure 5.10 ^{31}P nmr spectrum showing the inorganic phosphate product of BNPP (4mM) cleavage in the presence of $\text{Ce}(\text{ClO}_4)_3$ (20 mM) and NaOH (40 mM) in the presence of molecular oxygen in 50% H_2^{18}O and 50% D_2O . The Ce(III) was removed by complexation with EDTA after 30 minutes at 20 °C.

When BNPP (4 mM) was mixed with $\text{Ce}(\text{ClO}_4)_3$ (20 mM) and NaOH (40 mM) in the presence of molecular oxygen for 30 minutes at 20 °C in 50% H_2^{18}O , 50% D_2O the inorganic phosphate peak appeared as a triplet (Figure 5.10). This clearly indicates that labeled oxygen was incorporated from the solvent into the inorganic phosphate product. This suggests that in the case of the $\text{Ce}(\text{III})\cdot\text{O}_2$ mediated cleavage of BNPP, if the reaction involves nucleophilic attack by peroxide upon the coordinated BNPP (as described in chapter 3) the peroxyphosphate intermediate must decompose through displacement of the peroxide by hydroxide (pathway a, Scheme 5.4).

The incorporation of labeled oxygen from the water into the product is also consistent with Ce(III) or Ce(IV) promoted hydrolysis of BNPP where hydroxide rather than peroxide acts as a nucleophile; however, this does not explain why $\text{Ce}(\text{III})\cdot\text{O}_2$ cleaves BNPP 10^5 faster than the other lanthanide ions.

The proposal that, in the case of $\text{La}(\text{III})\cdot\text{HOOH}$ mediated cleavage of BNPP, the peroxyphosphate intermediate decomposes through disproportionation with hydrogen peroxide (Scheme 5.4a) whereas in the $\text{Ce}(\text{III})\cdot\text{O}_2$ system the same intermediate decomposes through an alternative mechanism (Scheme 5.4b) is reasonable since in the $\text{Ce}(\text{III})\cdot\text{O}_2$ system there is no excess hydrogen peroxide in solution available to reduce the peroxyphosphate.

5.4. Conclusion

The 34,000 fold increase in the rate of hydrolysis of BNPP upon the addition of 50 mM of hydrogen peroxide to 5 mM La(III) represents the first example of cooperativity between a metal ion and hydrogen peroxide in the hydrolysis of a phosphate diester. Analysis of the pH dependence, La(III) and

HOOH concentration dependence and the effect of hydrogen peroxide on the potentiometric titration of La(III) all indicate that it is a lanthanum dimer bridged by two peroxide dianions which is responsible for the rapid cleavage of BNPP. Incorporation of labeled oxygen from $\text{H}_2^{18}\text{O}_2$ into the inorganic phosphate product indicates that the coordinated peroxide dianion acts as a nucleophile and attacks the bound phosphate diester substrate which then releases a *p*-nitrophenoxide leaving group. The peroxyphosphate intermediate is then reduced to the phosphate by disproportionation with another equivalent of hydrogen peroxide.

The enormous cooperativity between La(III) and hydrogen peroxide lends support to the hypothesis that it is cooperativity between Ce(IV) and peroxide generated *in situ* from Ce(III) and molecular oxygen which is responsible for the reactivity of Ce(III) in the presence of molecular oxygen. It also suggests that by incorporating a peroxide nucleophile, La(III) and other metal ion catalysts can be transformed into a catalyst which rapidly cleaves DNA.

Very shortly after publication of our La(III) peroxide results (Takasaki & Chin, 1993), Schnaith *et al.* (1994) reported very similar cooperativity between a dinuclear iron complex and molecular oxygen in the hydrolytic cleavage of supercoiled plasmid DNA. They observe rapid hydrolytic cleavage of both strands of the plasmid to produce a linear piece of duplex DNA which could be religated by T4 DNA ligase. They propose that the mechanism involves nucleophilic attack of metal bound peroxide on the phosphodiester resulting in cleavage of the phosphate diester linkage with no destruction of the deoxyribose ring.

5.5. Experimental

5.5.1. Chemicals

$\text{La}(\text{ClO}_4)_3 \cdot 6\text{H}_2\text{O}$ and other lanthanide ion salts were purchased from Strem Chemicals and used as purchased. 30% Hydrogen peroxide was purchased from the A&C Chemical Company. The concentration of hydrogen peroxide of the stock solution was determined by titration with ceric ammonium nitrate. BNPP was purchased from Sigma Chemicals. H_2^{18}O and $\text{H}_2^{18}\text{O}_2$ were purchased from ICON Chemicals Inc..

5.5.2. UV-vis kinetics

The cleavage of BNPP was followed by monitoring the increase in absorbance at 400 nm due to the formation of the *p*-nitrophenoxide ion. All absorbance measurements were made on a Hewlett Packard HP 8452A UV-vis spectrophotometer equipped with a seven cell transport and jacketed cells attached to a circulating water bath for temperature control.

The data were acquired and saved using the Hewlett Packard software. All data analysis was done using software I developed using the Borland C++ programming environment. Rate constants were calculated by a non-linear least-squares fit of the first-order rate equation to the absorbance data. All reported rate constants are based on the analysis of 30-300 points representing at least 90% reaction.

5.5.3. Cleavage of 2',3'-cAMP

Cleavage of 2',3'-cAMP was monitored by HPLC using a Hewlett Packard 1090 series II Liquid Chromatograph. In a typical run, the $\text{La}(\text{III})$ (5 mM), hydrogen peroxide (50 mM) and 2',3'-cAMP (1 mM) were mixed in 0.1 M HEPES buffer (pH 8.0). At regular intervals, 50 μL aliquots of the reaction

solution were mixed with 50 μ L of 0.2 M inorganic phosphate (pH 5.5). The lanthanum phosphate precipitate was spun down for 3 minutes at 13200 rpm. 1 μ L of the supernatant was then injected onto a C-18 reversed phase column (5- μ m Hypersil maintained at 40 °C) and eluted for 5 min with $\text{NH}_4\text{H}_2\text{PO}_4$ (0.2 M pH 5.5) followed by a 0-100% linear gradient of $\text{NH}_4\text{H}_2\text{PO}_4$ (0.2 M pH 5.5) and methanol/water (3:2) solutions over 15 minutes with a flow rate of 0.5 mL/min. The retention times of 2',3'-cAMP (7.58 min), 2'-AMP (8.12 min), 3'-AMP (3.56 min) were all determined by injecting authentic samples of each compound.

5.5.4. ^{31}P nmr

Nmr spectra were recorded using a Varian XL-300 spectrophotometer. All reported chemical shifts are with respect to an external reference of 85% H_3PO_4 .

5.5.5. Potentiometric Titrations

All potentiometric titrations were performed using a Radiometer automated titration system. The raw data obtained from a strip chart recorder were digitized and transferred to an Apple Macintosh computer by first scanning the titration curve using the Apple Ofoto hardware and software. The pict file generated by Ofoto was then translated to Cartesian coordinates using the Flex-Trace application. These data points were then transferred to the Kaleidagraph application where the data were plotted and a non-linear least squares routine was used to fit the appropriate equation to the data.

Appendix 5.1 Pseudo First-Order Rate Constants

Table 5.1.1 pH-rate data for the hydrolysis of BNPP at 25° C in pH 7.0 0.10 M HEPES buffer and 0.10 M NaClO₄.

pH	$k_{\text{obs}} \times 10^3 \text{ (s}^{-1}\text{)}$	$\log(k_{\text{obs}})$
6.22	0.333 ± 0.02	-3.48
6.42	1.81 ± 0.009	-2.74
6.65	3.75 ± 0.008	-2.43
6.80	4.84 ± 0.01	-2.32
7.00	4.7 ± 0.01	-2.32
7.21	5.17 ± 0.02	-2.29
7.41	4.85 ± 0.01	-2.31

Table 5.1.2 La(III) Concentration Dependence of the Pseudo First-Order Rate Constant for the Cleavage of BNPP in the Presence of 30 mM Hydrogen Peroxide at pH 7.0 (0.10 M HEPES) at 25° C (data plotted in Figure 5.5).

[La(III)] (mM)	$k_{\text{obs}} \times 10^3 \text{ (s}^{-1}\text{)}$	$\log(k_{\text{obs}}/\text{s}^{-1})$
0.600	0.289 ± 0.002	-3.54
0.800	0.445 ± 0.004	-3.35
1.00	0.854 ± 0.004	-3.07
1.20	1.17 ± 0.006	-2.93
1.40	1.83 ± 0.01	-2.74

Table 5.1.3 Hydrogen Peroxide Concentration Dependence of the Pseudo First-Order Rate Constant for the Cleavage of BNPP in the Presence of 30 mM La(III) at pH 7.0 (0.10 M HEPES) at 25° C (data plotted in Figure 5.6).

[HOOH] (mM)	$k_{\text{obs}} \times 10^3 \text{ (s}^{-1}\text{)}$	$\log(k_{\text{obs}}/\text{s}^{-1})$
2.00	0.214 ± 0.0005	-3.67
3.00	0.509 ± 0.003	-3.29
4.00	0.945 ± 0.005	-3.02
5.00	0.133 ± 0.0004	-2.88

Table 5.1.4 La(III) Concentration Dependence of Pseudo First-Order Rate Constants for the Cleavage of BNPP (5×10^{-5} M) and Calculated Concentrations of 1 in the Presence of 30 mM Hydrogen Peroxide at pH 7.0 (0.10 M HEPES) at 25° C.

[La(III)] (mM)	[1] (mM)	$k_{\text{obs}} \times 10^3$ (s ⁻¹)
1.000	0.119	0.709 ± 0.005
2.000	0.348	2.86 ± 0.03
3.000	0.626	4.72 ± 0.04
4.000	0.933	6.15 ± 0.03
5.000	1.26	7.26 ± 0.06
6.000	1.60	7.83 ± 0.08

Chapter 6

The Effect of Lanthanide Ions on the Cleavage of RNA

6.1. Introduction

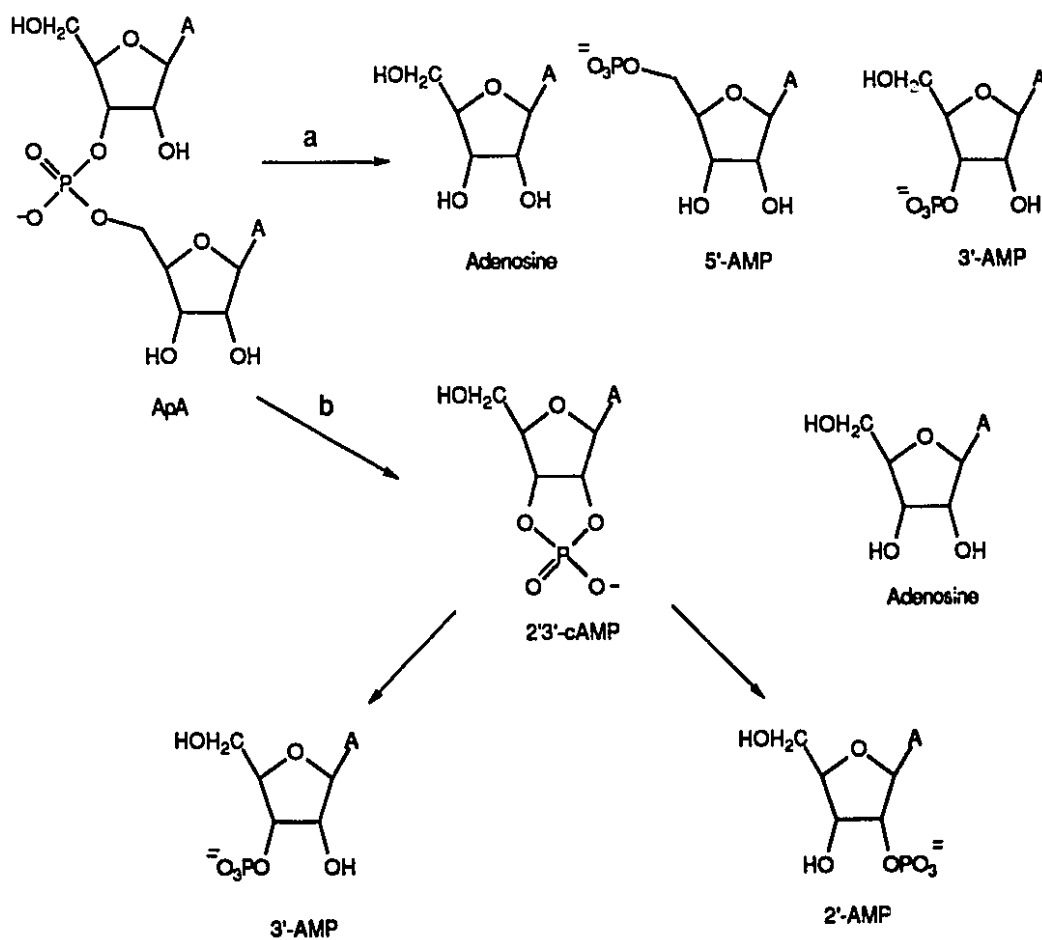
The work presented in this thesis began with the effect of lanthanide ions and lanthanide ion complexes on the rate of cleavage of an RNA analog (HPNPP). Chapters 2-5 dealt with the effect of Ce(III)•O₂ and La(III)•HOOH on the rate of cleavage of DNA and DNA analogs. In this chapter we return again to the effect of lanthanide ions on the rate of cleavage of RNA. However, we now bring new insight gained from our studies with DNA and DNA analogs.

As already described in chapter 2, the use of lanthanide ions in the cleavage of RNA and RNA analogs has recently been the focus of growing interest and research. The most impressive rate enhancement of an RNA dinucleotide was that achieved using 10 mM Tm(III) at 30 °C, pH 8 which Komiyama *et al.* (1992) found could cleave ApA with a half-life of 10 minutes. During the course of investigating the effects of Ce(III)•O₂ and La(III) on the cleavage of RNA, I discovered conditions under which La(III) cleaved ApA almost one hundred times more rapidly than previously reported.

Monitoring the cleavage of an RNA dinucleotide (ApA) by HPLC gives important information not obtained by monitoring the release of *p*-nitrophenoxide ion from HPNPP. Because HPLC allows one to monitor the

concentrations of the starting material and all of the products except inorganic phosphate, it is possible to discern whether it is attack by an external nucleophile which leads to cleavage (Scheme 6.1a) or the 2'-hydroxyl acting as a nucleophile which cleaves ApA and produces the 2'3'-cyclic monophosphate (Scheme 6.1b). It is also possible to determine the effect of the lanthanide ions on the lifetime of the phosphate monoester products.

Scheme 6.1



6.2. Results and Discussion

6.2.1. Ce(III) promoted cleavage of ApA

In order to test the efficiency of the peroxide nucleophile proposed for the $\text{Ce(III)} \cdot \text{O}_2$ promoted cleavage of DNA (dApdA), the same system was used to cleave a dinucleotide of RNA (ApA). If the peroxide nucleophile of the $\text{Ce(III)} \cdot \text{O}_2$ system is efficient enough to compete successfully with the internal 2'-hydroxyl nucleophile of the substrate then 5'-AMP and 3'-AMP should be produced but no 2'-AMP (Scheme 6.1a). If the 2'-hydroxyl acts as the nucleophile, leading to the 2',3'-cAMP then both the 2'- and 3'-monoesters should be produced with no 5'-AMP (Scheme 6.1b).

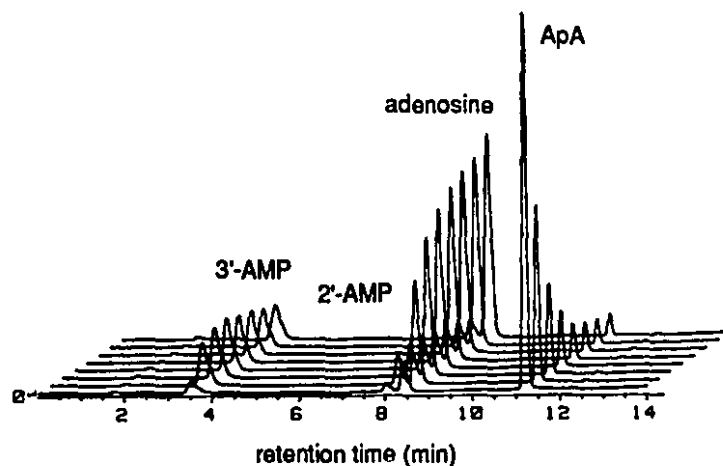


Figure 6.1 Stacked HPLC chromatograms showing the cleavage of ApA (1 mM) in the presence of $\text{Ce}(\text{ClO}_4)_3$ (20 mM) and O_2 at pH 8.15 and 20 °C. The chromatograms are taken at 3 minute intervals.

The HPLC chromatograms from the reaction of ApA (1 mM) with Ce(III) (20 mM) at pH 8.2, 20 °C show that the ApA is rapidly converted to adenosine ($k_{\text{obs}}=0.31 \text{ min}^{-1}$) and the 2'- and 3'-monoesters with no production of 5'-AMP (ret. time=1.62 min). The rapid cleavage of ApA ($t_{1/2}=2 \text{ min}$) observed with Ce(III) is approximately 5 times faster than that observed by

Fitting equations (6.1-3) to the observed concentrations of ApA and the 2' and 3' monophosphates (Figure 6.2) yields values for k_1 , k_4 , k_5 , r_1 and r_2 of $0.31 \pm 0.03 \text{ min}^{-1}$, $0.059 \pm 0.004 \text{ min}^{-1}$, $0.047 \pm 0.004 \text{ min}^{-1}$, 0.32 ± 0.2 and 0.63 ± 0.3 respectively. From the ratio of r_1 and r_2 the relative values of k_2 and k_3 can also be calculated ($k_3/k_2=1.97$). The values for k_4 and k_5 are in fairly good agreement with the values obtained independently for the cleavage of 2'-AMP ($k_4=0.028 \pm 0.002 \text{ min}^{-1}$) and 3'-AMP ($k_5=0.018 \pm 0.002 \text{ min}^{-1}$). The rate of conversion of the 2',3'-cAMP to the 2' and 3'-monophosphates was too rapid to be monitored by HPLC.

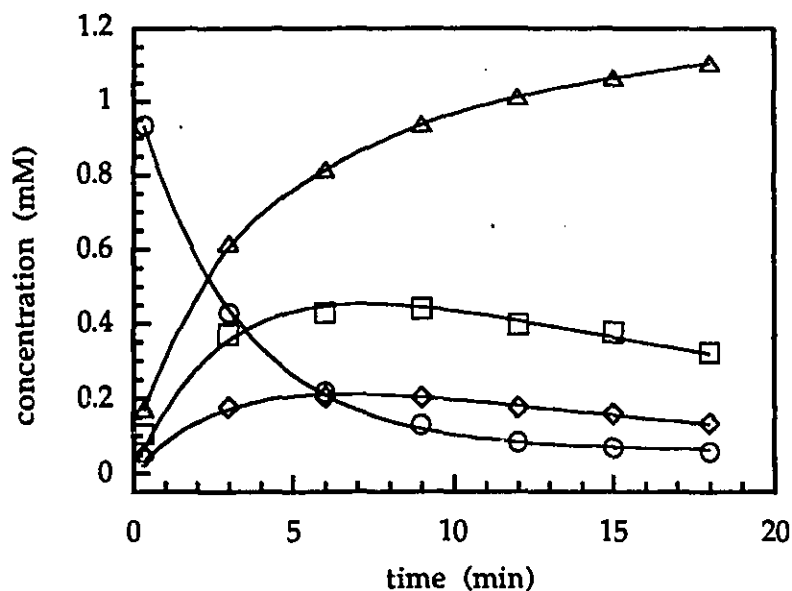


Figure 6.2 Kinetic plot showing the cleavage of ApA (1 mM) (circles) in the presence of $\text{Ce}(\text{ClO}_4)_3$ (20 mM) at pH 8.15, 20 °C to give adenosine (triangles), 2'-AMP (diamonds) and 3'-AMP (squares). The curves drawn through the points represent the non-linear least squares fit of equations (6.1), (6.2) and (6.3) to the data for [ApA], [2'-AMP] and [3'-AMP] respectively. The rate constants are given in the text. The curve drawn for [Adenosine] is simply a smooth curve through the data.

Interestingly, when the same reaction is done in the absence of molecular oxygen the ApA is still rapidly cleaved to give the 2' and 3' monophosphates; however, in the absence of molecular oxygen, the monophosphates themselves are not cleaved (Figure 6.3).

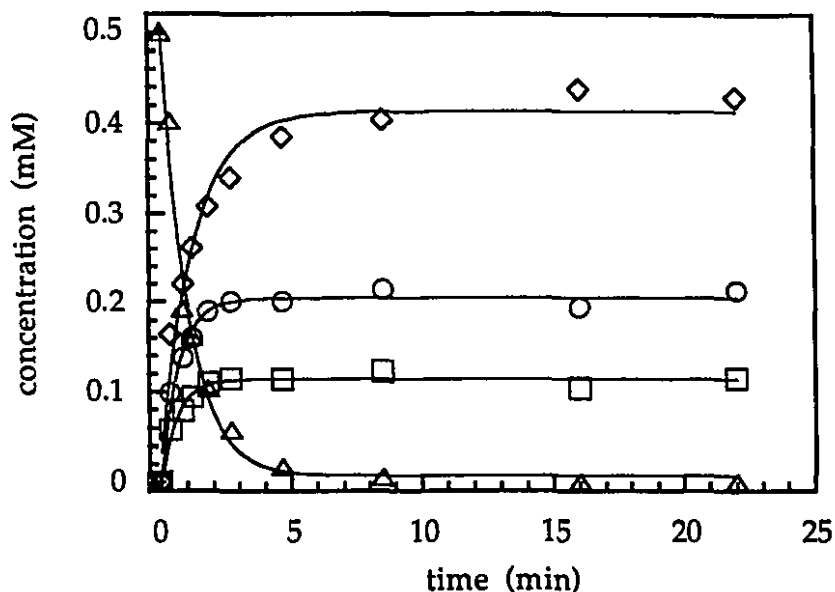


Figure 6.3 Kinetic plot showing the $\text{Ce}(\text{ClO}_4)_3$ (22.5 mM) promoted conversion of ApA (triangles) to adenosine (diamonds), 2'-AMP (squares) and 3'-AMP (circles) in the absence of molecular oxygen at pH 8.2, 20 °C.

Unlike in the case of dApdA, the removal of molecular oxygen does not suppress the Ce(III) promoted cleavage of ApA which is actually cleaved faster in the absence of molecular oxygen ($k_1=1.1 \text{ min}^{-1}$). The relative rate of conversion of 2',3'-cAMP to 2' and 3'-AMP is unaffected by the absence of molecular oxygen ($k_2/k_3=1.8$). The most striking effect of removing molecular oxygen from the system is the suppression of the cleavage of the monoesters. This is supported by the observation that the pseudo first-order rate constants for the Ce(III) promoted cleavage of the 2' and 3'-monophosphates ($k_4=0.0097 \pm .0005$; $k_5=0.0017 \pm .0004$ difficulty in keeping

oxygen out of the reaction may have inflated these values) are significantly lower than in the presence of oxygen .

The lack of Ce(III)•O₂ cooperativity in the cleavage of ApA and the production of only the 2' and 3'-monophosphates indicates that the peroxide nucleophile which is essential for the cleavage of DNA (dApdA) is unable to compete with the well positioned 2'-hydroxyl as a nucleophile. However, the oxygen dependence in the Ce(III) promoted cleavage of the monophosphates indicates that the peroxide nucleophile is essential for the cleavage of 2' and 3'-AMP. This result is not surprising since the 2'-hydroxyl cannot assist in the cleavage of 3'-AMP. Nucleophilic attack of the 2'-hydroxyl on the phosphate of 3'-AMP leads back to 2',3'-cAMP or 2'-AMP but not to adenosine and inorganic phosphate. Likewise, the attack of the 3'-hydroxyl on the phosphate of 2'-AMP does not lead to cleavage. In order to actually cleave the phosphate monoester, an external nucleophile is required. The observed Ce(III) molecular oxygen cooperativity in the cleavage of the monophosphates is therefore consistent with the proposal that the combination of Ce(III) generates the nucleophilic peroxide which then cleaves the monophosphates.

6.2.2. La(III) promoted hydrolysis of ApA

The rapid hydrolysis of ApA promoted by Ce(III) in the absence of molecular oxygen suggests that peroxide is not required for this reaction and therefore the same rate enhancement should be possible with other lanthanides even though they do not have the possibility of generating hydrogen peroxide *in situ*. Indeed, when La(III) (20 mM) is mixed with two equivalents of NaOH (40 mM) the resulting pH 8.7 solution at 20 °C rapidly hydrolyzes ApA (0.5 mM) to give adenosine and the 2' and 3'-

monophosphates ($k_{obs}=5.16 \text{ min}^{-1}$) with a half-life of only 8 seconds. Furthermore, like the results obtained with Ce(III) in the absence of molecular oxygen, with La(III) there is no detectable cleavage of the phosphate monoesters within the first twenty minutes of reaction (Figure 6.4).

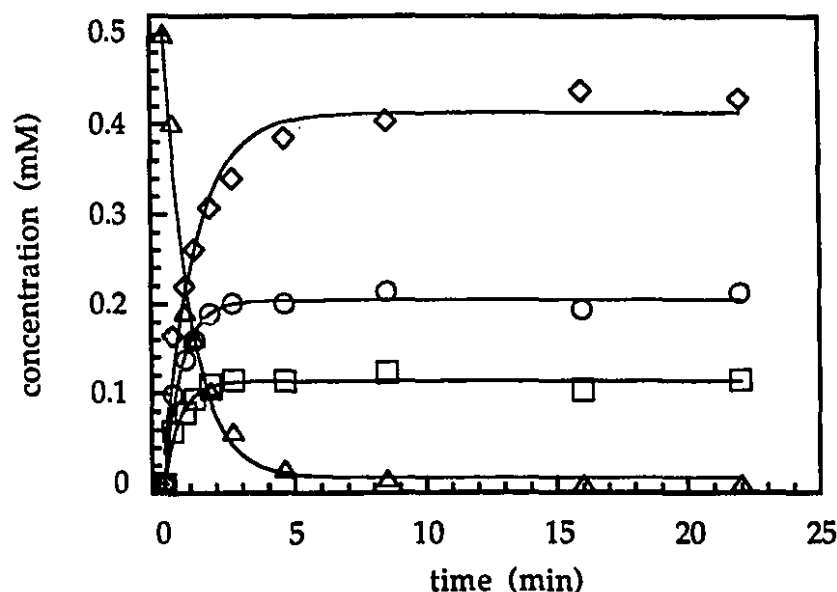


Figure 6.4 Kinetic plot showing the La(III) (20 mM) promoted hydrolysis of ApA (1 mM) (triangles) at pH 8.7, 20 °C to produce adenosine (diamonds), 2'-AMP (squares) and 3'-AMP (circles).

The rapid hydrolysis of ApA observed in the presence of La(III) and NaOH at pH 8.7 is 1.1×10^4 times faster than that observed in the presence of 20 mM La(III) buffered at pH 8.0 (0.5 M HEPES) ($k_{obs}=4.68 \pm 0.1 \times 10^{-4} \text{ min}^{-1}$). This enormous difference in reactivity suggests that a very reactive species is generated when La(III) is combined with two equivalents of NaOH. In order to learn more about the nature of this species the effects of pH and La(III) concentration on its reactivity were studied.

6.2.2.1. pH dependence

In order to probe the nature of the reactive La(III) hydroxide species it was first generated by mixing 8.33 mM La(III) with two equivalents of NaOH and it was then titrated with 0.1 M HCl (Figure 6.5). The freshly prepared solution of La(III)/OH⁻ takes up two equivalents of acid with a midpoint at pH 8.6 (Figure 6.5a). However, this species quickly decays to generate a second species which takes up two equivalents of acid with a midpoint at pH 7.25 (Figure 6.6 b&c).

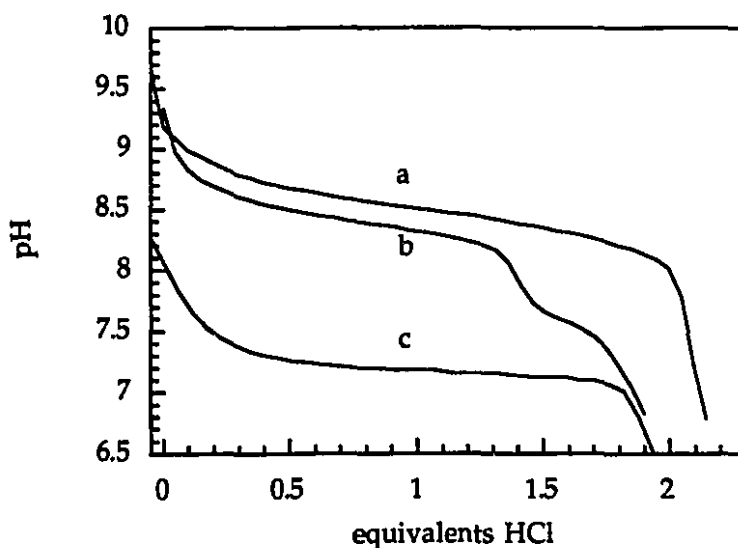


Figure 6.5 Potentiometric titration of the La(III)/OH⁻ species generated from mixing 8.33 mM La(ClO₄)₃ with two equivalents of NaOH. Titrations performed with 0.1 M HCl as titrant at 21 °C using (a) a freshly prepared solution of La(III)/OH⁻; (b) the same solution 11 minutes later; (c) after 1 hour.

It appears that it is the short lived species with an apparent $pK_a=8.6$ which is responsible for rapid cleavage of ApA. If the ApA is added to the La(III) and NaOH solution 30-40 minutes after it was made up, ApA is cleaved

20 times slower ($k_{\text{obs}}=0.25 \text{ min}^{-1}$) than when a fresh La(III)/NaOH solution is used.

The fact that it is the species with an apparent $\text{pK}_a=8.6$ which is the active species is further corroborated by the pH rate profile of the reaction (Figure 6.7) which shows a very steep (4th or 5th order) dependence on hydroxide ion between pH 8.0 and 8.6 but levels off to zero-order above pH 8.6.

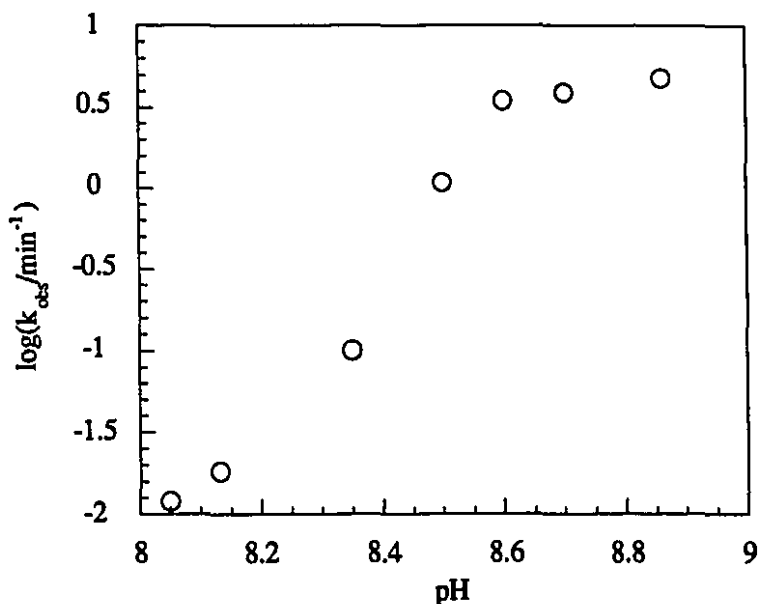


Figure 6.6 pH rate profile for the $\text{La}(\text{ClO}_4)_3$ (20 mM) + NaOH (40 mM) mediated cleavage of ApA (0.5 mM) at 20 °C.

The close agreement between the apparent pK_a of 8.6 derived from the potentiometric titration and the inflection point of 8.6 from the pH rate profile suggest that the behavior results from the same La(III)/ OH^- species. The potentiometric titration indicates that two equivalents of HCl are taken up at the endpoint which suggests that the active species incorporates two OH^- ions per La(III) (*ie.* $\text{La}(\text{OH})_2^+$). The fourth-order dependence on OH^- ion of the La(III)/ OH^- mediated cleavage of ApA suggests that either: two of the

$\text{La}(\text{OH})_2^+$ species are involved in the reaction; or that the active species is a $\text{La}(\text{OH})_2^+$ dimer ($\text{La}_2(\text{OH})_4^{2+}$). In either case, the reaction should be second-order in $\text{La}(\text{III})$ concentration.

6.2.2.2. $\text{La}(\text{III})$ Concentration Dependence

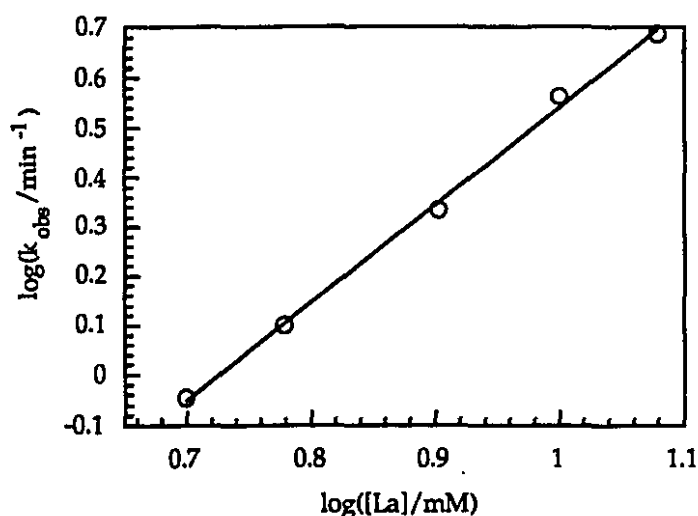


Figure 6.7 $\text{La}(\text{III})$ concentration dependence of $\text{La}(\text{III})/\text{OH}^-$ promoted cleavage of ApA (0.5 mM) at 20 °C at $\text{pH} > 9$ (pH independent region). (slope=1.97 $r=0.999$)

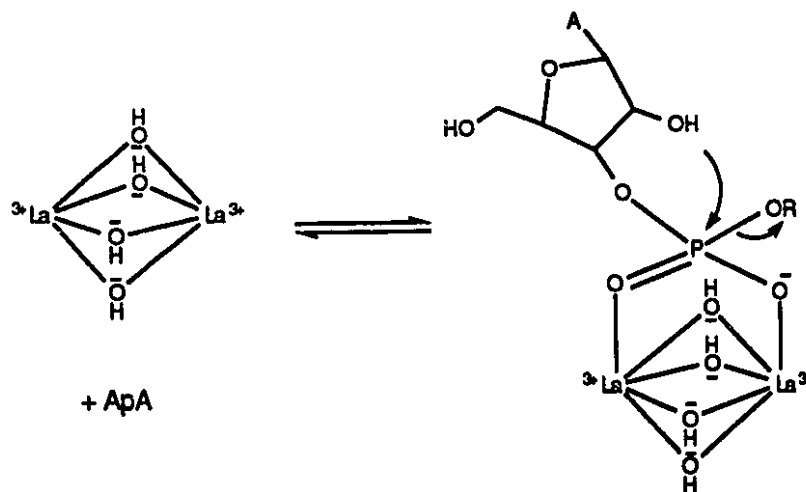
Figure 6.7 shows the $\log(k_{\text{obs}})$ vs. $\log([\text{La}(\text{III})])$ plot which confirms that the $\text{La}(\text{III})/\text{OH}^-$ promoted cleavage of ApA is indeed second-order in $\text{La}(\text{III})$ concentration. This supports the hypothesis that the reaction either involves two equivalents of $\text{La}(\text{OH})_2^+$ or one equivalent of $\text{La}_2(\text{OH})_4^{2+}$; however, it does not help differentiate between the two kinetically indistinguishable pathways.

While the two proposed mechanisms are kinetically indistinguishable, there is evidence from earlier studies that under basic conditions $\text{La}(\text{III})$ and other lanthanide salts hydrolyze to give polynuclear lanthanide(III) hydroxide

species (Biedermann & Ciavatta, 1961; Biedermann & Ciavatta, 1964; Biedermann & Newman, 1964).

The potentiometric titration studies by Biedermann (1961) only give information about the stoichiometry of the lanthanum hydroxide species with no structural information. This study has not revealed any further information about the structure of the proposed $\text{La}_2(\text{OH})_4^{2+}$ species; however, we can propose a structure which is analogous to that proposed for the $\text{Ce(III)} \cdot \text{O}_2$ species which is active in the cleavage of dApdA; and the $\text{La(III)} \cdot \text{HOOH}$ species which is active in the cleavage of BNPP. Both of these active species are thought to involve two lanthanide ions bridged by the peroxide dianion in a $\mu \eta^2: \eta^2$ fashion. A similar structure can be proposed for the $\text{La}_2(\text{OH})_4^{2+}$ species where the two La(III) ions are bridged by four hydroxide ions (Scheme 6.2). This structure could in turn give coordinate ApA as a bridging ligand thus giving double Lewis Acid activation of the coordinated substrate.

Scheme 6.2



6.3. Conclusion

In the second chapter of this thesis, the effect of lanthanide ions and lanthanide ion complexes on the rate of cleavage of an RNA analog (HPNPP) was studied. It was found that, in spite of the X-ray crystal structure which showed a phosphate diester bridging two lanthanide ions, the rate of HPNPP cleavage was not second-order in lanthanide concentration and the effect on the rate of HPNPP cleavage was modest. In chapters 3 and 4 it was discovered that the combination of Ce(III) with two equivalents of NaOH and molecular oxygen produces a reactive species capable of rapid cleavage of DNA (dApdA) and phosphate monoesters (3' and 5'-AMP). In this chapter it was discovered that the same combination of Ce(III), NaOH and O₂ rapidly cleaves RNA (ApA) except that the molecular oxygen is required only for the cleavage of the monophosphates.

The lack of Ce(III) oxygen cooperativity in the cleavage of ApA led to the discovery that the combination of La(III) and NaOH (pH 8.7) could cleave ApA with a half-life of only 8 seconds at 20 °C. This reaction is second-order in La(III) concentration and most likely takes advantage of double Lewis Acid activation of the coordinated substrate to give the enormous rate enhancement in the cleavage of ApA.

The observation that the trivalent lanthanide ions (La(III) and Ce(III) without O₂) cleave ApA even more rapidly than the Ce(IV) generated from Ce(III) + O₂ suggests that the Ce(IV) does not provide greater Lewis Acid activation than the trivalent lanthanide ions.

6.4. Experimental

6.4.1. ApA cleavage

ApA cleavage was monitored by HPLC using a Hewlett Packard HP 1090 series II LC. In a typical run, 50 μL aliquots of the reaction mixture were taken periodically and quenched with 50 μL of 0.2 M $(\text{NH}_4)_2\text{HPO}_4$. The CePO_4 precipitate was then spun down at 13,200 rpm for 3 minutes. 1 μL of the supernatant was then injected onto a C-18 reversed phase column (5- μm Hypersil maintained at 40 $^\circ\text{C}$) and eluted for 5 min with $\text{NH}_4\text{H}_2\text{PO}_4$ (0.2 M pH 5.5) followed by a 0-100% linear gradient of $\text{NH}_4\text{H}_2\text{PO}_4$ (0.2 M pH 5.5) and methanol/water (3:2) solutions over 10 minutes with a flow rate of 0.5 mL/min. The retention times of ApA (11.38 min), adenosine (8.46 min), 2'-AMP (8.05 min) and 3'-AMP (3.49 min) were determined by injecting authentic samples of each onto the column.

6.4.2. pH rate profile

The pH of fresh La(III)/OH^- solutions (25 mM La(III) & 50 mM HOOH) were adjusted with dilute HClO_4 and then mixed 5:1 with 2.5 mM ApA to give a mixture of 20 mM La(III) and 0.5 mM ApA after mixing. The progress of the reaction was monitored by HPLC as described above.

The pseudo first-order rate constants for the reactions done at pH 8.5 and higher were calculated from the non-linear least squares fit of the first-order rate equation to the concentration of ApA as a function of time. The pseudo first-order rate constants for the reactions done below pH 8.5 were estimated from the initial rate of disappearance of ApA.

6.4.3. La(III) Concentration Dependence

In a typical run, 10 mL of a solution containing the desired concentration of $\text{La}(\text{ClO}_4)_3$ with two equivalents of NaOH was prepared and the pH was adjusted to between 9 and 9.5 (well above the $\text{pK}_a=8.6$ where the reaction should be pH independent) and mixed 5:1 with 2.5 mM ApA. The reaction was monitored by HPLC as previously described. The pseudo first-order rate constants were all calculated from the non-linear least squares fit of the first-order rate equation of the concentration of ApA as a function of time.

6.4.4. Oxygen dependence of the Ce(III) reaction

The water used to make up all of the solutions were first degassed by bubbling N_2 gas for at least one hour prior to use. In the case of the reactions done in the presence of O_2 , once the Ce(III) and NaOH were combined the solution was exposed to the atmosphere for five minutes prior to mixing with the ApA. During this time the solution went from colourless to a pink/purple coloured solution. In the case of the reactions done in the absence of O_2 , the reaction was performed in a N_2 atmosphere.

6.4.5. Potentiometric Titration of La(III)/OH⁻

10 mL of a solution containing 25 mM $\text{La}(\text{ClO}_4)_3$ and 50 mM NaOH was freshly prepared. A 1.0 mL aliquot of this solution was mixed with 2.0 mL of distilled water and titrated with 1.0 M HCl at 20 °C using the Radiometer titration apparatus described earlier. The titration was repeated after 11 minutes and 1 hour using the same stock solution of La/OH⁻.

$$d[2'\text{-AMP}]/dt = k_2 k_1 [\text{ApA}] / (k_2 + k_3) - k_4 [2'\text{-AMP}] \quad (6.1.6)$$

substituting (6.1.2) into (6.1.6)

$$\frac{d[2'\text{-AMP}]}{dt} = \frac{k_2 k_1 [\text{ApA}]_0 e^{-k_1 t}}{k_2 + k_3} - k_4 [2'\text{-AMP}] \quad (6.1.7)$$

substituting $r_1 = k_2 / (k_2 + k_3)$ and integrating (6.1.7) gives:

$$[2'\text{-AMP}] = \frac{r_1 k_1 [\text{ApA}]_0}{k_4 - k_1} (e^{-k_1 t} - e^{-k_4 t}) \quad (6.1.8)$$

the same procedure can be applied for 3'-AMP to give:

$$[3'\text{-AMP}] = \frac{r_2 k_1 [\text{ApA}]_0}{k_5 - k_1} (e^{-k_1 t} - e^{-k_5 t}) \quad (6.1.9)$$

where $r_2 = k_3 / (k_2 + k_3)$

$$k_2 / k_3 = r_1 / r_2 \quad (6.1.10)$$

Appendix 6.2 Pseudo First-Order Rate Constants

Table 6.2.1 Pseudo First-Order Rate Constants for the La(III)/OH⁻ Mediated Cleavage of ApA as a Function of pH^a.

pH	k _{obs} (min ⁻¹)	log(k _{obs})
8.05	0.0120 ± 0.001	-1.92
8.13	0.0183 ± 0.004	-1.74
8.35	0.101 ± 0.02	-0.997
8.50	1.09 ± 0.2	0.0358
8.60	3.48 ± 0.4	0.542
8.70	3.89 ± 0.4	0.590
8.86	4.79 ± 0.3	0.680

^aData is plotted in Figure 6.6. [Ce(ClO₄)₃]=20 mM, [ApA]=0.5 mM, 20 °C.

Table 6.2.2 Pseudo First-Order Rate Constant for the La/OH⁻ Mediated Cleavage of ApA as a Function of La(III) Concentration^a.

[La] (mM)	k _{obs} (min ⁻¹)	log([La])	log(k _{obs})
5.00	0.900 ± 0.4	0.699	-0.0458
6.00	1.26 ± 0.3	0.778	0.100
8.00	2.20 ± 0.6	0.903	0.342
10.0	3.66 ± 0.3	1.00	0.563
12.0	4.88 ± 0.4	1.08	0.689

^aData plotted in Figure 6.7. [ApA]=0.5 mM, pH >9.0, 20 °C.

Chapter 7

Recent Developments in the use of Lanthanide Ions in the Development of Artificial Nucleases

During the course of the research described in this thesis, the use of lanthanide ions in the development of artificial nucleases has become an area of growing research interest. Several reports have been published in the past two years, which, while not directly influencing the research described in this thesis, are certainly relevant and deserving of mention.

Since the publication of their results obtained with lanthanide ions and the lanthanide ion schiff base complexes (Ln(III)L_2) on the cleavage of RNA (Morrow *et al.*, 1992b) and HPNPP (1992a) already described in chapter 2, Morrow and co-workers have focused their attention on designing a ligand which binds lanthanide ions tightly while maintaining their RNase activity. The development of such a ligand and its attachment to an RNA recognition group is essential for the use of lanthanide ions in the development of an artificial RNase capable of site-specific RNA cleavage. Because the imine of the schiff base ligand (L_2) is prone to hydrolysis (1992b) Morrow *et al.* have designed other more robust ligands consisting of the tetraazamacrocyclic cyclen (1,4,7,10-tetraazacyclododecane), N-alkylated with pendant arms containing ligating groups (Figure 7.1).

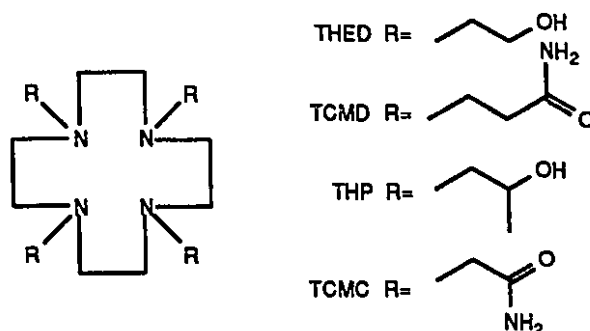


Figure 7.1 Structure and nomenclature of macrocyclic ligands with pendant ligating arms designed and synthesized by Morrow *et al.*.

Morrow *et al.* have synthesized and characterized the La(III) and Eu(III) complexes with THED (Morrow & Chin, 1993); the La(III)(TCMD) complex (Morrow *et al.*, 1993); the La(III), Eu(III) and Lu(III) complexes with THP (Chin *et al.*, 1994); and the La(III), Eu(III) and Dy(III) complexes with TCMC (Amin *et al.*, 1994); however, while all of these complexes are stable in solution, only the La(III)(TCMC) complex promotes the rapid cleavage of RNA oligomers and HPNPP. The pseudo first-order rate constant (0.57 hr^{-1}) for cleavage of adenylic acid oligomers ($A_{12}-A_{18}$) by La(III)(TCMC) (0.2 mM at 37°C , pH 7.6) (Amin *et al.*, 1994) is similar to that observed (1.5 hr^{-1}) with the Eu(III) L_2 complex (0.160 mM at 37°C , pH 7) (Morrow *et al.*, 1992b). The development of a ligand which forms a stable complex with a lanthanide ion while still preserving its ribonuclease activity represents an important step in the application of lanthanide ion promoted cleavage of RNA to the development of reagents capable of site-specific hydrolysis of RNA.

In a report that parallels and complements some of the work described at the beginning of the third chapter of this thesis Schneider and Rammo (1993) describe the effect of lanthanide ions on the rate of cleavage of BNPP. They report a value of $1.67 \times 10^{-4} \text{ s}^{-1}$ for the pseudo first-order rate constant for

the cleavage of BNPP at pH 7.0, 50 °C in the presence of 5 mM EuCl_3 . This agrees well with the range of values ($2 \times 10^{-6} - 7 \times 10^{-5} \text{ s}^{-1}$) obtained with other lanthanide ions (3.0 mM) at pH 7.0, 20 °C (section 3.2). Schneider and Rammo also report that complexation of the Eu(III) with different ligands usually results in a 50-90% reduction in the rate of cleavage of BNPP relative to that observed in the absence of the ligand. One notable exception is the [2,2,2]cryptand (Figure 7.2) which causes only a 8% loss of reactivity in the Eu(III) promoted cleavage of BNPP. This result, like that of Morrow *et al.*, suggest that it will be possible to design a ligand which will bind the lanthanide ions without sacrificing their nuclease activity.

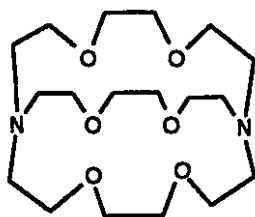


Figure 7.2 [2,2,2]cryptand

The work which most closely parallels the work presented in this thesis is that by Komiyama and co-workers. It appears that the remarkable reactivity of Ce(III) in the cleavage of DNA and DNA analogs was independently discovered by Komiyama's group at the University of Tokyo and in our lab at McGill. Although both groups report very similar results, the mechanisms proposed by the two groups to explain this phenomena differ.

In their first reports describing the unusual reactivity of Ce(III) , Sumaoka, Yashiro & Komiyama attribute the 10^{11} fold rate enhancement in the cleavage of 3',5'-cAMP to the formation of a $[\text{Ce}_3(\text{OH})_5]^{4+}$ cluster which

they suggest cleaves the 3',5'-cAMP by providing a metal-bound hydroxide ion as the nucleophile and metal-bound water which act as general acid catalysts (Sumaoka *et al.*, 1992a; 1992b).

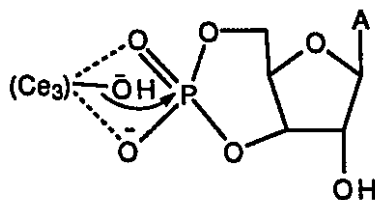
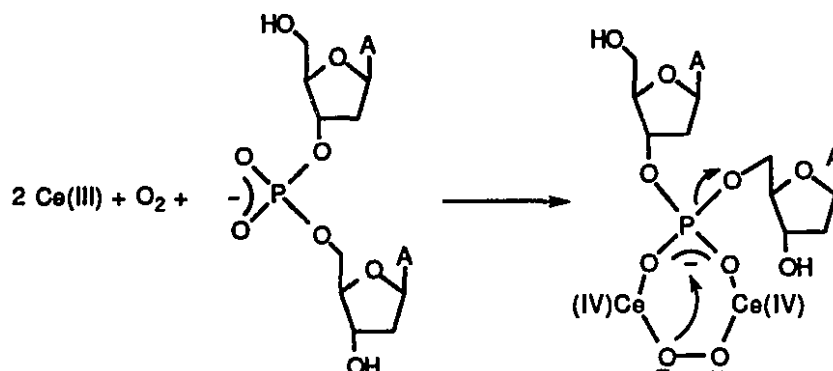


Figure 7.3 Proposed mechanism for the cAMP hydrolysis by the Ce(III) hydroxide cluster (Sumaoka *et al.*, 1992b).

In their reports describing the Ce(III) promoted conversion of supercoiled plasmid DNA to the nicked circular form (Matsumoto & Komiyama, 1992a; 1992b) and the Ce(III) promoted cleavage of thymidyl-(3'-5')thymidine (TpT) (Komiyama *et al.*, 1993) they explain the remarkable rate enhancement using the same mechanism they proposed for the Ce(III) promoted cleavage of 3',5'-cAMP.

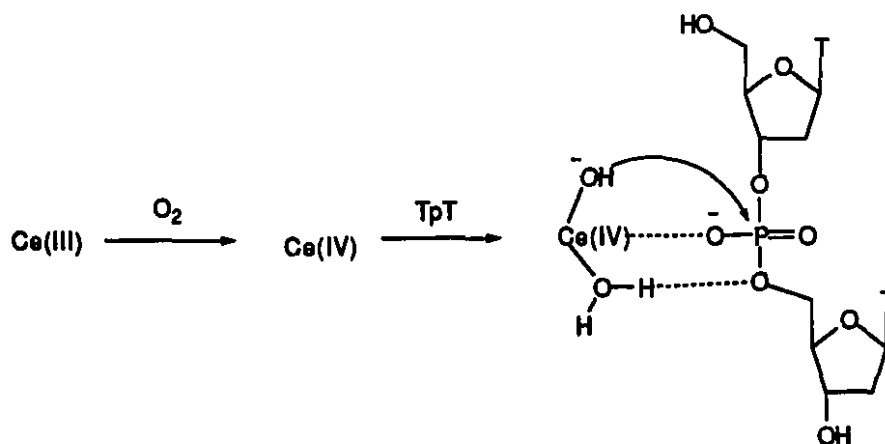
Independent of the work by Komiyama *et al.* on the Ce(III) promoted cleavage of TpT ($k_{\text{obs}}=3.2 \times 10^{-2} \text{ min}^{-1}$, 10 mM CeCl_3 at pH 7.2, 50 °C), I independently observed similar rates in the Ce(III)•O₂ promoted cleavage of dApdA ($k_{\text{obs}}=6.8 \times 10^{-3} \text{ min}^{-1}$, 20 mM $\text{Ce}(\text{ClO}_4)_3$ at pH 8.2, 37 °C). Based on the cooperativity between La(III) and hydrogen peroxide observed in the cleavage of BNPP (Takasaki & Chin, 1993) and the oxygen dependence of the Ce(III) promoted cleavage of dApdA, we proposed that the Ce(III)•O₂ promoted cleavage of dApdA resulted from the nucleophilic attack of peroxide (generated from the *in situ* reduction of molecular oxygen by Ce(III)) upon the coordinated substrate (Scheme 7.1 cf. Chapters 3 & 4) (Takasaki & Chin, 1994).

Scheme 7.1



It appears that Komiyama *et al.* independently discovered the oxygen dependence of the Ce(III) promoted cleavage of DNA and in their most recent publication they also report that Ce(III) is oxidized *in situ* to Ce(IV) by molecular oxygen (Komiyama *et al.*, 1994). However, they do not involve hydrogen peroxide in their proposed mechanism and suggest instead that the Ce(IV) promotes the cleavage of TpT by providing Lewis Acid activation of the coordinated substrate, nucleophilic attack of a metal-bound hydroxide and general acid catalysis by a metal bound water (Scheme 7.2).

Scheme 7.2



Both mechanisms (Schemes 7.1 and 7.2) are consistent with all of the reported data. They differ in how they account for the enormous difference in activity between $\text{Ce(III)}\cdot\text{O}_2$ and the other lanthanide ions. Sumaoko *et al.* report that Ce(III) is at least 700 times more reactive than the other lanthanide ions tested (Sumaoka *et al.*, 1992b). I found that none of the other lanthanide ions tested showed any detectable cleavage of dApdA after 68 hours under the same conditions used for Ce(III) mediated cleavage of dApdA (Takasaki & Chin, 1994). If we assume that 0.5% reaction is the minimum which can be detected by HPLC then the $\text{Ce(III)}\cdot\text{O}_2$ promoted cleavage of dApdA must be at least 5000 times faster than any of the other lanthanide ions tested. I also found that the rate of $\text{Ce(III)}\cdot\text{O}_2$ promoted cleavage of BNPP is 10^5 greater than that observed with any of the other lanthanide ions tested (Chapter 4).

Komiyama *et al.* suggest that the "overwhelming superiority of Ce(IV) over Ce(III) and other trivalent lanthanide metal ions is probably associated with the more effective acid catalysis by the coordination water: its pK_a (around 0) is much smaller than that of the coordination water of trivalent lanthanide ions (8-9). Furthermore, the tetravalent positive charge of Ce(IV) is favorable for the electrostatic stabilization of the negatively charged transition state of the hydrolysis." (Komiyama *et al.*, 1994) It is difficult to evaluate how much rate enhancement these factors can contribute to the overall rate enhancement. However, it seems unlikely that general acid catalysis by the more acidic water bound to the Ce(IV) can account for the greater reactivity of Ce(IV) ; since, at neutral pH the effect of a stronger Lewis Acid is counteracted by the fact that there will be 10^7 times less of the strong acid (pK_a 0) in the acid form than the weaker acid with a pK_a above 7. Furthermore, the observation that the Ce(IV) generated from the *in situ*

oxidation of Ce(III) does not appear to provide greater Lewis Acid activation of ApA than the unoxidized Ce(III) (Section 6.2).

In the ceric peroxide mechanism proposed in this thesis, it is proposed that the enormous superiority of Ce(III)•O₂ over the trivalent lanthanide ions is due to the presence of the peroxide nucleophile and the stronger Lewis Acidity of Ce(IV). It has been shown that cooperativity between La(III) and hydrogen peroxide provides an additional 34,000 fold rate enhancement in the cleavage of BNPP over the rate of La(III) promoted BNPP cleavage (Chapter 5) (Takasaki & Chin, 1993) and could therefore explain the extraordinary reactivity of the Ce(III)•O₂ system.

Contribution to Knowledge

The discovery of the remarkable cooperativity between Ce(III) and molecular oxygen to give the unprecedented 10^{10} - 10^{13} fold rate enhancement in the net hydrolytic cleavage of DNA and DNA analogs represents the first example of a non-enzymatic system which cleaves DNA rapidly ($t_{1/2}=100$ min.) without destruction of the deoxyribose sugar under mild conditions (pH 8.2, 37 °C).

To account for the remarkable cooperativity between Ce(III) and molecular oxygen, it has been proposed that the mechanism involves the *in situ* reduction of molecular oxygen by Ce(III) to give a reactive ceric peroxide complex which then cleaves the coordinated phosphate diester by nucleophilic attack of the peroxide upon the phosphorus center of the substrate.

The discovery of the significant cooperativity between La(III) and hydrogen peroxide in the cleavage of BNPP (The rate of BNPP cleavage with 2 mM La(III) + 20 mM HOOH is 3.4×10^4 times greater than with La(III) alone at pH 7.0, 25 °C) suggests that hydrogen peroxide should be a very important co-factor in the design of new DNA cleaving agents which do not destroy the deoxyribose sugar cf. (Schnaith *et al.*, 1994). The La(III) peroxide cooperativity also provides precedence for the ceric peroxide mechanism proposed to explain the Ce(III)•O₂ cooperativity.

On the basis of evidence from kinetic and equilibrium studies as well as oxygen labeling experiments a mechanism has been proposed which involves coordination of the substrate to a dimeric La(III) peroxide species $(La_2O_4)^{2+}$ followed by nucleophilic attack of the peroxide dianion upon the phosphorus and departure of the leaving group.

It has been shown that the formation of lanthanum hydroxide and cerium hydroxide clusters leads to cleavage of ApA at rates ($t_{1/2}=8$ sec. in the presence of La(III) (20 mM) + NaOH (40 mM) at pH 8.7, 20 °C) greater than previously observed with lanthanide ions. The observation that Ce(III)•O₂ cooperativity leads to the rapid cleavage of the monophosphates (2'-AMP & 3'-AMP) while La(III) and Ce(III) without O₂ do not, is consistent with the proposed generation of the peroxide nucleophile in the case of Ce(III)•O₂ cooperativity.

As a result of my Ph.D. study, the following papers have been published:

Bryan K. Takasaki and Jik Chin "Net Hydrolytic cleavage of the phosphate diester backbone of DNA with Ce(III) and molecular oxygen" *J. Am. Chem. Soc.* **116**, 1121-1122 (1994).

Bryan K. Takasaki and Jik Chin "Synergistic Effect between La(III) and Hydrogen peroxide in phosphate diester cleavage" *J. Am. Chem. Soc.* **115**, 9337-9338 (1993).

Bryan K. Takasaki, Jung Hee Kim, Erik Rubin and Jik Chin "Determination of the Equilibrium constant for coordination of an amide carbonyl to a metal complex in water" *J. Am. Chem. Soc.* **115**, 1157-1159 (1993).

References

- Abid, K. K., Fenton, D. E., Casellato, U., Vigato, P. A. & Graziani, R. (1984) *J. Chem. Soc., Dalton Trans.* , 351-354.
- Amin, S., Morrow, J. R., Lake, C. H. & Churchill, M. R. (1994) *Angew. Chem. Int. Ed. Engl.* 33, 773-775.
- Anslyn, E. & Breslow, R. (1989) *J. Am. Chem. Soc.* 111, 4473-4482.
- Arif, A. M., Backer-Dirks, J. D., Gray, C. J., Hart, F. A. & Hursthouse, M. B. (1987) *J. Chem. Soc., Dalton Trans.* , 1665-1673.
- Basile, L. A., Raphael, A. L. & Barton, J. K. (1987) *J. Am. Chem. Soc.* 109, 7550-7551.
- Benetollo, F., Bombieri, G., Cola, L. D., Polo, A., Smailes, D. L. & Vallarino, L. M. (1989) *Inorg. Chem.* 28, 3447-3452.
- Benetollo, F., Polo, A., Bombiere, G., Fonda, K. K. & Vallarino, L. M. (1990) *Polyhedron* 9, 1411-1422.
- Biedermann, G. & Ciavatta, L. (1961) *Acta Chem. Scand.* 15, 1347-1366.
- Biedermann, G. & Ciavatta, L. (1964) *Arkiv for Kemistry* 22, 253-279.
- Biedermann, G. & Newman, L. (1964) *Arkiv for Kemistry* 22, 303316.
- Blackburn, P. & Moore, S. (1982) *The Enzymes* 15, 317.
- Bombieri, G., Benetollo, F., Polo, A., Cola, L. D., Dmailes, D. L. & Vallarino, L. M. (1986) *Inorg. Chem.* 25, 1127-1132.
- Bombieri, G., Benetollo, F., Polo, A., Fonda, K. K. & Vallarino, L. M. (1991) *Polyhedron* 10, 1385.
- Breslow, R. & Huang, D.-L. (1990) *J. Am. Chem. Soc.* 112, 9621-9623.

- Breslow, R. & Huang, D.-L. (1991) *Proc. Natl. Acad. Sci. USA* 88, 4080.
- Breslow, R., Huang, D.-L. & Anslyn, E. (1989) *Proc. Natl. Acad. Sci. USA* 86, 1746-1750.
- Breslow, R. & Labelle, M. (1986) *J. Am. Chem. Soc.* 108, 2655-2659.
- Brown, D. M. & Usher, D. A. (1965) *J. Chem. Soc.* , 6558-6564.
- Bunzli, J.-C. & Wiessner, D. (1984) *Coord. Chem. Rev.* , 192-242.
- Butcher, W. W. & Westheimer, F. H. (1955) *J. Am. Chem. Soc.* 77, 2420-2424.
- Cech, T. R. (1990) *Angew. Chem. Int. Ed. Engl.* 29, 759-768.
- Cech, T. R., Herschlag, D., Piccirilli, J. A. & Pyle, A. M. (1992) *J. Biol. Chem.* 267, 17479-17482.
- Cech, T. R., Zaug, A. J. & Grabowski, P. J. (1981) *Cell* 27, 487-496.
- Celander, D. W. & Cech, T. R. (1991) *Science* 251, 401-407.
- Chen, C.-h. B. & Sigman, D. S. (1986) *Proc. Natl. Acad. Sci. USA* 83, 7147-7151.
- Chen, C.-H. B. & Sigman, D. S. (1987) *Science* 237, 1197-1201.
- Chen, C.-h. B. & Sigman, D. S. (1988) *J. Am. Chem. Soc.* 110, 6570-6572.
- Chin, J. (1991) *Acc. Chem. Res.* 24, 145.
- Chin, J., Banaszcyk, M., Jubian, V. & Zou, X. (1989) *J. Am. Chem. Soc.* 111, 186-190.
- Chin, J., Banaszcyk, M. & Jubian, V. (1988) *J. Chem. Soc., Chem. Commun.* , 734.
- Chin, K. O. A., Morrow, J. R., Lake, C. H. & Churchill, M. R. (1994) *Inorg. Chem.* 33, 656-664.
- Cohn, M. & Hu, A. (1978) *Proc. Natl. Acad. Sci. USA* 75, 200-203.
- Cox, J. R. & Ramsay, O. B. (1964) *Chem. Rev.* 64, 317-351.
- Dervan, P. B. (1986) *Science* 232, 464-471.
- Edwards, J. O. & Pearson, R. G. (1962) *J. Am. Chem. Soc.* 84, 16-24.
- Eichhorn, G. L. & Butzow, J. J. (1965) *J. Biopolymers* 3, 79.

- Epstein, J., Demek, M. M. & Rosenblatt, D. H. (1956) *J. Org. Chem.* 21, 796-798.
- Fersht, A. (1985). Enzyme Structure and Mechanism. In (pp. 426-433). New York: W. H. Freeman.
- Findlay, D., Herries, D. G., Mathias, A. P., Rabin, B. R. & Ross, C. A. (1961) *Nature* 190, 781.
- Goyne, T. E. & Sigman, D. S. (1987) *J. Am. Chem. Soc.* 109, 2846-2848.
- Griffin, L. C. & Dervan, P. B. (1989) *Science* 245, 967-971.
- Griffin, L. C., Kiessling, L. L., Beal, P. A., Gillespie, P. & Dervan, P. B. (1992) *J. Am. Chem. Soc.* 114, 7976-7982.
- Haake, P. C. & Westheimer, F. H. (1961) *J. Am. Chem. Soc.* 83, 1102-1109.
- Haim, A. (1992) *J. Am. Chem. Soc.* 114, 8384-8388.
- Hay, R. W. & Govan, N. (1990) *J. Chem. Soc., Chem. Commun.* , 714-715.
- Hendry, P. & Sargeson, A. M. (1990) *Inorg. Chem.* 29, 92-97.
- Herschlag, D. & Cech, T. R. (1990) *Nature* 344, 405.
- Kim, J. H. & Chin, J. (1992) *J. Am. Chem. Soc.* 114, 9792-9795.
- Kimball, A. S., Lee, J., Jayaram, M. & Tullius, T. D. (1993) *Biochem.* 32, 4698-4701.
- Koh, J. S. & Dervan, P. B. (1992) *J. Am. Chem. Soc.* 114, 1470-1478.
- Komiyama, M., Kodama, T., Takeda, N., Sumaoka, J., Shiiba, T., Matsumoto, Y. & Yashiro, M. (1994) *Journal of Biochemistry* 115, 809-810.
- Komiyama, M., Matsumura, K. & Matsumoto, Y. (1992) *J. Chem. Soc., Chem. Commun.* , 640-641.
- Komiyama, M., Matsumura, K., Yonezawa, K. & Matsumoto, Y. (1993) *Chem. Express* 8, 85-8.
- Kuwabara, M., Yoon, C., Goyne, T., Thederahn, T. & Sigman, D. S. (1986) *Biochem.* 25, 7401-7408.
- Larsson, L. (1958) *Acta Chem. Scand.* 12, 723-730.

- Latham, J. A. & Cech, T. R. (1989) *Science* 245, 276-282.
- Lowe, G. & Sproat, B. S. (1978) *J. Chem. Soc., Chem. Commun.* , 565-566.
- Matsumoto, Y. & Komiyama, M. (1992a) *Chem. Express* 7, 785-8.
- Matsumoto, Y. & Komiyama, M. (1992b) *Nucleic Acids Symp. Ser.* 27, 33-34.
- Menger, F. M. (1991) *J. Org. Chem.* 56, 6251-6252.
- Menger, F. M. & Haim, A. (1992) *Nature* 359, 666-668.
- Morrow, J. R., Amin, S., Lake, C. H. & Churchill, M. R. (1993) *Inorg. Chem.* 32, 4566-4572.
- Morrow, J. R., Buttrey, L. A. & Berback, K. A. (1992a) *Inorg. Chem.* 31, 16-20.
- Morrow, J. R., Buttrey, L. A., Shelton, V. M. & Berback, K. A. (1992b) *J. Am. Chem. Soc.* 114, 1903-1905.
- Morrow, J. R. & Chin, K. O. A. (1993) *Inorg. Chem.* 32, 3357-3361.
- Mrksich, M. & Dervan, P. B. (1993a) *J. Am. Chem. Soc.* 115, 2572-2576.
- Mrksich, M. & Dervan, P. B. (1993b) *J. Am. Chem. Soc.* 115, 9892-9899.
- Piccirilli, J. A., Vyle, J. S., Caruthers, M. H. & Cech, T. R. (1993) *Nature* 361, 85-88.
- Pyle, A. M. (1993) *Science* 261, 709-714.
- Rana, T. M. & Meares, C. F. (1991) *Proc. Natl. Acad. Sci. USA* 88, 10578-10582.
- Richards, R. M. & Wyckoff, H. W. (1961) *The Enzymes* 4, 648.
- Schnaith, L. M. T., Hanson, R. S. & Que, L. (1994) *Proc. Natl. Acad. Sci. USA* 91, 569-573.
- Schneider, H.-J. & Rammo, J. (1993) *Angew. Chem. Int. Ed. Engl.* 32, 1716-1719.
- Sigman, D. S. (1986) *Acc. Chem. Res.* 19.
- Sigman, D. S., Bruice, T. W., Mazumder, A. & Sutton, C. L. (1993) *Acc. Chem. Res.* 26, 98-104.
- Sigman, D. S., Graham, D. R., D'Aurora, V. & Stern, A. M. (1979) *J. Biol. Chem.* 254, 12269-12272.

- Sigman, D. S., Mazumder, A. & Perrin, D. M. (1993) *Chem. Rev.* 93, 2295-2316.
- Smith, P. H., Brainard, J. R., Morris, D. E., Jarvinen, G. D. & Ryan, R. R. (1989) *J. Am. Chem. Soc.* 111, 7437-7443.
- Strobel, S. A. & Dervan, P. B. (1991) *Nature* 350, 172.
- Sumaoka, J., Yashiro, M. & Komiyama, M. (1992a) *Nucleic Acids Symp. Ser.* 27, 37.
- Sumaoka, J., Yashiro, M. & Komiyama, M. (1992b) *J. Chem. Soc., Chem. Commun.* , 1707-1708.
- Takasaki, B. K. & Chin, J. (1993) *J. Am. Chem. Soc.* 115, 9337-9338.
- Takasaki, B. K. & Chin, J. (1994) *J. Am. Chem. Soc.* 116, 1121-1122.
- Thatcher, G. R. J. & Kluger, R. (1989). Mechanism and Catalysis of Nucleophilic substitution in Phosphate esters. In D. Bethell (Eds.), Advances in Physical Organic Chemistry (pp. 99-265). London: Academic Press.
- Tullius, T. D. & Dombroski, B. A. (1986) *Proc. Natl. Acad. Sci. USA* 83, 5469-5473.
- Tyeklar, Z. & Karlin, K. D. (1989) *Acc. Chem. Res.* 22, 241-248.
- Uhlmann, E. & Peyman, A. (1990) *Chem. Rev.* 90, 543-584.
- Wade, W. S., Mrkisch, M. & Dervan, P. B. (1992) *J. Am. Chem. Soc.* 114, 8783-8794.
- Weil, L. & Seibles, T. S. (1967) *BBA* 6, 1606.
- Westheimer, F. H. (1968) *Acc. Chem. Res.* 1, 70.
- Weintraub, H. M. (1990) *Scientific American* , 40-46.
- Xu, G.-X., Ren, J., Huang, C.-H. & Wu, J.-G. (1988) *Pure Appl. Chem.* 60, 1145-1152.
- Zaug, A. J., Been, M. D. & Cech, T. R. (1986) *Nature* 324, 429-433.
- Zaug, A. J. & Cech, T. R. (1986) *Science* 231, 470-475.

